HIGGS PARTICLES*

Conveners:

A. Djouadi^{1,2}, H.E. Haber³, P. Igo–Kemenes⁴, P. Janot⁵ and P.M. Zerwas¹

Working Group:

- A. Arhrib⁶, T. Binoth⁷, E. Chopin⁸, V. Driesen², W. Hollik², C. Jünger², J. Kalinowski⁹, W. Kilian¹, B.R. Kim¹⁰, M. Krämer¹, G. Kreyerhoff¹⁰, G. Moultaka⁶, S.K. Oh¹¹, P. Ohmann¹², J. Rosiek² and J.J. van der Bij⁷.
 - ¹ Deutsches Elektronen-Synchrotron DESY, D-22603 Hamburg, Germany.
 - 2 Institut für Theoretische Physik, Universität Karlsruhe, D-76128 Karlsruhe, Germany.
 - ³ Physikalisches Institut, Universität Heidelberg, D-6900 Heidelberg, Germany.
 - ⁴ Santa Cruz Institute for Particle Physics, University of California, Santa Cruz, CA 95064, USA.
 - ⁵ PPE Division, CERN, CH-1211, Geneva 23, Switzerland.
 - 6 Physique Mathématique et Théorique, E.S.A. du CNRS N o 5032, Université Montpellier II, F $\!-\!34095$ Montpellier, France
 - Albert-Ludwigs-Universität Freiburg, Fakultät für Physik, Hermann-Herder-Strasse 3, D-79104 Freiburg, Germany.
 - ⁸ Laboratoire de Physique Théorique ENSLAPP B.P.110, 74941 Annecy-Le-Vieux Cedex, France
 - ⁹ Institute of Theoretical Physics, Warsaw University, PL-00681 Warsaw, Poland.
 - 10 III Physikalisches Institute A, RWTH Aachen, D–52056 Aachen, Germany.
 - ¹¹ Institute for Advanced Physics, Kon–Kuk University, Seoul 143–701, Korea.
 - Department of Theoretical Physics, Oxford University, OX1 3NP Oxford, UK.
- * To appear in the Proceedings of the Workshop *Physics with* e^+e^- *Linear Colliders*, Annecy–Gran Sasso–Hamburg, Feb. 4 Sept. 1, 1995, P.M. Zerwas (editor).

HIGGS PARTICLES

Introduction and Summary

A. $DJOUADI^{1,2}$ and P.M. $ZERWAS^1$

The search for scalar Higgs particles and the exploration of the mechanism which breaks the electroweak symmetry, will be one of the major tasks at future high–energy e^+e^- colliders. In previous studies it has been shown that e^+e^- linear colliders operating in the energy range $\sqrt{s} \sim 300$ to 500 GeV with a luminosity of $\int \mathcal{L} \sim 20$ fb⁻¹ are ideal machines to search for light Higgs particles.

In the Standard Model (SM) the Higgs mass range $M_H \lesssim 200$ GeV is easy to cover at these energies. This intermediate Higgs mass range is one of the theoretically most favored ranges, allowing the particles to remain weakly interacting up to the GUT scale $\Lambda \sim 10^{16}$ GeV [a prerequisite for the perturbative renormalization of the electroweak mixing angle from the GUT symmetry value 3/8 down to the experimentally observed value at low energies]. The search of intermediate-mass Higgs bosons can be carried out in three different channels: the Higgs-strahlung process $e^+e^- \to ZH$ and the fusion mechanisms $WW/ZZ \to H$. The cross sections are large and the properties of the Higgs boson, in particular spin-parity quantum numbers and couplings to gauge bosons and fermions, can be thoroughly investigated, allowing for crucial tests of the Higgs mechanism.

In the Minimal Supersymmetric Standard Model (MSSM) the Higgs sector is extended to three neutral scalar and pseudoscalar particles h/H, A and a pair of charged particles H^{\pm} . The lightest Higgs boson h has a mass $M_h \lesssim 140$ GeV and can be detected in the entire MSSM parameter space either in the Higgs–strahlung process, $e^+e^- \to hZ$, or by the complementary mechanism of associated production with the pseudoscalar particle, $e^+e^- \to hA$. Moreover, there is a substantial area in the MSSM parameter space where the heavy Higgs bosons can be also found; for a total energy of 500 GeV this is possible if the H, A and H^{\pm} masses are less than 230 GeV. Similar to the SM, various properties of these Higgs bosons can be investigated.

Higher energies are required to sweep the entire mass range of the SM Higgs particle, $M_H \lesssim 1$ TeV. The high energies will also be needed to produce and to study the heavy scalar particles in extensions of the SM, such as the MSSM, if their masses are larger than ~ 250 GeV. Masses of the heavy Higgs bosons in this range are suggested by grand unified supersymmetric theories. In e^+e^- collisions, these experiments can be performed in the second phase of the colliders with a c.m. energy up to 1.5 to 2 TeV. In this report, we analyze the potential of a 1.5 TeV e^+e^- linear collider, with an integrated luminosity of $\int \mathcal{L} \sim 200$ fb⁻¹ per annum to compensate for the drop of the cross sections at high

¹ Deutsches Elektronen-Synchrotron DESY, D-22603 Hamburg, FRG.

² Institut für Theoretische Physik, Universität Karlsruhe, D-76128 Karlsruhe, FRG.

energies. We will study the heavy Higgs particles in the Standard Model, in the minimal supersymmetric extension and in other more speculative scenarios.

In the Standard Model, the main production mechanisms of Higgs particles, $e^+e^- \rightarrow HZ$ and $e^+e^- \rightarrow \nu\bar{\nu}H/e^+e^-H$, will be discussed and the cross sections, including the interference between the Higgs-strahlung and the fusion processes, will be given [2]. The double Higgs production process, in which the trilinear Higgs coupling can be determined [therefore leading to the first non-trivial test of the Higgs potential], will be discussed in Ref.[3]. Finally, possible effects of New Physics beyond the SM on production cross sections and angular distributions of Higgs bosons, will be summarized in Ref.[4]. Consequences of a model in which the Higgs boson interacts strongly with scalar singlet fields in a hidden sector, are described in Ref.[5].

Subsequently, we will investigate the properties of the heavy Higgs particles in supersymmetric extensions of the SM. We will restrict ourselves first to the minimal extension which is highly constrained, parameterized by only two free parameters at the tree-level: a Higgs mass parameter [generally the mass the pseudoscalar Higgs boson M_A] and the ratio of the vacuum expectation values of the two doublet fields responsible for the symmetry breaking, $tg\beta$, which in grand unified supersymmetric models with Yukawa coupling unification is forced to be either small, $tg\beta \sim 1.5$, or large, $tg\beta \sim 50$.

The various decay modes of the heavy CP-even Higgs boson H, the pseudoscalar boson A and the charged Higgs particles H^{\pm} will be analyzed in Ref.[6], in particular the decays into supersymmetric particles, charginos, neutralinos, squarks and sleptons. The production of the heavy Higgs particles, primarily through the channels $e^+e^- \to HA$ and H^+H^- , will be also discussed in Ref.[6] and the complete one-loop electroweak radiative corrections of the cross sections will be summarized [7,8]. We will finally discuss the multiple production of the SM and the light MSSM Higgs bosons in Refs.[9,10]. Some of these processes will allow us to determine the fundamental Higgs trilinear couplings.

A brief discussion of the Higgs sector in the next-to-minimal supersymmetric extension of the Standard Model, Ref.[11], concludes this report.

References

- [1] Proceedings of the Workshop e^+e^- Collisions at 500 GeV: The Physics Potential, DESY Reports 92–123 A+B, and 93–123 C, P.M. Zerwas ed.
- [2] W. Kilian, M. Krämer and P.M. Zerwas, Anomalous Couplings in the Higgs-Strahlung Process.
- [3] E. Chopin, Associated Pair Production of the SM Higgs and the Probing of the Higgs Self-Coupling.

- [4] W. Kilian, M. Krämer and P.M. Zerwas, Higgs-Strahlung and Vector Boson Fusion in e^+e^- Collisions.
- [5] E. T. Binoth and J.J. van der Bij, The Hidden Higgs Model at the NLC.
- [6] A. Djouadi, J. Kalinowski, P. Ohmann and P. M. Zerwas, Heavy SUSY Higgs Bosons at e^+e^- Linear Colliders.
- [7] V. Driesen, W. Hollik and J. Rosiek, Production of Heavy Neutral MSSM Higgs Bosons: a Complete 1-loop Calculation.
- [8] A. Arhrib and G. Moultaka, Radiative Corrections to $e^+e^- \to H^+H^-$.
- [9] A. Djouadi, H.E. Haber and P.M. Zerwas, Multiple Production of MSSM Neutral Higgs Bosons at High-Energy e⁺e⁻ Colliders.
- [10] A. Djouadi, V. Driesen and C. Jünger, Loop Induced Higgs Boson Pair Production.
- [11] B.R. Kim, G. Kreyerhoff and S.K. Oh, Search for Higgs Bosons of the NMSSM at Linear Colliders.

Higgs-strahlung and Vector Boson Fusion in e^+e^- Collisions

W. KILIAN, M. KRÄMER, AND P.M. ZERWAS Deutsches Elektronen-Synchrotron DESY, D-22603 Hamburg/FRG

Abstract

Higgs-strahlung $e^+e^- \to ZH$ and WW (ZZ) fusion $e^+e^- \to \bar{\nu}_e\nu_eH$ (e^+e^-H) are the most important mechanisms for the production of Higgs bosons at future e^+e^- linear colliders. We have calculated the cross sections and energy/angular distributions of the Higgs boson for these production mechanisms. When the Z boson decays into (electron-)neutrinos or e^+e^- , the two production amplitudes interfere. In the cross-over region between the two mechanisms the interference term is positive (negative) for $\bar{\nu}_e\nu_e$ (e^+e^-) decays, respectively, thus enhancing (reducing) the production rate.

The analysis of the mechanism which breaks the electroweak gauge symmetry $SU(2)_{\rm L} \times U(1)_{\rm Y}$ down to $U(1)_{\rm EM}$, is one of the key problems in particle physics. If the gauge fields involved remain weakly interacting up to high energies – a prerequisite for the (perturbative) renormalization of $\sin^2 \theta_W$ from the symmetry value 3/8 of grand-unified theories down to a value near 0.2 at low energies – fundamental scalar Higgs bosons [1] must exist which damp the rise of the scattering amplitudes of massive gauge particles at high energies. In the Standard Model (SM) an isoscalar doublet field is introduced to accommodate the electroweak data, leading to the prediction of a single Higgs boson. Supersymmetric extensions of the Standard Model expand the scalar sector to a spectrum of Higgs particles [2]. The Higgs particles have been searched for, unsuccessfully so far, at LEP1, setting a lower limit on the SM Higgs mass of $m_H > 65.2$ GeV [3]. The search for these particles and, if found, the exploration of their profile, will continue at LEP2 [2], the LHC [5], and future e^+e^- linear colliders [3].

Figure 1: Higgs-strahlung and vector boson fusion of (CP-even) Higgs bosons in e^+e^- collisions.

In this note (see also [7]) we will focus on the production of scalar Higgs bosons in e^+e^- collisions. The main production mechanisms for these particles are Higgs-strahlung [1] and WW (ZZ) fusion [9–11] [supplemented in supersymmetric theories by associated scalar/pseudoscalar Higgs pair production]. In particular, we will present a comprehensive

analysis of the interplay between the production mechanisms¹ (Fig.1)

Higgs-strahlung:
$$e^+e^- \to ZH \to \bar{\nu}\nu H$$
 (e^+e^-H)
 WW fusion : $e^+e^- \to \bar{\nu}_e\nu_e H$ (1)
 ZZ fusion : $e^+e^- \to e^+e^-H$

For $\bar{\nu}_e\nu_e$ and e^+e^- decays of the Z bosons, the two production amplitudes interfere. It turns out that the interference term is positive for $\bar{\nu}_e\nu_e$ and negative for e^+e^- decays, respectively, in the cross-over region between the two mechanisms. The interference effect had been noticed earlier [9,13]; however, we improve on these calculations by deriving analytic results for the energy and polar angular distribution of the Higgs particle (E_H, θ) in the final states of $e^+e^- \to H + \text{neutrinos}$ and $e^+e^- \to He^+e^-$. This representation can comfortably serve as input for Monte Carlo generators like PYTHIA/JETSET [14] and HZHA [15] which include the leading QED bremsstrahlung corrections and the important background processes.

Total cross sections. The cross section for the Higgs-strahlung process can be written in the following compact form:

$$\sigma(e^+e^- \to ZH) = \frac{G_F^2 m_Z^4}{96\pi s} \left(v_e^2 + a_e^2\right) \lambda^{\frac{1}{2}} \frac{\lambda + 12m_Z^2/s}{(1 - m_Z^2/s)^2}$$
(2)

where \sqrt{s} is the center-of-mass energy, and $a_e = -1$, $v_e = -1 + 4\sin^2\theta_W$ are the Z charges of the electron; $\lambda = (1 - (m_H + m_Z)^2/s) (1 - (m_H - m_Z)^2/s)$ is the usual two-particle phase space function. So long as the non-zero width of the Z boson² is not taken into account, the cross section rises steeply at threshold $\sim (s - (m_H + m_Z)^2)^{1/2}$. After reaching a maximum [about 25 GeV above threshold in the LEP2 energy range], the cross section falls off at high energies, according to the scaling law $\sim g_W^4/s$ asymptotically. Thus, Higgs-strahlung is the dominant production process for moderate values of the energy. The cross section (2) for Higgs-strahlung is reduced by a factor $3 \times \mathrm{BR}_{\nu} = 20\%$ if the final state of Z decays is restricted to neutrino pairs.

The total cross section for the WW (ZZ) fusion of Higgs particles can be cast into a similarly compact form³ [17]:

$$\sigma = \frac{G_F^3 m_V^4}{64\sqrt{2}\pi^3} \int_{x_H}^1 dx \int_x^1 \frac{dy}{[1 + (y - x)/x_V]^2} \left[(v^2 + a^2)^2 f(x, y) + 4v^2 a^2 g(x, y) \right]$$
(3)

¹ We will concentrate first on the Standard Model (SM); the extension to the Minimal Supersymmetric Standard Model (MSSM) is trivial as will be demonstrated in the last section of this note.

²The results presented in this note are insensitive to non-zero width effects of the Higgs boson [16]. For SM Higgs masses below 100 GeV, Γ_H is at least three orders of magnitude smaller than Γ_Z ; for larger Higgs masses, m_H can be reinterpreted as the effective invariant mass of the Higgs decay products.

³The variable x is the invariant mass squared of ν_e plus H, (x-y) the 4-momentum transfer squared from e^+ to $\bar{\nu}_e$ (all momenta in units of the total energy).

where V denotes either W or Z, the charges are $v = a = \sqrt{2}$ ($v = v_e$ and $a = a_e$) for WW (ZZ) fusion, respectively, and

$$f(x,y) = \left(\frac{2x}{y^3} - \frac{1+2x}{y^2} + \frac{2+x}{2y} - \frac{1}{2}\right) \left[\frac{z}{1+z} - \log(1+z)\right] + \frac{x}{y^3} \frac{z^2(1-y)}{1+z}$$

$$g(x,y) = \left(-\frac{x}{y^2} + \frac{2+x}{2y} - \frac{1}{2}\right) \left[\frac{z}{1+z} - \log(1+z)\right]$$

with $x_H = m_H^2/s$, $x_V = m_V^2/s$ and $z = y(x - x_H)/(xx_V)$. For moderate Higgs masses and energies, the cross section, being $\mathcal{O}(g_W^6)$, is suppressed with respect to Higgs-strahlung by the additional electroweak coupling. The smaller value of the Z-electron coupling suppresses the ZZ fusion process by an additional order of magnitude compared to WW fusion. At high energies, the WW fusion process becomes leading, nevertheless, since the size of the cross section is determined by the W mass, in contrast to the scale-invariant Higgs-strahlung process,

$$\sigma(e^+e^- \to \bar{\nu}_e\nu_e H) \approx \frac{G_F^3 m_W^4}{4\sqrt{2}\pi^3} \left[\left(1 + \frac{m_H^2}{s} \right) \log \frac{s}{m_H^2} - 2\left(1 - \frac{m_H^2}{s} \right) \right]$$

$$\to \frac{G_F^3 m_W^4}{4\sqrt{2}\pi^3} \log \frac{s}{m_H^2}$$

$$(4)$$

The cross section rises logarithmically at high energies, as to be anticipated for this t-channel exchange process.

Differential cross section and interference for WW fusion. The compact form (3) for the fusion cross section cannot be maintained once the interference term between vector boson fusion and Higgs-strahlung is included. Moreover, since in the case of WW fusion the integration variables x and y do not correspond to observable quantities, the formula is useful only for calculating the total cross section without experimental cuts. Nevertheless, similarly compact expressions can be derived in this general case by choosing the energy E_H and the polar angle θ of the Higgs particle as the basic variables in the e^+e^- c.m. frame. The overall cross section that will be observed experimentally for the process

$$e^+e^- \rightarrow H + \bar{\nu}\nu$$

receives contributions $3 \times \mathcal{G}_S$ from Higgs-strahlung with Z decays into three types of neutrinos, \mathcal{G}_W from WW fusion, and \mathcal{G}_I from the interference term between fusion and Higgs-strahlung for $\bar{\nu}_e \nu_e$ final states. We find⁴ for energies \sqrt{s} above the Z resonance:

$$\frac{d\sigma(H\bar{\nu}\nu)}{dE_H d\cos\theta} = \frac{G_F^3 m_Z^8 p}{\sqrt{2}\pi^3 s} \left(3\mathcal{G}_S + \mathcal{G}_I + \mathcal{G}_W\right)$$
 (5)

⁴The analytic result for \mathcal{G}_W had first been obtained in Ref.[11].

Figure 2: Total cross sections for the processes $e^+e^- \to H\bar{\nu}\nu$ and $e^+e^- \to He^+e^-$ as a function of the Higgs mass. The cross sections are broken down to the three components Higgs-strahlung, vector boson fusion, and the interference term. "thr" denotes the maximum Higgs mass for on-shell ZH production, "tot" is the total cross section. In $e^+e^- \to H\bar{\nu}\nu$ (above) the interference term is negative for small Higgs masses, for large Higgs masses positive. In $e^+e^- \to He^+e^-$ (below), the interference term is of opposite sign.

with

$$\mathcal{G}_{S} = \frac{v_{e}^{2} + a_{e}^{2}}{96} \frac{ss_{\nu} + s_{1}s_{2}}{(s - m_{Z}^{2})^{2} \left[(s_{\nu} - m_{Z}^{2})^{2} + m_{Z}^{2} \Gamma_{Z}^{2} \right]}$$

$$\mathcal{G}_{I} = \frac{(v_{e} + a_{e}) \cos^{4} \theta_{W}}{8} \frac{s_{\nu} - m_{Z}^{2}}{(s - m_{Z}^{2}) \left[(s_{\nu} - m_{Z}^{2})^{2} + m_{Z}^{2} \Gamma_{Z}^{2} \right]}$$

$$\times \left[2 - (h_{1} + 1) \log \frac{h_{1} + 1}{h_{1} - 1} - (h_{2} + 1) \log \frac{h_{2} + 1}{h_{2} - 1} + (h_{1} + 1)(h_{2} + 1) \frac{\mathcal{L}}{\sqrt{r}} \right]$$

$$\mathcal{G}_{W} = \frac{\cos^{8} \theta_{W}}{s_{1}s_{2}r} \left\{ (h_{1} + 1)(h_{2} + 1) \left[\frac{2}{h_{1}^{2} - 1} + \frac{2}{h_{2}^{2} - 1} - \frac{6s_{\chi}^{2}}{r} + \left(\frac{3t_{1}t_{2}}{r} - c_{\chi} \right) \frac{\mathcal{L}}{\sqrt{r}} \right]$$

$$- \left[\frac{2t_{1}}{h_{2} - 1} + \frac{2t_{2}}{h_{1} - 1} + \left(t_{1} + t_{2} + s_{\chi}^{2} \right) \frac{\mathcal{L}}{\sqrt{r}} \right] \right\}$$
(8)

The cross section is written explicitly in terms of the Higgs momentum $p = \sqrt{E_H^2 - m_H^2}$, and the energy $\epsilon_{\nu} = \sqrt{s} - E_H$ and invariant mass squared $s_{\nu} = \epsilon_{\nu}^2 - p^2$ of the neutrino pair. In addition, the following abbreviations have been adopted from Ref.[11],

$$s_{1,2} = \sqrt{s}(\epsilon_{\nu} \pm p \cos \theta)$$

$$t_{1,2} = h_{1,2} + c_{\chi}h_{2,1}$$

$$t_{1,2} = h_{1,2} + c_{\chi}h_{2,1}$$

$$r = h_1^2 + h_2^2 + 2c_{\chi}h_1h_2 - s_{\chi}^2$$

$$c_{\chi} = 1 - 2ss_{\nu}/(s_1s_2)$$

$$s_{\chi}^2 = 1 - c_{\chi}^2$$

$$\mathcal{L} = \log \frac{h_1h_2 + c_{\chi} + \sqrt{r}}{h_1h_2 + c_{\chi} - \sqrt{r}}$$

To derive the total cross section $\sigma(e^+e^- \to H\bar{\nu}\nu)$, the differential cross section must be integrated over the region

$$-1 < \cos \theta < 1 \quad \text{and} \quad m_H < E_H < \frac{\sqrt{s}}{2} \left(1 + \frac{m_H^2}{s} \right) \tag{9}$$

Differential cross section and interference for ZZ fusion. Similarly, the overall cross section for the process

$$e^+e^- \to H + e^+e^-$$

receives contributions \mathcal{G}_S from Higgs-strahlung with Z decays into electron-positron pairs, \mathcal{G}_Z from ZZ fusion, and \mathcal{G}_I from the interference term between fusion and Higgs-strahlung:

$$\frac{d\sigma(He^{+}e^{-})}{dE_{H} d\cos\theta} = \frac{G_{F}^{3}m_{Z}^{8}p}{\sqrt{2}\pi^{3}s} \left(\mathcal{G}_{S} + \mathcal{G}_{I} + \mathcal{G}_{Z1} + \mathcal{G}_{Z2}\right)$$
(10)

with

$$\mathcal{G}_{S} = \frac{\left(v_{e}^{2} + a_{e}^{2}\right)^{2}}{192} \frac{ss_{e} + s_{1}s_{2}}{\left(s - m_{Z}^{2}\right)^{2} \left[\left(s_{e} - m_{Z}^{2}\right)^{2} + m_{Z}^{2}\Gamma_{Z}^{2}\right]}$$

$$\mathcal{G}_{I} = \frac{\left(v_{e}^{2} + a_{e}^{2}\right)^{2} + 4v_{e}^{2}a_{e}^{2}}{64} \frac{s_{e} - m_{Z}^{2}}{\left(s - m_{Z}^{2}\right) \left[\left(s_{e} - m_{Z}^{2}\right)^{2} + m_{Z}^{2}\Gamma_{Z}^{2}\right]}$$
(11)

$$\times \left[2 - (h_1 + 1) \log \frac{h_1 + 1}{h_1 - 1} - (h_2 + 1) \log \frac{h_2 + 1}{h_2 - 1} + (h_1 + 1)(h_2 + 1) \frac{\mathcal{L}}{\sqrt{r}} \right] \tag{12}$$

$$\mathcal{G}_{Z1} = \frac{(v_e^2 + a_e^2)^2 + 4v_e^2 a_e^2}{32 \, s_1 s_2 r} \left\{ (h_1 + 1)(h_2 + 1) \left[\frac{2}{h_1^2 - 1} + \frac{2}{h_2^2 - 1} - \frac{6s_\chi^2}{r} + \left(\frac{3t_1 t_2}{r} - c_\chi \right) \frac{\mathcal{L}}{\sqrt{r}} \right] - \left[\frac{2t_1}{h_2 - 1} + \frac{2t_2}{h_1 - 1} + \left(t_1 + t_2 + s_\chi^2 \right) \frac{\mathcal{L}}{\sqrt{r}} \right] \right\}$$

$$\mathcal{G}_{Z2} = \frac{(v_e^2 - a_e^2)^2}{16 \, s_1 s_2 r} (1 - c_\chi) \left[\frac{2}{h_1^2 - 1} + \frac{2}{h_2^2 - 1} - \frac{6s_\chi^2}{r} + \left(\frac{3t_1 t_2}{r} - c_\chi \right) \frac{\mathcal{L}}{\sqrt{r}} \right] \tag{14}$$

where the same abbreviations as in the formulae following Eq.(5), with the appropriate replacements $\nu \to e$ and $W \to Z$, have been used.

To interpret the results, we display the three components of the total cross sections $\sigma(e^+e^- \to H\bar{\nu}\nu)$ and $\sigma(e^+e^- \to He^+e^-)$ in Fig.2 for the linear collider energy $\sqrt{s} = 500$ GeV in the cross-over region.⁵

While the energy distribution of the Higgs particle peaks at $E_H \sim (s+m_H^2-m_Z^2)/2\sqrt{s}$ for Higgs-strahlung, it is nearly flat for WW fusion (Fig.3, left). Only with rising total energy the lower part of the Higgs spectrum becomes more pronounced. The angular distribution for Higgs-strahlung is almost isotropic at threshold while the standard $\sin^2\theta$ law is approached, in accordance with the equivalence principle, at asymptotic energies (Fig.3, right). The angular distribution peaks, by contrast, in the WW fusion process at $\theta \to 0$ and π for high energies as expected for t-channel exchange processes.

Polarized beams. At linear colliders the incoming electron and positron beams can be polarized longitudinally. Higgs-strahlung and WW fusion both require opposite helicities of the electrons and positrons. If $\sigma_{U,LR,RL}$ denote the cross sections in $e^+e^- \to H\bar{\nu}\nu$ for unpolarized electrons/positrons, left-handed electrons/right-handed positrons, and right-handed electrons/left-handed positrons, respectively, we can easily derive, in the notation of Eq.(5):

$$\sigma_U \propto 3 \mathcal{G}_S + \mathcal{G}_I + \mathcal{G}_W$$
 (15)

$$\sigma_{LR} \propto 6 \mathcal{G}_S + 4 \mathcal{G}_I + 4 \mathcal{G}_W \tag{16}$$

$$\sigma_{RL} \propto 6 \mathcal{G}_S$$
 (17)

The cross section for WW fusion of Higgs particles increases by a factor four, compared with unpolarized beams, if left-handed electrons and right-handed positrons are used. By using right-handed electrons, the WW fusion mechanism is switched off. [The interference term cannot be separated from the WW fusion cross section.]

 $^{^5}$ Note that Higgs-strahlung dominates WW fusion at 500 GeV for moderate Higgs masses only if the total ZH cross section is considered.

For the process $e^+e^- \to He^+e^-$, the pattern is slightly more complicated:

$$\sigma_U \propto \mathcal{G}_S + \mathcal{G}_I + \mathcal{G}_{Z1} + \mathcal{G}_{Z2}$$
 (18)

$$\sigma_{LR} \propto 2 \frac{(v_e + a_e)^2}{(v_e^2 + a_e^2)} \mathcal{G}_S + 2 \frac{(v_e + a_e)^4}{(v_e^2 + a_e^2)^2 + 4v_e^2 a_e^2} (\mathcal{G}_I + \mathcal{G}_{Z1})$$
 (19)

$$\sigma_{RL} \propto 2 \frac{(v_e - a_e)^2}{(v_e^2 + a_e^2)} \mathcal{G}_S + 2 \frac{(v_e - a_e)^4}{(v_e^2 + a_e^2)^2 + 4v_e^2 a_e^2} (\mathcal{G}_I + \mathcal{G}_{Z1})$$
 (20)

$$\sigma_{LL} = \sigma_{RR} \quad \propto \quad 2 \, \mathcal{G}_{Z2}. \tag{21}$$

However, since $v_e \ll a_e$, the difference between σ_{RL} and σ_{LR} is suppressed.

Supersymmetric CP-even Higgs bosons. It is trivial to transfer all these results from the Standard Model to the Minimal Supersymmetric Standard Model (MSSM). Since the couplings to Z/W gauge bosons in the MSSM are shared [20] by the CP-even light and heavy scalar Higgs bosons, h and H, respectively, only the overall normalization of the cross sections is modified with respect to the Standard Model:

$$\sigma(h)_{\text{MSSM}} = \sin^2(\beta - \alpha) \times \sigma(H)_{\text{SM}}$$
 (22)

$$\sigma(H)_{\text{MSSM}} = \cos^2(\beta - \alpha) \times \sigma(H)_{\text{SM}}$$
 (23)

Higgs-strahlung, vector boson fusion, and the interference term are affected in the same way. [The angle α is the mixing angle in the CP-even Higgs sector while the mixing angle β is determined by the ratio of the vacuum expectation values of the two neutral Higgs fields in the MSSM. A recent discussion of the size of the coefficients $\sin^2/\cos^2(\beta - \alpha)$ may be found in Ref.[21].]

References

- P.W. Higgs, Phys. Rev. Lett. 12 (1964) 132, and Phys. Rev. D145 (1966) 1156; F. Englert and R. Brout, Phys. Rev. Lett. 13 (1964) 321; G.S. Guralnik, C.R. Hagen, and T.W. Kibble, Phys. Rev. Lett. 13 (1964) 585.
- [2] P. Fayet, Nucl. Phys. B90 (1975) 104.
- [3] J.-F. Grivaz, Proceedings of the International EPS Conference on High–Energy Physics, Bruxelles 1995.
- [4] M. Carena et al., *Higgs Physics*, in: Proceedings of the Workshop *Physics with LEP2*, eds. G. Altarelli and F. Zwirner, CERN 1995.
- [5] G. Altarelli, Proceedings of the ECFA LHC-Workshop, eds. G. Jarlskog and D. Rein, Aachen 1990, CERN 90/10.

- [6] Proceedings of the Workshop e⁺e⁻ Collisions at 500 GeV: The Physics Potential, Munich-Annecy-Hamburg, ed. P.M. Zerwas, Reports DESY 92-123A,B; 93-123C.
- [7] W. Kilian, M. Krämer, and P.M. Zerwas, Phys. Lett. B373 (1996) 135.
- [8] J. Ellis, M.K. Gaillard, and D.V. Nanopoulos, Nucl. Phys. B106 (191976) 292; B.L. Ioffe and V.A. Khoze, Sov. J. Part. Nucl. 9 (1978) 50; B.W. Lee, C. Quigg, and H.B. Thacker, Phys. Rev. D16 (1977) 1519; J.D. Bjorken, Proc. Summer Institute on Particle Physics, SLAC Report 198 (1976).
- [9] D.R.T. Jones and S.T. Petcov, Phys. Lett. B84 (1979) 440.
- [10] R.N. Cahn and S. Dawson, Phys. Lett. B136 (1984) 96; G.L. Kane, W.W. Repko, and W.B. Rolnick, Phys. Lett. B148 (1984) 367; R.N. Cahn, Nucl. Phys. B255 (1985) 341; B.A. Kniehl, Z. Phys. C55 (1992) 605.
- [11] G. Altarelli, B. Mele, and F. Pitolli, Nucl. Phys. B287 (1987) 205.
- [12] S. Katsanevas et al., in preparation.
- [13] E. Boos, M. Sachwitz, H. Schreiber, and S. Shichanin, Int. J. Mod. Phys. A10 (1995) 2067.
- [14] T. Sjöstrand, The PYTHIA 5.7 and JETSET 7.4 Manual, LU-TP. 95/20 and CERN-TH 112/93, and Comput. Phys. Commun. 82 (1994) 74.
- [15] P. Janot, The HZHA Generator Program, in preparation.
- [16] A. Djouadi, M. Spira, and P.M. Zerwas, Z. Phys. C70 (1996) 427.
- [17] A. Djouadi, D. Haidt, B.A. Kniehl, B. Mele, and P.M. Zerwas, in Ref.[3].
- [18] V.N. Baĭer, V.S. Fadin, and V.A. Khoze, Sov. Phys. JETP 23 (1966) 104.
- [19] E. Boos et al., Report SNUTP-94-116.
- [20] J.F. Gunion and H.E. Haber, Nucl. Phys. B272 (1986) 1; B278 (1986) 449; B307 (1988) 445; Erratum *ibid.* B402 (1993) 567; A. Djouadi, J. Kalinowski, and P.M. Zerwas, Z. Phys. C57 (1993) 569.
- [21] A. Djouadi, J. Kalinowski, and P.M. Zerwas, Z. Phys. C70 (1996) 435.

Figure 3: Energy distribution (left) and angular distribution (right) of the Higgs bosons for the three components of the cross section [Hs = Higgs-strahlung; WW = fusion; intf = interference term]. The individual curves are normalized to the total cross section. The Hs peak extends up to maximal values of $0.22 \, \mathrm{GeV}^{-1}$. The total cross section is $69.4 \, \mathrm{fb}$.

Associated Pair Production of the SM Higgs and the Probing of the Higgs Self-Coupling

E. CHOPIN

Laboratoire de Physique Théorique ENSLAPP ¹
B.P.110, 74941 Annecy-Le-Vieux Cedex, France
E-mail: chopin@lapphp0.in2p3.fr

1 Associated Higgs Pair Production

The interest in double Higgs production is the probing of the triple Higgs self coupling. It has been considered in e^+e^- sometime ago[1]. The most efficient means for double Higgs production is $e^+e^- \to \nu_e \bar{\nu}_e HH$ (see fig. 1). Double Higgs bremstrahlung ($e^+e^- \to ZHH$) is only competing at relatively low energies where the event sample is too low to be useful. The equivalent loop-induced double Higgs production in e^+e^- has been found to be much too small[4] and is not sensitive to the H^3 coupling. However, the $\gamma\gamma$ mode can form a $J_Z=0$ state and therefore $\gamma\gamma\to HH$ is a candidate for testing the H^3 coupling[3]. It has been pointed out recently that another interesting process is $\gamma\gamma\to W^+W^-HH$ [2] that is expected to compete with double Higgs production in e^+e^- . The reason is that in the TeV range, W fusion processes are very much enhanced. The sub-process involved is $W^+W^-\to HH$, where the dominant helicity amplitude is:

$$\tilde{\mathcal{M}}_{LL} = \frac{g^2}{2} \left\{ \frac{1}{\beta_H \beta_W^3} \left(\frac{1}{x - x_0} - \frac{1}{x + x_0} \right) \left(r \frac{M_H^2}{s} + \beta_H^2 + \beta_W^4 \right) + \frac{1}{\beta_W^2} \left(2 - \beta_W^2 - r \right) + \frac{3h_3 r}{4} \left(\frac{1 + \beta_W^2}{1 - M_H^2 / s} \right) \right\} \rightarrow \frac{g^2}{4} r (3h_3 - 2) + \dots \tag{1}$$

Where h_3 is the anomaly in the triple Higgs coupling g, i.e. $g = h_3 g_{sm}$ where g_{sm} is the minimal standard model coupling of H^3 . We also denote $\beta_{W,H} = \sqrt{1 - 4M_{W,H}^2/s}$, $r = M_H^2/M_W^2$, $x_0 = (1 + \beta_H^2)/2\beta_W\beta_H$, $x = \cos\theta$.

Figure 2 shows that at 2TeV, the cross sections drops precipitously with increasing Higgs mass. One can also notice that in $\gamma\gamma \to W^+W^-HH$ the external outgoing W (mainly transverse) are produced at small angle and take a large amount of energy. For the fusion diagrams of this process, the internal W triggers $W^+W^- \to HH$, which implies that these diagrams dominate for a heavy Higgs. When convoluting with the much advertised photon spectra of[5] and for $M_H=100GeV$ the cross section of $\gamma\gamma \to W^+W^-HH$ drops by about at least a factor of 2 compared with the result without convolution. For W-fusion-like processes, the internal W's are almost on shell and one may wonder if some structure functions could reproduce the exact results.

¹ URA 14-36 du CNRS, associée à l'E.N.S de Lvon et à l'Université de Savoie.

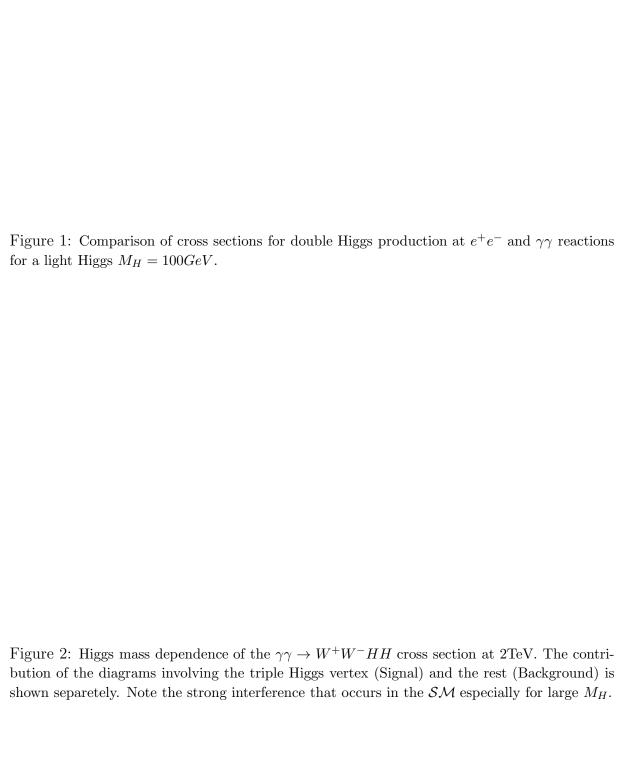


Figure 3: Comparing the result of the W_L effective approximation (σ^{EWA}) to the exact result σ^{exact} for $e^+e^- \to \nu_e\bar{\nu}_eHH$ (left) and $\gamma\gamma \to W^+W^-HH$ (right) for a light Higgs and a heavy Higgs. Also shown is the asymptotic analytical cross section σ^{EWA}_{∞} . σ^{TT} is the cross section with both outgoing W's transverse.

2 The structure function approach

There have been numerous derivations of the distribution (or structure function) of the W inside the light fermions (quarks and electrons) [6]. For the effective W approximation, the most interesting aspect concerns the W_L content, which has been used to investigate manifestations of models of symmetry breaking and Higgs production. The W_L distribution inside the photon has only very recently been studied [7]. For the case of the heavy Higgs the approximation is excellent, already at 2TeV. However, for a light Higgs, the approximation is not good and reproduce only the energy behaviour. If one makes the further approximation that the hard process cross section is independent of the energy, this additional "asymptotic" approximation only reproduces the energy behaviour as well as the order of magnitude (even for a heavy Higgs, see figs. 3).

Figure 4: The distribution in the reconstructed angle θ^* for the signal, background and the interference in the case of $\gamma\gamma \to W^+W^-HH$ without convolution with photon spectra.

3 Identifying and measuring the Higgs triple vertex

There is a specific signature of the H^3 coupling in all processes that we have studied. Once we note that the two Higgses that originate from this vertex can be regarded as produced by a scalar H^* then in the centre of mass system of the pair, the angular distribution of the Higgses is flat. Therefore, we suggest to reconstruct the angle, θ^* , measured in the centre-of-mass of the pair, between the Higgs direction and the boost axis or the direction of the beam. For the "signal" the distribution is flat, while the "background" is peaked in the forward/backward direction (see fig. 4). We therefore consider the ratio R of events that verify $|\cos(\theta^*)| < \cos(\theta_0^*)^3$, over the number of events outside this region. Assuming a total integrated luminosity of $300 fb^{-1}$, and a 50% efficiency for the reconstruction of the double Higgs events one obtain $\sim 68 e^+e^- \rightarrow \nu_e \bar{\nu}_e HH$ events for $M_H = 100 GeV$. Here the criterion for detection of an anomaly in h_3 is a 50% deviation in the expected number of events, provided one has at least 30 events. We conclude that with the total

²We call "signal" the part of the amplitude that include the H^3 vertex. The rest is called "background".

 $^{^{3}\}cos\theta_{0}^{\star}=0.5$ is taken in the following.

Figure 5: Dependence of the ratio R on h_3 .

cross section one would only be able to claim New Physics if $\delta h_3 < -0.75$ or $\delta h_3 > 2$. For $M_H = 400 GeV$, \mathcal{SM} values will not lead to a measurement, however if $|\delta h_3| > 1$ a signal will be recorded (with more than 30 events) and would be a clear indication for an anomalous h_3 coupling. For $M_H = 100 GeV$ where one has enough events for a \mathcal{SM} value, the ratio R is much more powerful in constraining the coupling. First the event sample within $|\cos\theta^{\star}| < 0.5$ is about 7 out of 60 outside this region. Assuming that the ratio can be measured at 20%, we find $-.10 < |\delta h_3| < .15$ (see fig. 5) which means a precision of about 10% on h_3 . For $\gamma\gamma \to W^+W^-HH$ and considering the effective $\gamma\gamma$ luminosity, for $M_H = 100 GeV$, one can hope to collect 15 events. In view of this number the criterion for detection of non-standard values is 100% deviation in the number of events. However, for a Higgs mass of 400GeV the effect of an anomalous H^3 coupling are dramatic and, by far, much more interesting than in e^+e^- . Requiring observation of at least 15 events for $M_H = 400 \text{GeV}$ (within the \mathcal{SM} one expects only 3) useful constraints on the coupling can be set: $-.7 < \delta h_3 < 0.5$. There is thus a complementarity between the e^+e^- and the $\gamma\gamma$ depending on the Higgs mass in probing the Higgs triple vertex. As for the ratio R, taking $M_H = 100 GeV$ it is unlikely that with the number of total WWHH events at $\gamma\gamma$ one would be able to make such a measurement, nonetheless even if this ratio were measured with the same precision as in e^+e^- one would not constrain the couplings further than what is achieved in the classic e^+e^- mode. For $M_H > 600 GeV$, $\gamma\gamma \to HH$ is the only reaction where useful limits can be set. Thus, there is at a 2TeV collider a very nice coverage of the h_3 sensitivity by all three reactions.

4 Conclusions

We have seen that a 2TeV e^+e^- collider with the realistic luminosities expected for this machine one may hope to achieve a measurement of the tri-linear couplings at the level of 10% (for a light Higgs). The results are also encouraging in the sense that the e^+e^- and the $\gamma\gamma$ modes can cover different ranges of the Higgs mass. We find that for a light Higgs (up to 250GeV) the best limits on the H^3 couplings come from $e^+e^- \to \nu_e\bar{\nu}_e HH$. However, for heavier Higgses up to mass of 500GeV, the best channel is the associated double Higgs production in $\gamma\gamma$. For still heavier masses, the one-loop induced $\gamma\gamma \to HH$ is by far better. The variable R clearly helps in discriminating the triple Higgs vertex. As a by-product we have verified the validity of the distribution function describing the longitudinal W content of the photon. We should also insist on the complementarity of the e^+e^- and the $\gamma\gamma$ modes of the linear collider for these studies.

References

- V. Barger, T. Han and R. J. N Phillips, Phys. Rev. **D38** (1988) 2766.
 V. Barger, T. Han, Mod. Phys. Lett. **A5** (1990) 667.
- [2] F. Boudjema, E. Chopin, hep-ph/9507396, submitted to Z. Phys. C.
- [3] G.V. Jikia and Yu.F. Pirogov, *Phys. Let.* B283 (1992) 135.
 G.V. Jikia, Nucl. Phys. B412 (1994) 57.
- [4] K.J.F. Gaemers, F. Hoogeveen, Z. Phys. C26 (1984) 249.
 A. Djouadi, V. Driesen, C. Jünger, hep-ph/9602341, KA-TP-02-96 (Feb. 96).
- [5] I.F. Ginzburg et al., Nucl. Instrum. Meth. 205 (1983) 47.
 I.F. Ginzburg et al., Nucl. Instrum. Meth. 219 (1984) 5.
 V.I. Telnov, Nucl. Instrum. Meth. A294 (1990) 72.
- [6] S. Dawson, Nucl. Phys. **B249** (1984) 42.
 W.B. Rolnick, Nucl. Phys. **B274** (1986) 171.
 Z. Kunszt and D.E. Soper, Nucl. Phys. **B296** (1988) 253.
- [7] M. Baillargeon, G. Bélanger and F. Boudjema, in Proceedings of Two-Photon Physics from DAΦNE to LEP200 and Beyond, Paris, 1994, edited by F. Kapusta and J. Parisi (world Scientific, Singapore, 1995), p.267.

Anomalous Couplings in the Higgs-strahlung Process

W. KILIAN, M. KRÄMER, AND P.M. ZERWAS
Deutsches Elektronen-Synchrotron DESY, D-22603 Hamburg/FRG

Abstract

The angular distributions in the Higgs-strahlung process $e^+e^- \to HZ \to H\bar{f}f$ are uniquely determined in the Standard Model. We study how these predictions are modified if non-standard couplings are present in the ZZH vertex, as well as lepton-boson contact terms. We restrict ourselves to the set of operators which are singlets under standard $SU_3 \times SU_2 \times U_1$ transformations, CP conserving, dimension 6, helicity conserving, and custodial SU_2 conserving.

The Higgs-strahlung process [1]

$$e^+e^- \to HZ \to H\bar{f}f$$
 (1)

together with the WW fusion process, are the most important mechanisms for the production of Higgs bosons in e^+e^- collisions [2,3]. Since the ZZH vertex is uniquely determined in the Standard Model (SM), the production cross section of the Higgs-strahlung process, the angular distribution of the HZ final state as well as the fermion distribution in the Z decays can be predicted if the mass of the Higgs boson is fixed [4]. These predictions may be modified when deviations from the pointlike coupling are present, which can occur in models with non-pointlike character of the Higgs boson itself or through interactions beyond the SM at high energy scales. Since the effective energy scale of the Higgs-strahlung process is set by the c.m. energy \sqrt{s} , while the fusion processes are essentially low-energy processes with an effective scale of the order M_W , new interactions manifest themselves more clearly in the total cross section and angular distributions for the Higgs-strahlung process (see also [5]).

Operator basis. Deviations from the pointlike coupling can occur in models with non-pointlike character of the Higgs boson itself or through interactions beyond the SM at high energy scales. We need not specify the underlying theory but instead we will adopt the usual assumption that these effects can globally be parameterized by introducing a set of dimension-6 operators

$$\mathcal{L} = \mathcal{L}_{SM} + \sum_{i} \frac{\alpha_i}{\Lambda^2} \mathcal{O}_i \tag{2}$$

The coefficients are in general expected to be of the order $1/\Lambda^2$, where Λ denotes the energy scale of the new interactions. However, if the underlying theory is weakly interacting, the α_i can be significantly smaller than unity, in particular for loop-induced operators. [It is assumed a priori that the ratio of the available c.m. energy to Λ is small enough for the expansion in powers of $1/\Lambda$ to be meaningful.]

If we restrict ourselves to operators [6] which are singlets under $SU_3 \times SU_2 \times U_1$ transformations of the SM gauge group, CP conserving, and conserving the custodial SU_2 symmetry, the following bosonic operators are relevant for the Higgs-strahlung process:

$$\mathcal{O}_{\partial\varphi} = \frac{1}{2} |\partial_{\mu}(\varphi^{\dagger}\varphi)|^2 \tag{3}$$

$$\mathcal{O}_{\varphi W} = \frac{1}{2} \varphi^{\dagger} \vec{W}_{\mu\nu}^2 \varphi \tag{4}$$

$$\mathcal{O}_{\varphi B} = \frac{1}{2} \varphi^{\dagger} B_{\mu\nu}^2 \varphi \tag{5}$$

where the gauge fields W^3 , B are given by the Z, γ fields. This set of operators is particularly interesting because it does not affect, at tree level, observables which do not involve the Higgs particle explicitly. [It is understood that the fields and parameters are (re-)normalized in the Lagrangian \mathcal{L} in such a way that the particle masses and the electromagnetic coupling retain their physical values.]

In addition, we consider the following helicity-conserving fermionic operators which induce contact terms contributing to $e^+e^- \to ZH$:

$$\mathcal{O}_{L1} = (\varphi^{\dagger} i D_{\mu} \varphi) (\bar{\ell}_L \gamma^{\mu} \ell_L) + \text{h.c.}$$
 (6)

$$\mathcal{O}_{L3} = (\varphi^{\dagger} \tau^a i D_{\mu} \varphi) (\bar{\ell}_L \tau^a \gamma^{\mu} \ell_L) + \text{h.c.}$$
 (7)

$$\mathcal{O}_R = (\varphi^{\dagger} i D_{\mu} \varphi) (\bar{e}_R \gamma^{\mu} e_R) + \text{h.c.}$$
 (8)

 $[\ell_L]$ and e_R denote the left-handed lepton doublet and the right-handed singlet, respectively. The vacuum expectation value of the Higgs field is given by $\langle \varphi \rangle = (0, v/\sqrt{2})$ with $v = 246 \,\text{GeV}$, and the covariant derivative acts on the Higgs doublet as $D_{\mu} = \partial_{\mu} - \frac{i}{2}g\tau^a W_{\mu}^a + \frac{i}{2}g'B_{\mu}$.] Helicity-violating fermionic operators do not interfere with the SM amplitude, so that their contribution to the cross section is suppressed by another power of Λ^2 . The helicity-conserving fermionic operators modify the SM Zee couplings and are therefore constrained by the measurements at LEP1; however, it is possible to improve on the existing limits by measuring the Higgs-strahlung process at a high-energy e^+e^- collider since the impact on this process increases with energy [7].

Figure 1: Anomalous $ZZH/\gamma ZH$ couplings and e^+e^-ZH contact terms in the Higgs-strahlung process.

The effective ZZH and the induced γZH interactions (Fig.1, left diagram) may be written

$$\mathcal{L}_{ZZH} = g_Z M_Z \left(\frac{1 + a_0}{2} Z_{\mu} Z^{\mu} H + \frac{a_1}{4} Z_{\mu\nu} Z^{\mu\nu} H \right)$$
 (9)

$$\mathcal{L}_{\gamma ZH} = g_Z M_Z \frac{b_1}{2} Z_{\mu\nu} A^{\mu\nu} H \tag{10}$$

where $g_Z = M_Z \sqrt{4\sqrt{2}G_F}$. Additional operators $Z_\mu Z^{\mu\nu} \partial_\nu H$ and $Z_\mu A^{\mu\nu} \partial_\nu H$ are redundant in this basis: They may be eliminated in favor of the other operators and the contact terms by applying the equations of motion. The remaining coefficients are given by

$$a_0 = -\frac{1}{2}\alpha_{\partial\varphi} v^2/\Lambda^2 \tag{11}$$

$$a_1 = 4g_Z^{-2} \left(c_W^2 \alpha_{\varphi W} + s_W^2 \alpha_{\varphi B} \right) / \Lambda^2 \tag{12}$$

$$b_1 = 4g_Z^{-2}c_W s_W \left(-\alpha_{\varphi W} + \alpha_{\varphi B}\right)/\Lambda^2 \tag{13}$$

where s_W and c_W are the sine and cosine of the weak mixing angle, respectively.

In the same way the $e\bar{e}HZ$ contact interactions (Fig.1, right diagram) can be defined for left/right-handed electrons and right/left-handed positrons

$$\mathcal{L}_{eeZH} = g_Z M_Z \left[c_L \bar{e}_L Z e_L H + c_R \bar{e}_R Z e_R H \right] \tag{14}$$

with

$$c_L = -2g_Z^{-1} (\alpha_{L1} + \alpha_{L3}) / \Lambda^2 \tag{15}$$

$$c_R = -2g_Z^{-1}\alpha_R/\Lambda^2 (16)$$

Some consequences of these operators for Higgs production in e^+e^- collisions have been investigated in the past. Most recently, the effect of novel ZZH vertex operators and $\ell\ell ZH$ contact terms on the total cross sections for Higgs production has been studied in Ref.[7]. The impact of vertex operators on angular distributions has been analyzed in Refs.[8] and [9]. We expand on these analyses by studying the angular distributions for the more general case where both novel vertex operators and contact interactions are present. The analysis of angular distributions in the Higgs-strahlung process (1) allows us to discriminate between various novel interactions. In fact, the entire set of parameters a_0, a_1, b_1 and c_L, c_R can be determined by measuring the polar and azimuthal angular distributions as a function of the beam energy if the electron/positron beams are unpolarized. As expected, the energy dependence of the polar angular distribution is sufficient to provide a complete set of measurements if longitudinally polarized electron beams are available¹.

Total cross section and polar angular distribution. Denoting the polar angle between the Z boson and the e^+e^- beam axis by θ , the differential cross section for the process $e^+e^-_{L,R} \to ZH$ may be written as

$$\frac{d\sigma^{L,R}}{d\cos\theta} = \frac{G_F^2 M_Z^4}{96\pi s} \left(v_e \pm a_e\right)^2 \lambda^{1/2} \frac{\frac{3}{4}\lambda \sin^2\theta \left(1 + \alpha^{L,R}\right) + 6\left(1 + \beta^{L,R}\right) M_Z^2/s}{(1 - M_Z^2/s)^2}$$
(17)

¹Since we can restrict ourselves to helicity-conserving couplings, as argued before, additional positron polarization need not be required.

Figure 2: Polar and azimuthal angles in the Higgs-strahlung process. [The polar angle θ_* is defined in the Z rest frame.]

and the integrated cross section

$$\sigma = \frac{G_F^2 M_Z^4}{96\pi s} \left(v_e \pm a_e \right)^2 \lambda^{1/2} \frac{\lambda \left(1 + \alpha^{L,R} \right) + 12 \left(1 + \beta^{L,R} \right) M_Z^2 / s}{(1 - M_Z^2 / s)^2}$$
(18)

The Z charges of the electron are defined as usual by $a_e = -1$ and $v_e = -1 + 4s_W^2$. s is the c.m. energy squared, and λ the two-particle phase space coefficient $\lambda = [1 - (m_H + m_Z)^2/s] \times [1 - (m_H - m_Z)^2/s]$. The coefficients $\alpha(s)^{L,R}$ and $\beta(s)^{L,R}$ can easily be determined for the interactions in Eqs.(9) and (14):

$$\alpha(s)^{L,R} = 2a_0 + (s - M_Z^2) \frac{8c_W s_W}{v_e \pm a_e} c_{L,R}$$
(19)

$$\beta(s)^{L,R} = \alpha(s)^{L,R} + 2\gamma\sqrt{s} M_Z \left[a_1 + \frac{4c_W s_W}{v_e \pm a_e} \left(1 - \frac{M_Z^2}{s} \right) b_1 \right]$$
 (20)

where the boost of the Z boson is given by $\gamma = (s + M_Z^2 - M_H^2)/2M_Z\sqrt{s}$.

The modification of the cross section by the new interaction terms has a simple structure. The coefficient a_0 just renormalizes the SM cross section. By contrast, the contact interactions grow with s. [The ratio s/Λ^2 is assumed to be small enough for the restriction to dimension-6 operators to be meaningful.] The operators $\mathcal{O}_{\varphi W}$, $\mathcal{O}_{\varphi B}$ affect the coefficient in the cross section which is independent of θ . They damp the fall-off of this term, changing the $1/s^2$ to a 1/s behavior; however, these contributions remain subleading since they are associated with transversely polarized Z bosons which are suppressed at high energies compared with the longitudinal components. To illustrate the size of the modifications $\alpha(s)^{L,R}$ and $\beta(s)^{L,R}$, we have depicted these functions in Fig.3(a) for the special choice $\alpha_i = 1$.

Azimuthal distributions. The azimuthal angle ϕ_* of the fermion f is defined as the angle between the $[e^-, Z]$ production plane and the [Z, f] decay plane (Fig.2). It corresponds to the azimuthal angle of f in the Z rest frame with respect to the $[e^-, Z]$ plane. On general grounds, the ϕ_* distribution must be a linear function of $\cos \phi_*$, $\cos 2\phi_*$, and $\sin \phi_*$, $\sin 2\phi_*$, measuring the helicity components of the decaying spin-1 Z state. The coefficients of the sine terms vanish for CP invariant theories. The $\cos \phi_*$ and $\cos 2\phi_*$ terms correspond to P-odd and P-even combinations of the fermion currents. The general azimuthal distributions are quite involved [4,8,9]. We therefore restrict ourselves to the simplified case in which all polar angles are integrated out, i.e., the polar angle θ of the Z boson in the laboratory frame and the polar angle θ_* of f in the Z rest frame. In this way we find for the azimuthal ϕ_* distribution:

$$\frac{d\sigma^{L,R}}{d\phi_*} \sim 1 \mp \frac{9\pi^2}{32} \frac{2v_f a_f}{v_f^2 + a_f^2} \frac{\gamma}{\gamma^2 + 2} \left(1 + f_1^{L,R}\right) \cos\phi_* + \frac{1}{2(\gamma^2 + 2)} \left(1 + f_2^{L,R}\right) \cos 2\phi_* \quad (21)$$

with

$$f_1(s)^{L,R} = M_Z \sqrt{s} \frac{(\gamma^2 - 1)(\gamma^2 - 2)}{\gamma(\gamma^2 + 2)} \left[a_1 + \frac{4s_W c_W}{v_e \pm a_e} \left(1 - \frac{M_Z^2}{s} \right) b_1 \right]$$
(22)

$$f_2(s)^{L,R} = 2M_Z \sqrt{s} \frac{\gamma(\gamma^2 - 1)}{\gamma^2 + 2} \left[a_1 + \frac{4s_W c_W}{v_e \pm a_e} \left(1 - \frac{M_Z^2}{s} \right) b_1 \right]$$
 (23)

The cross section flattens with increasing c.m. energy in the Standard Model, i.e. the coefficients of $\cos \phi_*$ and $\cos 2\phi_*$ decrease asymptotically proportional to $1/\sqrt{s}$ and 1/s, respectively. The anomalous contributions modify this behavior: The $\cos \phi_*$ term receives contributions which increase proportional to \sqrt{s} with respect to the total cross section, while the $\cos 2\phi_*$ term receive contributions from the transversal couplings that approaches a constant value asymptotically. The size of the new terms in $f_{1,2}^{L,R}$ is shown in Fig.3(b) as a function of the energy. [The special choice $\alpha_i = 1$ we have adopted for illustration, implies $f_{1,2}^L = f_{1,2}^R$.]

High-energy limit. It is instructive to study the high-energy behavior of the coefficients in the limit $M_Z^2 \ll s \ll \Lambda^2$. In this case we obtain the simplified relations:

$$\alpha(s)^{L,R} \simeq \mp s \cdot 8s_W c_W c_{L,R} + \mathcal{O}(v_e) \tag{24}$$

$$\beta(s)^{L,R} \simeq \alpha(s)^{L,R} + s(a_1 \mp 4s_W c_W b_1) + \mathcal{O}(v_e)$$
 (25)

and

$$f_1(s)^{L,R} \simeq \frac{s}{2} (a_1 \mp 4s_W c_W b_1) + \mathcal{O}(v_e)$$
 (26)

$$f_2(s)^{L,R} \simeq s(a_1 \mp 4s_W c_W b_1) + \mathcal{O}(v_e)$$
 (27)

Terms which are proportional to $v_e = -1 + 4s_W^2$ are suppressed by an order of magnitude. If longitudinally polarized electrons are available, the asymptotic value of the coefficients

 a_1, b_1, c_L and c_R can be determined by measuring the polar angular distribution without varying the beam energy. The analysis of the azimuthal ϕ_* distribution provides two additional independent measurements of the coefficients a_1 and b_1 . On the other hand, the set of measurements remains incomplete for fixed energy if only unpolarized electron/positron beams are used at high energies; in this case the coefficients cannot be disentangled completely without varying the beam energy within the preasymptotic region.

References

- J. Ellis, M.K. Gaillard, and D.V. Nanopoulos, Nucl. Phys. B106 (1976) 292; B.L. Ioffe and V.A. Khoze, Sov. J. Part. Nucl. 9 (1978) 50; B.W. Lee, C. Quigg, and H.B. Thacker, Phys. Rev. D16 (1977) 1519; J.D. Bjorken, Proc. Summer Institute on Particle Physics, SLAC Report 198 (1976).
- [2] M. Carena, P.M. Zerwas (conv.) et al., *Higgs Physics*, in: Proceedings of the Workshop *Physics with LEP2*, eds. G. Altarelli, T. Sjöstrand, and F. Zwirner, CERN Yellow Report 96-01.
- [3] Proceedings of the Workshop e^+e^- Collisions at 500 GeV: The Physics Potential, Munich-Annecy-Hamburg, ed. P.M. Zerwas, Reports DESY 92-123A,B; 93-123C.
- [4] V. Barger, K. Cheung, A. Djouadi, B. Kniehl, and P.M. Zerwas, Phys. Rev. D49 (1994) 79.
- [5] W. Kilian, M. Krämer, and P.M. Zerwas, Report DESY-95-217, to appear in Phys. Lett. B.
- [6] W. Buchmüller and D. Wyler, Nucl. Phys. B268 (1986) 621.
- [7] B. Grzadkowski and J. Wudka, Phys. Lett. B364 (1995) 49.
- [8] K. Hagiwara and M.L. Stong, Z. Phys. C62 (1994) 99.
- [9] G.J. Gounaris, F.M. Renard, and N.D. Vlachos, Nucl. Phys. B459 (1996) 51; G.J. Gounaris, J. Laissac, J.E. Paschalis, F.M. Renard, and N.D. Vlachos, Preprint PM/96-08.

Figure 3: Coefficients of the angular distributions as a function of the beam energy. Parameters are described in the text; in particular, $\alpha_i = 1$ has been chosen in the effective Lagrangian Eq.(2). [The L, R coefficients of the azimuthal distribution coincide for the special choice $\alpha_i = 1$.]

The hidden Higgs model at the NLC

T. BINOTH AND J. J. VAN DER BIJ Albert-Ludwigs-Universität Freiburg, Fakultät für Physik, Hermann-Herder-Strasse 3, 79104 Freiburg, Germany

Abstract

We investigate the influence of massless scalar singlets on Higgs signals at the NLC. An exclusion bound is presented which restricts large regions of the parameter space but on the other hand implies that for strong interactions between the Higgs boson and the singlet fields of the hidden sector, detection of such a non standard Higgs signal can become impossible.

1. Introduction

Understanding of the electroweak symmetry breaking mechanism is one of the main tasks in particle physics. The determination of its nature would be a break-through in our knowledge about matter. So it is important to think about alternatives to the Standard Model Higgs sector. Various such extensions are available. Maybe the best motivated one is the supersymmetrized Standard Model with its important phenomenological implication of a light Higgs boson and which allows a consistent frame for grand unified theories. Another well understood extension – though in its minimal version disfavoured by the precision experiments at LEP – are technicolor theories. Though these theories avoid fundamental scalars, a rich bosonic spectrum of techniquark condensates may exist. Thus in both theories, as long as they do not occur in their minimal form, light bosonic matter could be present modifying the standard Higgs signals we are looking for at present and future colliders. If such bosons appear as singlets under the Standard Model gauge group, they do not feel the color or electroweak forces, but they can couple to the Higgs particle. As a consequence radiative corrections to weak processes are not sensitive to the presence of singlets in the theory, because no Feynman graphs containing singlets appear at the one-loop level. Since effects at the two-loop level are below the experimental precision, the presence of a singlet sector is not ruled out by any of the LEP1 precision data. The only connection to such a hidden sector is a possible Higgs-singlet coupling, leading to a nonstandard invisible Higgs decay. The invisible decay of the Higgs boson with a narrow width leads to relatively sharp missing energy signals, well known from discussions on Majoron models [2]. However a strongly coupled hidden sector could lead to fast Higgs decay and thereby to wide resonances. This would disturb the signal to background ratio if necessary cuts are imposed.

To check the influence of a hidden sector we will study the coupling of a Higgs boson to an O(N) symmetric set of scalars, which is one of the simplest possibilities, introducing only a few extra parameters in the theory. The effect of the extra scalars is practically the presence of a possibly large invisible decay width of the Higgs particle. When the coupling is large enough the Higgs resonance can become wide even for a light Higgs boson. It was

shown earlier that there will be a range of parameters, where such a Higgs boson can be seen neither at LEP nor at the LHC [1,2].

In the next section we will introduce the model together with its theoretical constraints and in the last section we will discuss exclusion limits at the NLC.

2. The model

The scalar sector of the model consists of the usual Higgs sector coupled to a real N-component vector $\vec{\varphi}$ of scalar fields, denoted by phions in the following. The Lagrangian density is given by,

$$\mathcal{L} = -\partial_{\mu}\phi^{+}\partial^{\mu}\phi - \lambda(\phi^{+}\phi - v^{2}/2)^{2} - 1/2 \partial_{\mu}\vec{\varphi}\partial^{\mu}\vec{\varphi} - 1/2 m^{2} \vec{\varphi}^{2} - \kappa/(8N) (\vec{\varphi}^{2})^{2} - \omega/(2\sqrt{N}) \vec{\varphi}^{2} \phi^{+}\phi$$

where ϕ is the standard Higgs doublet. Couplings to fermions and vector bosons are the same as in the Standard Model. The ordinary Higgs field acquires the vacuum expectation value $v/\sqrt{2}$. For positive ω the $\vec{\varphi}$ -field acquires no vacuum expectation value. After spontaneous symmetry breaking one is left with the ordinary Higgs boson, coupled to the phions into which it decays. Also the phions receive an induced mass from the spontaneous symmetry breaking which is suppressed by a factor $1/\sqrt{N}$. If the factor N is taken to be large, the model can be analysed with 1/N-expansion techniques. By taking this limit the phion mass remains small, but as there are many phions, the decay width of the Higgs boson can become large. Therefore the main effect of the presence of the phions is to give a large invisible decay rate to the Higgs boson. The invisible decay width is given by

$$\Gamma_H = \frac{\omega^2 v^2}{32\pi M_H} = \frac{\omega^2 (\sin \theta_W \cos \theta_W M_Z)^2}{32\pi^2 \alpha_{em} M_H}$$

The Higgs width is compared with the width in the Standard Model for various choices of the coupling ω in Fig. 1. The model is different from Majoron models [2], since the width is not necessarily small. The model is similar to the technicolor–like model of Ref. [4].

Consistency of the model requires two conditions. One condition is the absence of a Landau pole below a certain scale Λ . The other follows from the stability of the vacuum up to a certain scale. An example of such limits is given in Fig. 2, where $\kappa=0$ was taken at the scale $2m_Z$, which allows for the widest parameter range. The regions of validity up to a given scale Λ are sandwiched between the lower–left and the upper–right contour lines in the figure. The first stem from instability of the vacuum, the second from the presence of a Landau pole at that scale.

To search for the Higgs boson there are basically two channels, one is the standard decay, which is reduced in branching ratio due to the decay into phions. The other is the invisible decay, which rapidly becomes dominant, eventually making the Higgs resonance wide (see Fig. 1). In order to give the bounds we neglect the coupling κ as this is a small effect. We also neglect the phion mass. For other values of the phion mass the bounds can be found by rescaling the decay widths with the appropriate phase space factor. Now we confront this two dimensional parameter space with the experimental potential of the NLC.

Figure 1: Higgs width in comparison with the Standard Model.

3. NLC bounds

At the NLC the upper limits on the couplings in the present model come essentially from the invisible decay, as the branching ratio into visible particles drops with increasing φ -Higgs coupling (ω) , whereas for small ω one has to consider visible Higgs decays, too. Since the main source for Higgs production, the WW-fusion process, can not be used to look for invisible Higgs decay, one is in principle left with the Higgsstrahlung und ZZfusion reaction. For energies up to 500 GeV the Higgsstrahlungs cross section is dominant and is of comparable size to the ZZ-fusion process even if one is folding in the branching ratio $B(Z \to e^+e^-, \mu^+\mu^-)$. The possibility to tag an on-shell Z boson via a leptonic system which is extremely useful for the discrimination of possible backgrounds makes Higgsstrahlung to be the preferred production mechanism. Thus we only have considered reactions containing an on shell Z boson with its decay into e^+e^- or $\mu^+\mu^-$. One should be aware that a few events from the huge WW background may survive [3], but that the $Z\nu\nu$ background is dominant after imposing the cuts defined below. Then the signal cross section is the well known Higgsstrahlungs cross section modified by the non standard Higgs width due to phion decay. With the invariant mass of the invisible phion system, s_I , it has the form:

$$\sigma_{(e^+e^- \to Z + \cancel{E})} = \int ds_I \, \sigma_{(e^+e^- \to ZH)}(s_I) \, \frac{\sqrt{s_I} \quad \Gamma(H \to \cancel{E})}{\pi((M_H^2 - s_I)^2 + s_I \, \Gamma(H \to \text{All})^2)}$$

We calculated the $Z\nu\nu$ background with the standard set of graphs for Z production (ZZproduction, WW-fusion and Z initial, final state radiation) by a Monte Carlo program

Figure 2: Theoretical limits on the parameters of the model in the ω vs. M_H plane. The contour lines correspond to the cutoff scales $\Lambda = 10^{19}$, 10^6 , 10^4 and 10^3 GeV.

(see Ref. [5]). To reduce the background we used the fact that the angular distribution of the Z-boson for the signal peaks for small values of $|\cos\theta_Z|$ in contrast to the background. Thus we imposed the cut $|\cos\theta_Z| < 0.7$. Because we assume the reconstruction of the on-shell Z-boson we use the kinematical relation $E_Z = (s + M_Z^2 - s_I)/(2\sqrt{s})$ between the Z energy and the invariant mass of the invisible system to define a second cut. Since the differential cross section $d\sigma/ds_I$ contains the Higgs resonance at $s_I = M_H^2$, we impose the following condition on the Z energy:

$$\frac{s + M_Z^2 - (M_H + \Delta_H)^2}{2\sqrt{s}} < E_Z < \frac{s + M_Z^2 - (M_H - \Delta_H)^2}{2\sqrt{s}}$$

For the choice of Δ_H a comment is in order. As long as the Higgs width is small, one is allowed to use small Δ_H , which reduces the background considerably keeping most of the signal events. But in the case of large φ -Higgs coupling, ω , one looses valuable events. To compromise between both effects we took $\Delta_H = 30$ GeV.

For the exclusion limits we assumed an integrated luminosity of $20 \, fb^{-1}$. To define the 95% confidence level we used Poisson statistics similar to the description of Ref. [2]. The result is given in Fig. 3. One notices the somewhat reduced sensitivity for $M_H \simeq M_Z$ due to a resonating Z boson in the ZZ background. For larger values of M_H the limit stems from the other $Z\nu\nu$ backgrounds with W bosons in the t-channel and kinematical constrains. For large ω the signal ceases to dominate over the background because the Higgs peak is smeared out to an almost flat distribution.

Figure 3: Exclusion limits at the NLC due to Higgs searches. The dashed line corresponds to the invisible, the full line to all Higgs decay modes.

We conclude from this analysis that the NLC can put further limits on the parameter space of our invisible Higgs model. Note that within the kinematic range very strong limits on ω can be set. Again there is a range where the Higgs boson will not be discovered, even if it does exist in this mass range. This has already been shown for the Higgs search at LEP and also holds true for the heavy Higgs search at LHC. We see that a sufficiently wide nonstandard Higgs resonance would make it very difficult to test the mechanism of electroweak symmetry breaking at future colliders.

References

- [1] T. Binoth, J. J. van der Bij, Quarks 94, Vladimir, Freiburg-THEP-94/26, hep-ph/9409332.
- [2] M. Carena, P.M. Zerwas (conv) et al., Higgs Physics, Proceedings of the Workshop Physics at LEP2, CERN Yellow Report 96-01.
- [3] O. J. P. Eboli et al., e^+e^- -collisions at 500 GeV, part C, DESY 93-123C, 55 (1993).
- [4] R. S. Chivukula, M. Golden, Phys. Lett. B267, 233 (1991).
- [5] Ambrosanio S., Mele B., Nucl. Phys. B374, 3 (1992).

Heavy SUSY Higgs Bosons at e^+e^- Linear Colliders

A. Djouadi^{1,2}, J. Kalinowski³, P. Ohmann^{1,4} and P.M. Zerwas¹

Abstract

The production mechanisms and decay modes of the heavy neutral and charged Higgs bosons in the Minimal Supersymmetric Standard Model are investigated at future e^+e^- colliders in the TeV energy regime. We generate supersymmetric particle spectra by requiring the MSSM Higgs potential to produce correct radiative electroweak symmetry breaking, and we assume a common scalar mass m_0 , gaugino mass $m_{1/2}$ and trilinear coupling A, as well as gauge and Yukawa coupling unification at the Grand Unification scale. Particular emphasis is put on the low $\mathrm{tg}\beta$ solution in this scenario where decays of the Higgs bosons to Standard Model particles compete with decays to supersymmetric charginos/neutralinos as well as sfermions. In the high $\mathrm{tg}\beta$ case, the supersymmetric spectrum is either too heavy or the supersymmetric decay modes are suppressed, since the Higgs bosons decay almost exclusively into b and τ pairs. The main production mechanisms for the heavy Higgs particles are the associated AH production and H^+H^- pair production with cross sections of the order of a few fb.

1. Introduction

Supersymmetric theories [1,2] are generally considered to be the most natural extensions of the Standard Model (SM). This proposition is based on several points. In these theories, fundamental scalar Higgs bosons [5,6] with low masses can be retained in the context of high unification scales. Moreover, the prediction [8] of the renormalized electroweak mixing angle $\sin^2\theta_W=0.2336\pm0.0017$, based on the spectrum of the Minimal Supersymmetric Standard Model (MSSM) [10], is in striking agreement with the electroweak precision data which yield $\sin^2\theta_W=0.2314(3)$ [11]. An additional attractive feature is provided by the opportunity to generate the electroweak symmetry breaking radiatively [9]. If the top quark mass is in the range between ~ 150 and ~ 200 GeV, the universal squared Higgs mass parameter at the unification scale decreases with decreasing energy and becomes negative at the electroweak scale, thereby breaking the SU(2)_L × U(1)_Y gauge symmetry while leaving the U(1) electromagnetic and SU(3) color gauge symmetries intact [9]. The analysis of the electroweak data prefers a light Higgs mass [11,9] as

¹ Deutsches Elektronen-Synchrotron DESY, D-22603 Hamburg, FRG.

² Institut für Theoretische Physik, Universität Karlsruhe, D-76128 Karlsruhe, FRG.

³ Institute of Theoretical Physics, Warsaw University, PL-00681 Warsaw, Poland.

⁴ Department of Theoretical Physics, Oxford University, OX1 3NP, Oxford, UK.

predicted in supersymmetric theories; however since the radiative corrections depend only logarithmically on the Higgs mass [10], the dependence is weak and no firm conclusions can yet be drawn.

The more than doubling the spectrum of states in the MSSM gives rise to a rather large proliferation of parameters. This number of parameters is however reduced drastically by embedding the low–energy supersymmetric theory into a grand unified (GUT) framework. This can be achieved in supergravity models [9], in which the effective low–energy supersymmetric theory [including the interactions which break supersymmetry] is described by the following parameters: the common scalar mass m_0 , the common gaugino mass $m_{1/2}$, the trilinear coupling A, the bilinear coupling B, and the Higgs–higgsino mass parameter μ . In addition, two parameters are needed to describe the Higgs sector: one Higgs mass parameter [in general the mass of the pseudoscalar Higgs boson, M_A] and the ratio of the vacuum expectation values, $tg\beta = v_2/v_1$, of the two Higgs doublet fields which break the electroweak symmetry.

The number of parameters can be further reduced by introducing additional constraints which are based on physically rather natural assumptions:

- (i) Unification of the b and τ Yukawa couplings at the GUT scale [11] leads to a correlation between the top quark mass and $tg\beta$ [12,13,14]. Adopting the central value of the top mass as measured at the Tevatron [15], $tg\beta$ is restricted to two narrow ranges around $tg\beta \sim 1.7$ and 50, with the low $tg\beta$ solution theoretically somewhat favored [14].
- (ii) If the electroweak symmetry is broken radiatively, then the bilinear coupling B and the Higgs-higgsino mass parameter μ are determined up to the sign of μ . [The sign of μ might be determined by future precision measurements of the radiative b decay amplitude.]
- (iii) It turns out a posteriori that the physical observables are nearly independent of the GUT scale value of the trilinear coupling A_G , for $|A_G| \lesssim 500$ GeV.

Mass spectra and couplings of all supersymmetric particles and Higgs bosons are determined after these steps by just two mass parameters along with the sign of μ ; we shall choose to express our results in terms of the pseudoscalar Higgs boson A mass M_A and the common GUT gaugino mass $m_{1/2}$.

In this paper we focus on heavy Higgs particles A, H and H^{\pm} with masses of a few hundred GeV, and therefore close to the decoupling limit [16]. The pattern of Higgs masses is quite regular in this limit. While the upper limit on the mass of the lightest CP-even Higgs boson h is a function of $tg\beta$ [17],

$$M_h \lesssim 100 \text{ to } 150 \text{ GeV} \text{ [for low to high tg}\beta]}$$
 (1.1)

the heavy Higgs bosons are nearly mass degenerate [c.f. Fig.1]

$$M_A \simeq M_H \simeq M_{H^{\pm}}$$
 (1.2)

Moreover, the properties of the lightest CP-even Higgs boson h become SM-like in this limit. The production of the heavy Higgs bosons becomes particularly simple in e^+e^- collisions; the heavy Higgs bosons can only be pair-produced,

$$e^+e^- \rightarrow AH$$
 (1.3)

$$e^+e^- \rightarrow H^+H^- \tag{1.4}$$

Close to this decoupling limit, the cross section for H Higgs-strahlung $e^+e^- \to ZH$ is very small and the cross section for the WW fusion mechanism $e^+e^- \to \nu_e\bar{\nu}_eH$ is appreciable only for small values of $\mathrm{tg}\beta$, $\mathrm{tg}\beta \sim 1$, and relatively small H masses, $M_H \lesssim 350$ GeV. The cross section for ZZ fusion of the H is suppressed by an order of magnitude compared to WW fusion. The pseudoscalar A particle does not couple to W/Z boson pairs at the tree level.

The decay pattern for heavy Higgs bosons is rather complicated in general. For large $\mathrm{tg}\beta$ the SM fermion decays prevail. For small $\mathrm{tg}\beta$ this is true above the $t\bar{t}$ threshold of $M_{H,A}\gtrsim 350~\mathrm{GeV}$ for the neutral Higgs bosons and above the $t\bar{b}$ threshold of $M_{H^\pm}\gtrsim 180~\mathrm{GeV}$ for the charged Higgs particles. Below these mass values many decay channels compete with each other: decays to SM fermions $f\bar{f}$ [and for H to gauge bosons VV], Higgs cascade decays, chargino/neutralino $\chi_i\chi_j$ decays and decays to supersymmetric sfermions $\tilde{f}\bar{f}$

$$H \rightarrow f\bar{f} , VV , hh , \chi_i\chi_j , \tilde{f}\bar{\tilde{f}}$$
 (1.5)

$$A \rightarrow f\bar{f} , hZ , \chi_i\chi_j , \tilde{f}\bar{\tilde{f}}$$
 (1.6)

$$H^{\pm} \rightarrow f\bar{f}', hW^{\pm}, \chi_i\chi_j, \tilde{f}\bar{\tilde{f}}'$$
 (1.7)

In this paper, we analyze in detail the decay modes of the heavy Higgs particles and their production at e^+e^- linear colliders. The analysis will focus on heavy particles for which machines in the TeV energy range are needed. The paper is organized in the following way. In the next section we define the physical set—up of our analysis in the framework of the MSSM embedded into a minimal supergravity theory. In section 3, we discuss the production cross sections of the heavy Higgs bosons. In the subsequent sections, we discuss the widths of the various decay channels and the final Higgs decay products.

2. The Physical Set-Up

The Higgs sector of the Minimal Supersymmetric Standard Model is described at tree-level by the following potential

$$V_{0} = (m_{H_{1}}^{2} + \mu^{2})|H_{1}|^{2} + (m_{H_{2}}^{2} + \mu^{2})|H_{2}|^{2} - m_{3}^{2}(\epsilon_{ij}H_{1}^{i}H_{2}^{j} + \text{h.c.})$$

$$+ \frac{1}{8}(g^{2} + g'^{2})\left[|H_{1}|^{2} - |H_{2}|^{2}\right]^{2} + \frac{1}{2}g^{2}|H_{1}^{i*}H_{2}^{i}|^{2}$$
(2.1)

The quadratic Higgs terms associated with μ and the quartic Higgs terms coming with the electroweak gauge couplings g and g' are invariant under supersymmetric transformations. m_{H_1} , m_{H_2} and m_3 are soft–supersymmetry breaking parameters with $m_3^2 = B\mu$. ϵ_{ij} [i,j=1,2 and $\epsilon_{12}=1]$ is the antisymmetric tensor in two dimensions and $H_1 \equiv (H_1^1,H_1^2)=(H_1^0,H_1^-)$, $H_2 \equiv (H_2^1,H_2^2)=(H_2^+,H_2^0)$ are the two Higgs-doublet fields. After the symmetry breaking, three out of the initially eight degrees of freedom will be absorbed to generate the W^\pm and Z masses, leaving a quintet of scalar Higgs particles: two CP–even Higgs bosons h and H, a CP–odd [pseudoscalar] boson A and two charged Higgs particles H^\pm .

Retaining only the [leading] Yukawa couplings of the third generation

$$\lambda_t = \frac{\sqrt{2}m_t}{v\sin\beta} , \quad \lambda_b = \frac{\sqrt{2}m_b}{v\cos\beta} \quad \text{and} \quad \lambda_\tau = \frac{\sqrt{2}m_\tau}{v\cos\beta}$$
 (2.2)

where $\operatorname{tg}\beta = v_2/v_1$ [with $v^2 = v_1^2 + v_2^2$ fixed by the W mass, v = 246 GeV] is the ratio of the vacuum expectation values of the fields H_2^0 and H_1^0 , the superpotential is given in terms of the superfields Q = (t, b) and $L = (\tau, \nu_{\tau})$ by

$$W = \epsilon_{ij} \left[\lambda_t H_2^i Q^j t^c + \lambda_b H_1^i Q^j b^c + \lambda_\tau H_1^i L^j \tau^c - \mu H_1^i H_2^j \right]$$
 (2.3)

Supersymmetry is broken by introducing the soft–supersymmetry breaking bino \tilde{B} , wino \tilde{W}^a [a=1-3] and gluino \tilde{q}^a [a=1-8] mass terms,

$$\frac{1}{2} M_1 \overline{\tilde{B}} \tilde{B} + \frac{1}{2} M_2 \overline{\tilde{W}}^a \tilde{W}^a + \frac{1}{2} M_3 \overline{\tilde{g}}^a \tilde{g}^a , \qquad (2.4)$$

soft-supersymmetry breaking trilinear couplings,

$$\epsilon_{ij} \left[\lambda_t A_t H_2^i \tilde{Q}^j \tilde{t}^c + \lambda_b A_b H_1^i \tilde{Q}^j \tilde{b}^c + \lambda_\tau A_\tau H_1^i \tilde{L}^j \tilde{\tau}^c - \mu B H_1^i H_2^j \right]$$
 (2.5)

and soft-supersymmetry breaking squark and slepton mass terms

$$M_O^2[\tilde{t}_L^* \tilde{t}_L + \tilde{b}_L^* \tilde{b}_L] + M_U^2 \tilde{t}_R^* \tilde{t}_R + M_D^2 \tilde{b}_R^* \tilde{b}_R + M_L^2 [\tilde{\tau}_L^* \tilde{\tau}_L + \tilde{\nu}_{\tau_L}^* \tilde{\nu}_{\tau_L}] + M_E^2 \tilde{\tau}_R^* \tilde{\tau}_R + \cdots$$
 (2.6)

where the ellipses stand for the soft mass terms corresponding to the first and second generation sfermions.

The minimal SUSY-GUT model emerges by requiring at the GUT scale M_G :

(i) the unification of the U(1), SU(2) and SU(3) coupling constants $\alpha_i = g_i^2/4\pi$ [i = 1–3],

$$\alpha_3(M_{\rm G}) = \alpha_2(M_{\rm G}) = \alpha_1(M_{\rm G}) = \alpha_G \tag{2.7}$$

¹Note that our convention for the sign of μ is consistent with Ref.[18], which is opposite to the one adopted in Ref.[19].

(ii) a common gaugino mass; the M_i with i = 1-3 at the electroweak scale are then related through renormalization group equations (RGEs) to the gauge couplings,

$$M_{i} = \frac{\alpha_{i}(M_{Z})}{\alpha_{G}} m_{1/2} \longrightarrow M_{3}(M_{Z}) = \frac{\alpha_{3}(M_{Z})}{\alpha_{2}(M_{Z})} M_{2}(M_{Z}) = \frac{\alpha_{3}(M_{Z})}{\alpha_{1}(M_{Z})} M_{1}(M_{Z})$$
(2.8)

(iii) a universal trilinear coupling A

$$A_G = A_t(M_G) = A_b(M_G) = A_\tau(M_G)$$
 (2.9)

(iii) a universal scalar mass m_0

$$m_0 = M_Q = M_U = M_D = M_L = M_E$$

= $m_{H_1}(M_G) = m_{H_2}(M_G)$ (2.10)

Besides the three parameters $m_{1/2}$, A_G and m_0 the supersymmetric sector is described at the GUT scale by the bilinear coupling B_G and the Higgs-higgsino mass parameter μ_G . The theoretically attractive assumption that the electroweak symmetry is broken radiatively constrains the latter two parameters. Indeed, radiative electroweak symmetry breaking results in two minimization conditions [see Ref.[19] for details] of the Higgs potential; at the low-energy scale in the tree approximation, they are given by

$$\frac{1}{2}M_Z^2 = \frac{m_{H_1}^2 - m_{H_2}^2 \tan^2 \beta}{\tan^2 \beta - 1} - \mu^2 \tag{2.11}$$

$$B\mu = \frac{1}{2}(m_{H_1}^2 + m_{H_2}^2 + 2\mu^2)\sin 2\beta \tag{2.12}$$

For given values of the GUT parameters $m_{1/2}$, m_0 , A_G as well as $\operatorname{tg}\beta$, the first minimization equation can be solved for μ [to within a sign]; the second equation can then be solved for B. Since $m_{H_1}^2$ and $m_{H_2}^2$ are related to M_A through the RGEs, the solution for μ and B can be approximately expressed as a function of M_A and $\operatorname{tg}\beta$. The power of supergravity models with radiative electroweak symmetry breaking becomes apparent when one includes the one-loop contributions to the Higgs potential. It is through these one-loop terms that most of the supersymmetric particle masses are determined; the minimization conditions [which are also solved for μ to within a sign and B] fix the masses in order that the electroweak symmetry is broken correctly, i.e. with the correct value of M_Z . [U(1)_{EM} and SU(3) remain unbroken of course]. The one-loop contributions and the minimization equations are given in Ref.[19] to which we refer for details.

A heavy top quark is required to break the electroweak symmetry radiatively, since it is the large top Yukawa coupling which will drive one of the Higgs mass parameters squared to a negative value. As emphasized before, the additional condition of unification of the b- τ Yukawa couplings gives rise to stringent constraints on $tg\beta$. The attractive idea of explaining the large top Yukawa coupling as a result of a fixed point solution of the RGEs leads to a relationship between M_t and the angle β , $M_t \simeq (200 \text{ GeV}) \sin \beta$ for

 $tg\beta \lesssim 10$, giving a further constraint on the model.

To limit the parameter space further, one could require that the SUGRA model is not fine—tuned and the SUSY breaking scale should not be too high, a constraint which can be particularly restrictive in the small $tg\beta$ region. However, the degree of fine—tuning which can be considered acceptable is largely a matter of taste, so we disregard this issue in our analysis.

We now detail the calculations of the supersymmetric particle spectrum more precisely. We incorporate boundary conditions at both electroweak and GUT scales, adopting the ambidextrous approach of Ref.[19]. We specify the values of the gauge and Yukawa couplings at the electroweak scale, in particular M_t , $\mathrm{tg}\beta$ and α_s . The gauge and Yukawa couplings are then evolved to the GUT scale M_G [defined to be the scale $\tilde{\mu}$ for which $\alpha_1(\tilde{\mu}) = \alpha_2(\tilde{\mu})$] using the two-loop RGEs [13]. At M_G we specify the soft supersymmetry breaking parameters $m_{1/2}$, m_0 and A_G . We then evolve parameters down to the electroweak scale where we apply the one-loop minimization conditions derived from the one-loop effective Higgs potential and solve for μ to within a sign and B [we then can integrate the RGEs back to M_G and obtain μ_G and B_G]. By this procedure, the supersymmetric spectrum is completely specified; that is, we generate a unique spectrum corresponding to particular values of $m_{1/2}$, m_0 , A_G , $\mathrm{tg}\beta$ and the sign of μ . It turns out that the spectrum is nearly independent of A_G , for $|A_G| \lesssim 500$ GeV. In most of our calculations, we substitute a particular value of M_A for m_0 in order to introduce a mass parameter which can be measured directly.

We discuss the SUSY spectrum and its phenomenological implications for two representative points in the M_t -tan β plane². We choose $M_t^{\rm pole}=175~{\rm GeV}$, consistent with the most recent Tevatron analyses [15] throughout our calculations, and values of ${\rm tg}\beta=1.75$ and 50, which are required (within uncertainties) by b- τ unification at M_G . In particular, we emphasize the low ${\rm tg}\beta$ solutions; they are theoretically favored from considerations such as $b\to s\gamma$ [21] and cosmological constraints [22]. The low ${\rm tg}\beta$ solutions generate much lighter SUSY spectra, more likely to be seen at future e^+e^- colliders. In both the low and high ${\rm tg}\beta$ regions we take³ $\alpha_s(M_Z)=0.118$ [23] and $A_G=0$, though the qualitative behavior in each region should not depend greatly on these parameters.

(a) Low $\tan \beta$

As a typical example of the low $\tan \beta$ region we consider the point $M_t^{\text{pole}} = 175 \text{ GeV}$ and $\tan \beta = 1.75$ for which $\lambda_t(M_G)$ lies in its "fixed-point" region [12,14]. If M_A is fixed, the scalar mass parameter m_0 can be calculated as a function of the common gaugino mass parameter $m_{1/2}$ so that all Higgs and supersymmetric particle masses can in principle be parameterized by $m_{1/2}$. The correlation between m_0 and $m_{1/2}$ is shown in Fig.2 for three

²Our numerical analysis is consistent with the numbers obtained in Ref.[20], once their value of A_{τ} in Tab.2 is corrected. We thank W. de Boer for a discussion on this point.

³This corresponds to the $\sin^2 \theta_W$ value quoted and compared with the high-precision electroweak analyses in the Introduction.

values of $M_A = 300,600$ and 900 GeV in the low $\text{tg}\beta$ region.

Some of the parameter space is already eliminated by experimental bounds on the light Higgs mass, the chargino/neutralino masses, the light stop mass, the slepton masses and the squark/gluino masses from LEP1/1.5 and the Tevatron [24]. The lower limits are indicated by the non–solid lines in Fig.2. Low values of $m_{1/2} \lesssim 60$ GeV are excluded by the lower bound on the gaugino masses. For $\mu > 0$, the bound from the negative search of charginos at LEP1.5 almost rules out completely the scenario with $M_A \lesssim 300$ GeV. If the h boson is not discovered at LEP2, i.e. if $M_h \gtrsim 95$ GeV, the whole $\mu < 0$ scenario [for $m_{1/2}, m_0 < 500$ GeV] can be excluded, while for $\mu > 0$ only the $m_{1/2} > 200$ GeV range [which implies very large values of M_A] would survive. The requirement that the lightest neutralino is the LSP, and therefore its mass is larger than the lightest $\tilde{\tau}$ mass, excludes a small edge of the parameter space [dotted line] at small m_0 with $m_{1/2} > 200$ GeV in the $\mu < 0$ case.

The masses of the Higgs bosons are shown in Fig.3a as a function of $m_{1/2}$ for $\mathrm{tg}\beta=1.75$, both signs of μ and for two representative values of $m_0=100$ and 500 GeV. The lightest Higgs boson has a rather small tree-level mass and M_h comes mainly from radiative corrections; the maximal values [for $m_{1/2} \sim 400$ GeV] are $M_h^{\mathrm{max}} \sim 90$ GeV for $\mu < 0$ and ~ 100 for $\mu > 0$. Because the pseudoscalar mass is approximately given by $M_A^2 \sim B\mu/\sin 2\beta \sim B\mu$ [at the tree-level] and since $B\mu$ turns out to be large in this scenario, the pseudoscalar A is rather heavy especially for large values of m_0 , and thus is almost mass degenerate with the heavy CP-even and charged Higgs bosons, $M_A \sim M_H \simeq M_{H^\pm}$. Note that M_A is below the $t\bar{t}$ threshold, $M_A \lesssim 350$ GeV, only if m_0 and $m_{1/2}$ are both of $\mathcal{O}(100)$ GeV.

The chargino/neutralino and sfermion masses are shown Fig.3b-d as a function of $m_{1/2}$ for the two values $M_A=300$ and 600 GeV and for both signs of μ . In the case of charginos and neutralinos, the masses are related through RGEs by the same ratios that describe the gauge couplings at the electroweak scale. The LSP is almost bino-like [with a mass $m_{\chi_1^0} \sim M_1$] while the next-to-lightest neutralino and the lightest chargino are wino-like [with masses $m_{\chi_2^0} \sim m_{\chi_1^+} \sim M_2 \sim 2 m_{\chi_1^0}$]. The heavier neutralinos and chargino are primarily higgsinos with masses $m_{\chi_3^0} \sim m_{\chi_4^0} \sim m_{\chi_2^+} \sim |\mu|$. Note that the masses approximately scale as M_A and that the decay of the heavy scalar and pseudoscalar Higgs bosons into pairs of the heaviest charginos and neutralinos is kinematically not allowed.

The left– and right–handed charged sleptons and sneutrinos are almost mass degenerate, the mass differences not exceeding $\mathcal{O}(10)$ GeV; the mixing in the τ sector is rather small for small $\mathrm{tg}\beta$, allowing one to treat all three generations of sleptons on the same footing. In the case of squarks, only the first two generations are degenerate, with left– and right–handed squarks having approximately the same mass. The mixing in the stop as well as in the sbottom sector leads to a rather substantial splitting between the two stop or sbottom mass eigenstates. Only for small values of M_A and for $\mu < 0$ is \tilde{b}_1 the lightest squark; otherwise \tilde{t}_1 is the lightest squark state. Note that the squark masses

increase with $m_{1/2}$ and that they scale as M_A i.e. as $|\mu|$. The slepton masses decrease with increasing $m_{1/2}$: this is due to the fact that when $m_{1/2}$ increases and M_A is held constant, m_0 decreases [see Fig.2], and the dependence of the slepton masses on m_0 is stronger [for fixed m_0 , the slepton masses would increase with increasing $m_{1/2}$].

(b) High $\tan \beta$

In this region we take $\operatorname{tg}\beta=50$ as a representative example, a value consistent with the unification of the t, b and τ Yukawa couplings. The set of possible solutions in the parameter space $[m_{1/2}, m_0]$ for $M_A=300$ and 600 GeV is shown in Fig.4. At $\operatorname{tg}\beta=50$ and $M_t^{\text{pole}}=175$ GeV, we find solutions only for $\mu<0$; this is a result of the large one-loop contribution to M_A , the sign of which depends on μ [25]. The boundary contours given in the figure correspond to tachyonic solutions in the parameter space: $m_{\tilde{\tau}_1}^2<0$, $M_A^2<0$ or $M_h^2<0$ at the tree-level. The latter constraint is important for algorithmic reasons: M_h^2 at the tree-level enters into the minimization equations in the form of a logarithm [19]. Also the requirement of the lightest neutralino to be the LSP excludes a small edge of the parameter space at small values of m_0 ; this explains why the curves for $M_A=300$ and 600 GeV do not terminate for low m_0 values.

Particle	Mass (GeV)	Mass (GeV)	Mass (GeV)	Mass (GeV)
M_A	300	300	600	600
$(m_{1/2}, m_0)$	(364,250)	(352,800)	(603,300)	(590,800)
$ ilde{g}$	940	910	1557	1524
$ ilde{t_1}, ilde{t_2}$	662,817	753,896	1115,1285	1156,1325
$\widetilde{b_1}, \widetilde{b_2}$	689,787	804,894	1159,1260	1220,1312
$ ilde{u_1}, ilde{u_2}$	881,909	1144,1164	1431,1479	1586,1628
$ ilde{d_1}, ilde{d_2}$	878,912	1142,1167	1425,1481	1582,1630
$ ilde{ au_1}, ilde{ au_2}; ilde{ u_ au}$	165,365; 325	567,740; 729	255,517; 485	586,812; 799
$ ilde{e_1}, ilde{e_2}; ilde{ u_e}$	290,360; 351	813,838; 835	381,519; 513	833,901; 898
χ_i^\pm	268,498	261,536	452,764	443,779
χ_i^0	144,268,485,496	139,261,526,534	239,452,754,763	234,443,771,778
$M_A, M_{H^{\pm}}, M_H, M_h$	300,315,300,124	300,315,300,124	600,608,600,131	600,608,600,131

Tab.1: Particle spectra for $M_t^{\text{pole}} = 175 \text{ GeV}$, $\tan \beta = 50 \text{ for selected } M_A, m_{1/2} \text{ and } m_0 \text{ values.}$

The sparticle spectra for $M_A = 300$ and 600 GeV and two sets of $m_{1/2}$ and (extreme) m_0 values are shown in Table 1. In all these cases, the particle spectrum is very heavy; hence most of the SUSY decay channels of the Higgs particles are shut for large $\operatorname{tg}\beta$. The

only allowed decay channels are $H, A \to \tilde{\tau}_1 \tilde{\tau}_1, \chi_1^0 \chi_1^0$ and $H^{\pm} \to \tilde{\tau}_1 \tilde{\nu}$ [for large M_A values]. However, the branching ratios of these decay channels are suppressed by large $b\bar{b}$ and $t\bar{b}$ widths of the Higgs particles for large $tg\beta$: while the supersymmetric decay widths are of the order $\mathcal{O}(0.1 \text{ GeV})$, the decays involving b quarks have widths $\mathcal{O}(10 \text{ GeV})$ and dominate by 2 orders of magnitude.

(c) Additional Constraints

There are additional experimental constraints on the parameter space for both high and low $tg\beta$; the most important of these are the $b \to s\gamma$, $Z \to b\bar{b}$, and dark matter [relic LSP abundance] constraints. These constraints are much more restrictive in the high $tg\beta$ case.

Recent studies [21] have indicated that the combination of $b \to s\gamma$, dark matter and m_b constraints disfavor the high $tg\beta$ solution for which the t, b and τ Yukawa couplings are equal, in particular the minimal SUSY-SO(10) model with universal soft-supersymmetry breaking terms at M_G . This model can, however, be saved if the soft terms are not universal [implying a higgsino-like lightest neutralino], and there exist theoretical motivations for non–universal soft terms at M_G [26]. The presently favored $Z \to b\bar{b}$ decay width would favor a very low A mass for large $tg\beta$.

For low $tg\beta$, these additional constraints do not endanger the model, yet they can significantly reduce the available parameter space. In particular the $Z \to b\bar{b}$ constraint favors a light chargino and light stop for small to moderate values of $tg\beta$ [27,28] so that they could be detected at LEP2 [28]. The dark matter constraint essentially places an upper limit on m_0 and $m_{1/2}$ [29]. The $b \to s\gamma$ constraint [30], on the other hand, is plagued with large theoretical uncertainties mainly stemming from the unknown next-toleading QCD corrections and uncertainties in the measurement of $\alpha_s(M_Z)$. However, it is consistent with the low $tg\beta$ solution and may in the future be useful in determining the sign of μ [31].

3. Production Mechanisms

The main production mechanisms of neutral Higgs bosons at e^+e^- colliders are the Higgsstrahlung process and pair production,

(a) Higgs-strahlung
$$e^+e^- \rightarrow (Z) \rightarrow Z + h/H$$

(a) Higgs-strahlung
$$e^+e^- \rightarrow (Z) \rightarrow Z + h/H$$

(b) pair production $e^+e^- \rightarrow (Z) \rightarrow A + h/H$

as well as the WW and ZZ fusion processes,

(c) fusion processes
$$e^+e^- \rightarrow \bar{\nu}\nu \ (WW) \rightarrow \bar{\nu}\nu + h/H$$

 $e^+e^- \rightarrow e^+e^-(ZZ) \rightarrow e^+e^- + h/H$

The \mathcal{CP} -odd Higgs boson A cannot be produced in the Higgs-strahlung and fusion processes to leading order since it does not couple to VV pairs.] The charged Higgs particle can be pair produced through virtual photon and Z boson exchange,

(d) charged Higgs
$$e^+e^- \rightarrow (\gamma, Z^*) \rightarrow H^+H^-$$

[For masses smaller than ~ 170 GeV, the charged Higgs boson is also accessible in top decays, $e^+e^- \to t\bar{t}$ with $t \to H^+b$.]

The production cross sections⁴ for the neutral Higgs bosons are suppressed by mixing angle factors compared to the SM Higgs production,

$$\sigma(e^+e^- \to Zh)$$
, $\sigma(VV \to h)$, $\sigma(e^+e^- \to AH) \sim \sin^2(\beta - \alpha)$ (3.1)

$$\sigma(e^+e^- \to ZH) , \ \sigma(VV \to H) , \ \sigma(e^+e^- \to Ah) \sim \cos^2(\beta - \alpha)$$
 (3.2)

while the cross section for the charged Higgs particle does not depend on any parameter other than $M_{H^{\pm}}$.

In the decoupling limit, $M_A \gg M_Z$, the HVV coupling vanishes, while the hVV coupling approaches the SM Higgs value

$$g_{HVV} = \cos(\beta - \alpha) \to M_Z^2 \sin 4\beta / 2M_A^2 \to 0$$
 (3.3)

$$g_{hVV} = \sin(\beta - \alpha) \rightarrow 1 - \mathcal{O}(M_Z^4/M_A^4) \rightarrow 1$$
 (3.4)

Hence, the only relevant mechanisms for the production of the heavy Higgs bosons in this limit will be the associated pair production (b) and the pair production of the charged Higgs particles (d). The cross sections, in the decoupling limit and for $\sqrt{s} \gg M_Z$, are given by [we use $M_H \sim M_A$]

$$\sigma(e^+e^- \to AH) = \frac{G_F^2 M_Z^4}{96\pi s} (v_e^2 + a_e^2) \beta_A^3$$
 (3.5)

$$\sigma(e^{+}e^{-} \to H^{+}H^{-}) = \frac{2G_F^2 M_W^4 s_W^4}{3\pi s} \left[1 + \frac{v_e v_H}{8s_W^2 c_W^2} + \frac{(a_e^2 + v_e^2) v_H^2}{256c_W^4 s_W^4} \right] \beta_{H^{\pm}}^3$$
(3.6)

where $\beta_j = (1 - 4M_j^2/s)^{1/2}$ is the velocity of Higgs bosons, the Z couplings to electrons are given by $a_e = -1$, $v_e = -1 + 4\sin^2\theta_W$, and to the charged Higgs boson by $v_H = -2 + 4\sin^2\theta_W$. The cross sections for hA and HZ production vanish in the decoupling limit since they are proportional to $\cos^2(\beta - \alpha)$.

The cross section for the fusion process, $e^+e^- \to \bar{\nu}_e\nu_e H$, is enhanced at high energies since it scales like $M_W^{-2} \log s/M_H^2$. This mechanism provides therefore a useful channel for H production in the mass range of a few hundred GeV below the decoupling limit and small values of $\mathrm{tg}\beta$, where $\mathrm{cos}^2(\beta-\alpha)$ is not prohibitively small; the cross section, though,

⁴The complete analytical expressions of the cross sections can be found, e.g., in Ref.[32]. Note that in this paper there are a few typos that we correct here: in eq.(20), the factor 92 should replaced by 96; in the argument of the λ function of the denominator in eq.(21), the parameter M_A^2 should be replaced by M_Z^2 ; finally, the minus sign in the interference term in eq.(25) should be replaced by a plus sign.

becomes gradually less important for increasing M_H and vanishes in the decoupling limit. In the high energy regime, the $WW \to H$ fusion cross section is well approximated by the expression

$$\sigma(e^+e^- \to \bar{\nu}_e\nu_e H) = \frac{G_F^3 M_W^4}{4\sqrt{2}\pi^3} \left[\left(1 + \frac{M_H^2}{s} \right) \log \frac{s}{M_H^2} - 2\left(1 - \frac{M_H^2}{s} \right) \right] \cos^2(\beta - \alpha) \quad (3.7)$$

obtained in the effective longitudinal W approximation. Since the NC couplings are small compared to the CC couplings, the cross section for the ZZ fusion process is $\sim 16\cos^4\theta_W$, i.e. one order of magnitude smaller than for WW fusion.

Numerical results for the cross sections are shown in Fig.5 at high–energy e^+e^- colliders as a function of \sqrt{s} TeV for the two values $\mathrm{tg}\beta=1.75$ and 50, and for pseudoscalar masses $M_A=300$, 600 and 900 GeV [note that $M_H\simeq M_{H^\pm}\simeq M_A$ as evident from Figs. 1 and 3a]. For a luminosity of $\int \mathcal{L}=200~\mathrm{fb}^{-1}$, typically a sample of about 1000 HA and H^+H^- pairs are predicted for heavy Higgs masses of $\sim 500~\mathrm{GeV}$ at $\sqrt{s}=1.5~\mathrm{TeV}$. For small $\mathrm{tg}\beta$ values, $\mathrm{tg}\beta\lesssim 2$, a few hundred events are predicted in the $WW\to H$ fusion process for H masses $\sim 300~\mathrm{GeV}$. The cross sections for the hA and HZ processes are too low, less than $\sim 0.1~\mathrm{fb}$, to be useful for $M_H\gtrsim 300~\mathrm{GeV}$; Fig.5b.

Note that the cross sections for the production of the lightest Higgs boson h in the decoupling limit and for $\sqrt{s} \gg M_Z, M_h$ are simply given by

$$\sigma(e^+e^- \to ZZ) \simeq \frac{G_F^2 M_Z^4}{96\pi s} (v_e^2 + a_e^2)$$
 (3.8)

$$\sigma(e^+e^- \to \bar{\nu}_e\nu_e h) \simeq \frac{G_F^3 M_W^4}{4\sqrt{2}\pi^3} \log \frac{s}{M_h^2}$$
 (3.9)

The cross sections are the same as for the SM Higgs particle and are very large ~ 100 fb, especially for the WW fusion mechanism.

4. Decay Modes

4.1 Decays to standard particles

For large $tg\beta$ the Higgs couplings to down–type fermions dominate over all other couplings. As a result, the decay pattern is in general very simple. The neutral Higgs bosons will decay into $b\bar{b}$ and $\tau^+\tau^-$ pairs for which the branching ratios are close to $\sim 90\%$ and $\sim 10\%$, respectively. The charged Higgs particles decay into $\tau\nu_{\tau}$ pairs below and into tb pairs above the top–bottom threshold.

The partial decay widths of the neutral Higgs bosons⁵, $\Phi = H$ and A, to fermions are given by [6]

$$\Gamma(\Phi \to \bar{f}f) = N_c \frac{G_F M_\Phi}{4\sqrt{2}\pi} g_{\Phi ff}^2 m_f^2 \beta_f^p \tag{4.1}$$

 $^{^5}$ We refrain from a discussion of the h decays which become SM-like in the decoupling limit. In addition, we discuss only the dominant two-body decay modes of the heavy Higgs bosons; for an updated and more detailed discussion, including also three-body decays, see Ref.[33].

with p = 3(1) for the CP-even (odd) Higgs bosons; $\beta_f = (1 - 4m_f^2/M_{\Phi}^2)^{1/2}$ is the velocity of the fermions in the final state, N_c the color factor. For the decay widths to quark pairs, the QCD radiative corrections are large and must be included; for a recent update and a more detailed discussion, see Ref.[34].

The couplings of the MSSM neutral Higgs bosons [normalized to the SM Higgs coupling $g_{H_{\rm SM}ff} = \left[\sqrt{2}G_F\right]^{1/2}m_f$ and $g_{H_{\rm SM}VV} = 2\left[\sqrt{2}G_F\right]^{1/2}M_V^2$] are given in Table 2.

Φ	$g_{\Phi ar{u}u}$	$g_{\Phi ar{d}d}$	$g_{\Phi VV}$
h H A	$ \cos \alpha / \sin \beta \\ \sin \alpha / \sin \beta \\ 1/ \operatorname{tg} \beta $	$-\sin\alpha/\cos\beta$ $\cos\alpha/\cos\beta$ $tg\beta$	$ \begin{array}{c} \sin(\beta - \alpha) \\ \cos(\beta - \alpha) \\ 0 \end{array} $

Tab. 2: Higgs boson couplings in the MSSM to fermions and gauge bosons relative to the SM Higgs couplings.

In the decoupling limit, $M_A \gg M_Z$, we have

$$\cos \alpha \sim \sin \beta - \cos \beta \frac{M_Z^2}{2M_A^2} \sin 4\beta \to \sin \beta$$
 (4.2)

$$\sin \alpha \sim -\cos \beta + \sin \beta \frac{M_Z^2}{2M_A^2} \sin 4\beta \rightarrow -\cos \beta$$
 (4.3)

Therefore the hff couplings reduce to the SM Higgs couplings, while the Hff couplings become equal to those of the pseudoscalar boson A,

$$\cos \alpha / \sin \beta \rightarrow 1$$

$$-\sin \alpha / \cos \beta \rightarrow 1$$

$$-\sin \alpha / \sin \beta \rightarrow 1/ \operatorname{tg} \beta$$

$$\cos \alpha / \cos \beta \rightarrow \operatorname{tg} \beta$$
(4.4)

The partial width of the decay mode $H^+ \to u\bar{d}$ is given by

$$\Gamma(H^{+} \to u\bar{d}) = \frac{N_{c}G_{F}}{4\sqrt{2}\pi} \frac{\lambda_{ud,H^{\pm}}^{1/2}}{M_{H^{\pm}}} |V_{ud}|^{2} \times \left[(M_{H^{\pm}}^{2} - m_{u}^{2} - m_{d}^{2}) \left(m_{d}^{2} \operatorname{tg}^{2}\beta + m_{u}^{2} \operatorname{ctg}^{2}\beta \right) - 4m_{u}^{2} m_{d}^{2} \right]$$
(4.5)

with V_{ud} the CKM-type matrix element for quarks and λ is the two-body phase space function defined by

$$\lambda_{ij,k} = (1 - M_i^2 / M_k^2 - M_j^2 / M_k^2)^2 - 4M_i^2 M_j^2 / M_k^4$$
(4.6)

For decays into quark pairs, the QCD corrections must be also included.

Below the $\bar{t}t$ threshold, a variety of channels is open for the decays of the heavy CP– even Higgs bosons, the most important being the cascade decays $H \to \Phi\Phi$ with $\Phi = h$ or A, with a partial width [for real light Higgs bosons]

$$\Gamma(H \to \Phi\Phi) = \frac{G_F}{16\sqrt{2}\pi} \frac{M_Z^4}{M_H} g_{H\Phi\Phi}^2 \beta_{\Phi}$$
(4.7)

where $\beta_{\Phi} = (1 - 4M_{\Phi}^2/M_H^2)^{1/2}$ and the radiatively corrected three-boson self-couplings [to leading order], in units of $g_Z' = (\sqrt{2}G_F)^{1/2}M_Z^2$, are given by

$$g_{Hhh} = 2\sin 2\alpha \sin(\beta + \alpha) - \cos 2\alpha \cos(\beta + \alpha) + 3\frac{\epsilon}{M_Z^2} \frac{\sin \alpha \cos^2 \alpha}{\sin \beta}$$

$$g_{HAA} = -\cos 2\beta \cos(\beta + \alpha) + \frac{\epsilon}{M_Z^2} \frac{\sin \alpha \cos^2 \beta}{\sin \beta}$$

$$(4.8)$$

In contrast to the previous couplings, the leading m_t^4 radiative corrections cannot be absorbed entirely in the redefinition of the mixing angle α , but they are renormalized by an explicit term depending on the parameter ϵ given by $[M_S]$ is the common squark mass at the electroweak scale

$$\epsilon = \frac{3G_F}{\sqrt{2}\pi^2} \frac{m_t^4}{\sin^2 \beta} \log \left(1 + \frac{M_S^2}{m_t^2} \right) \tag{4.9}$$

In the decoupling limit, these couplings approach the values

$$g_{Hhh} \rightarrow \frac{3}{2}\sin 4\beta$$

$$g_{HAA} \rightarrow -\frac{1}{2}\sin 4\beta \tag{4.10}$$

In the mass range above the WW and ZZ thresholds, where the HVV couplings are not strongly suppressed for small values of $tg\beta$, the partial widths of the H particle into massive gauge bosons can also be substantial; they are given by

$$\Gamma(H \to VV) = \frac{\sqrt{2}G_F \cos^2(\alpha - \beta)}{32\pi} M_H^3 (1 - 4\kappa_V + 12\kappa_V^2) (1 - 4\kappa_V)^{1/2} \, \delta_V' \qquad (4.11)$$

with $\kappa_V = M_V^2/M_H^2$ and $\delta_V' = 2(1)$ for V = W(Z).

For small values of $tg\beta$ and below the $\bar{t}t$ and the $t\bar{b}$ thresholds, the pseudoscalar and charged Higgs bosons can decay into the lightest Higgs boson h and a gauge boson; however these decays are suppressed by $\cos^2(\beta - \alpha)$ and therefore are very rare for large A masses. The partial decay widths are given by

$$\Gamma(A \to hZ) = \frac{G_F \cos^2(\beta - \alpha)}{8\sqrt{2}\pi} \frac{M_Z^4}{M_A} \lambda_{Zh,A}^{1/2} \lambda_{Ah,Z}$$

$$\Gamma(H^+ \to hW^+) = \frac{G_F \cos^2(\beta - \alpha)}{8\sqrt{2}\pi} \frac{M_W^4}{M_{H^{\pm}}} \lambda_{Wh,H^{\pm}}^{\frac{1}{2}} \lambda_{H^{\pm}h,W}$$
(4.12)

In the decoupling limit, the partial widths of all decays of the heavy CP-even, CP-odd and charged Higgs bosons involving gauge bosons vanish since $\cos^2(\beta - \alpha) \to 0$. In addition, the $H \to hh$ decay width is very small since it is inversely proportional to M_H , and $H \to AA$ is not allowed kinematically. Therefore, the only relevant channels are the decays into $\bar{b}b/\bar{t}t$ for the neutral and $t\bar{b}$ for the charged Higgs bosons. The total decay widths of the three bosons H, A and H^{\pm} , into standard particles can be approximated in this limit by

$$\Gamma(H_k \to \text{all}) = \frac{3G_F}{4\sqrt{2}\pi} M_{H_k} \left[m_b^2 \text{tg}^2 \beta + m_t^2 \text{ctg}^2 \beta \right]$$
(4.13)

[We have neglected the small contribution of the decays into τ leptons for large $tg\beta$.]

4.2 Decays to charginos and neutralinos

The decay widths of the Higgs bosons H_k [k = (1, 2, 3, 4) correspond to (H, h, A, H^{\pm})] into neutralino and chargino pairs are given by [35]

$$\Gamma(H_k \to \chi_i \chi_j) = \frac{G_F M_W^2}{2\sqrt{2}\pi} \frac{M_{H_k} \lambda_{ij,k}^{1/2}}{1 + \delta_{ij}} \quad \left[(F_{ijk}^2 + F_{jik}^2) \left(1 - \frac{m_{\chi_i}^2}{M_{H_k}^2} - \frac{m_{\chi_j}^2}{M_{H_k}^2} \right) - 4\eta_k \epsilon_i \epsilon_j F_{ijk} F_{jik} \frac{m_{\chi_i} m_{\chi_j}}{M_{H_k}^2} \right]$$
(4.14)

where $\eta_{1,2,4} = +1$, $\eta_3 = -1$ and $\delta_{ij} = 0$ unless the final state consists of two identical (Majorana) neutralinos in which case $\delta_{ii} = 1$; $\epsilon_i = \pm 1$ stands for the sign of the *i*'th eigenvalue of the neutralino mass matrix [the matrix Z is defined in the convention of Ref.[18], and the eigenvalues of the mass matrix can be either positive or negative] while $\epsilon_i = 1$ for charginos; $\lambda_{ij,k}$ is the usual two-body phase space function given in eq.(4.4).

In the case of neutral Higgs boson decays, the coefficients F_{ijk} are related to the elements of the matrices U, V for charginos and Z for neutralinos,

$$H_k \to \chi_i^+ \chi_j^- : F_{ijk} = \frac{1}{\sqrt{2}} \left[e_k V_{i1} U_{j2} - d_k V_{i2} U_{j1} \right]$$
 (4.15)

$$H_k \to \chi_i^0 \chi_j^0$$
 : $F_{ijk} = \frac{1}{2} (Z_{j2} - \tan \theta_W Z_{j1}) (e_k Z_{i3} + d_k Z_{i4}) + i \leftrightarrow j$ (4.16)

with the coefficients e_k and d_k given by

$$e_1/d_1 = \cos \alpha / - \sin \alpha , \ e_2/d_2 = \sin \alpha / \cos \alpha , \ e_3/d_3 = -\sin \beta / \cos \beta$$
 (4.17)

For the charged Higgs boson, the coupling to neutralino/chargino pairs are given by

$$F_{ij4} = \cos \beta \left[Z_{j4} V_{i1} + \frac{1}{\sqrt{2}} \left(Z_{j2} + \tan \theta_W Z_{j1} \right) V_{i2} \right]$$

$$F_{ji4} = \sin \beta \left[Z_{j3} U_{i1} - \frac{1}{\sqrt{2}} \left(Z_{j2} + \tan \theta_W Z_{j1} \right) U_{i2} \right]$$
(4.18)

The matrices U, V for charginos and Z for neutralinos can be found in Ref.[18].

Since in most of the parameter space discussed in Section 2, the Higgs-higgsino mass parameter $|\mu|$ turned out to be very large, $|\mu| \gg M_1, M_2, M_Z$, it is worth discussing the Higgs decay widths into charginos and neutralinos in this limit. First, the decays of the neutral Higgs bosons into pairs of [identical] neutralinos and charginos $H_k \to \chi_i \chi_i$ will be suppressed by powers of M_Z^2/μ^2 . This is due to the fact that neutral Higgs bosons mainly couple to mixtures of higgsino and gaugino components, and in the large μ limit, neutralinos and charginos are either pure higgsino— or pure gaugino—like. For the same reason, decays $H^+ \to \chi_{1,2}^0 \chi_1^+$ and $\chi_{3,4}^0 \chi_2^+$ of the charged Higgs bosons will be suppressed. Furthermore, since in this case M_A is of the same order as $|\mu|$, decays into pairs of heavy charginos and neutralinos will be kinematically forbidden. Therefore, the channels

$$H, A \rightarrow \chi_1^0 \chi_{3,4}^0, \chi_2^0 \chi_{3,4}^0 \text{ and } \chi_1^{\pm} \chi_2^{\mp}$$
 $H^+ \rightarrow \chi_1^+ \chi_{3,4}^0 \text{ and } \chi_2^+ \chi_{1,2}^0$ (4.19)

will be the dominant decay channels of the heavy Higgs particles. Up to the phase space suppression [i.e. for M_A sufficiently larger than $|\mu|$], the partial widths of these decay channels, in units of $G_F M_W^2 M_{H_k}/(4\sqrt{2}\pi)$, are given by [35]

$$\Gamma(H \to \chi_1^0 \chi_{3,4}^0) = \frac{1}{2} \tan^2 \theta_W (1 \pm \sin 2\beta)
\Gamma(H \to \chi_2^0 \chi_{3,4}^0) = \frac{1}{2} (1 \pm \sin 2\beta)
\Gamma(H \to \chi_1^{\pm} \chi_2^{\mp}) = 1$$

$$\Gamma(A \to \chi_1^0 \chi_{4,3}^0) = \frac{1}{2} \tan^2 \theta_W (1 \pm \sin 2\beta)
\Gamma(A \to \chi_2^0 \chi_{4,3}^0) = \frac{1}{2} (1 \pm \sin 2\beta)
\Gamma(A \to \chi_1^{\pm} \chi_2^{\mp}) = 1$$

$$\Gamma(A \to \chi_1^{\pm} \chi_2^{\mp}) = 1$$

$$\Gamma(H^+ \to \chi_1^+ \chi_{3,4}^0) = 1$$

$$\Gamma(H^+ \to \chi_2^+ \chi_1^0) = 1$$

$$\Gamma(H^+ \to \chi_2^+ \chi_2^0) = \tan^2 \theta_W$$
(4.22)

[We have used the fact that in the decoupling limit $\sin 2\alpha = -\sin 2\beta$.] If all these channels are kinematically allowed, the total decay widths of the heavy Higgs bosons to chargino and neutralino pairs will be given by the expression

$$\Gamma(H_k \to \sum \chi_i \chi_j) = \frac{3G_F M_W^2}{4\sqrt{2}\pi} M_{H_k} \left(1 + \frac{1}{3} \tan^2 \theta_W \right)$$
(4.23)

which holds universally for all the three Higgs bosons H, A, H^{\pm} .

4.3 Decays to squarks and sleptons

Decays of the neutral and charged Higgs bosons, $H_k = h, H, A, H^{\pm}$, to sfermion pairs can be written as

$$\Gamma(H_k \to \tilde{f}_i \tilde{f}_j) = \frac{N_C G_F}{2\sqrt{2}\pi M_{H_k}} \lambda_{\tilde{f}_i \tilde{f}_j, H_k}^{1/2} g_{H_k \tilde{f}_i \tilde{f}_j}^2$$

$$\tag{4.24}$$

 \tilde{f}_i with i=1,2 are the sfermion mass eigenstates which are related to the current eigenstates \tilde{f}_L, \tilde{f}_R by

$$\tilde{f}_{1} = \tilde{f}_{L} \cos \theta_{f} + \tilde{f}_{R} \sin \theta_{f}
\tilde{f}_{2} = -\tilde{f}_{L} \sin \theta_{f} + \tilde{f}_{R} \cos \theta_{f}$$
(4.25)

The mixing angles θ_f are proportional to the masses of the partner fermions and they are important only in the case of third generation sfermions. The couplings $g_{H_k\tilde{f}_i\tilde{f}'_j}$ of the neutral and charged Higgs bosons H_k to sfermion mass eigenstates are superpositions of the couplings of the current eigenstates,

$$g_{H_k \tilde{f}_i \tilde{f}'_j} = \sum_{\alpha, \beta = L, R} T_{ij\alpha\beta} \ g_{\Phi \tilde{f}_\alpha \tilde{f}'_\beta} \tag{4.26}$$

The elements of the 4×4 matrix T are given in Tab.3a. The couplings $g_{H_k \tilde{f}_{\alpha} \tilde{f}'_{\beta}}$, in the current eigenstate basis $\tilde{f}_{\alpha,\beta} = \tilde{f}_{L,R}$ [normalized to $2(\sqrt{2}G_F)^{1/2}$] may be written as [6,35]

$$g_{H_{k}\tilde{f}_{L}\tilde{f}_{L}} = m_{f}^{2}g_{1}^{\Phi} + M_{Z}^{2}(T_{3}^{f} - e_{f}s_{W}^{2})g_{2}^{\Phi}$$

$$g_{H_{k}\tilde{f}_{R}\tilde{f}_{R}} = m_{f}^{2}g_{1}^{\Phi} + M_{Z}^{2}e_{f}s_{W}^{2}g_{2}^{\Phi}$$

$$g_{H_{k}\tilde{f}_{L}\tilde{f}_{R}} = -\frac{1}{2}m_{f}\left[\mu g_{3}^{\Phi} - A_{f}g_{4}^{\Phi}\right]$$
(4.27)

for the neutral Higgs bosons, $H_k=h,H,A$. $T_3=\pm 1/2$ is the isospin of the [left-handed] sfermion and e_f its electric charge. The coefficients g_i^{Φ} are given in Tab.3b; in the decoupling limit, the coefficients g_2^{Φ} reduce to

$$\cos(\beta + \alpha) \rightarrow \sin 2\beta$$

$$\sin(\beta + \alpha) \rightarrow -\cos 2\beta \tag{4.28}$$

[for the other coefficients, see eqs.(4.2)]. For the charged Higgs bosons, the couplings [also normalized to $2(\sqrt{2}G_F)^{1/2}$] are

$$g_{H^+\tilde{u}_{\alpha}\tilde{d}_{\beta}} = -\frac{1}{\sqrt{2}} \left[g_1^{\alpha\beta} + M_W^2 g_2^{\alpha\beta} \right] \tag{4.29}$$

with the coefficients $g_{1/2}^{\alpha\beta}$ with $\alpha, \beta = L, R$ listed in Table 3c.

$\boxed{i,j \ / \ \alpha,\beta}$	LL	RR	LR	RL
11 12 21 22	$\cos \theta_f \cos \theta_{f'} - \cos \theta_f \sin \theta_{f'} - \sin \theta_f \cos \theta_{f'} - \sin \theta_f \sin \theta_{f'}$	$\sin \theta_f \sin \theta_{f'}$ $\sin \theta_f \cos \theta_{f'}$ $\cos \theta_f \sin \theta_{f'}$ $\cos \theta_f \cos \theta_{f'}$	$\cos \theta_f \sin \theta_{f'}$ $\cos \theta_f \cos \theta_{f'}$ $-\sin \theta_f \sin \theta_{f'}$ $-\sin \theta_f \cos \theta_{f'}$	$ \sin \theta_f \cos \theta_{f'} \\ -\sin \theta_f \sin \theta_{f'} \\ \cos \theta_f \cos \theta_{f'} \\ -\cos \theta_f \sin \theta_{f'} $

Tab. 3a: Transformation matrix for the Higgs couplings to sfermions in the presence of mixing.

$ ilde{f}$	Φ	g_1^Φ	g_2^Φ	g_3^Φ	g_4^Φ
\tilde{u}	h H A	$\cos \alpha / \sin \beta$ $\sin \alpha / \sin \beta$	$-\sin(\alpha+\beta)\\\cos(\alpha+\beta)\\0$	$-\sin\alpha/\sin\beta$ $\cos\alpha/\sin\beta$	$\cos \alpha / \sin \beta$ $\sin \alpha / \sin \beta$ $-1/tg\beta$
$ ilde{d}$	$egin{array}{c} h \\ H \\ A \end{array}$	$-\sin\alpha/\cos\beta$ $\cos\alpha/\cos\beta$ 0	$-\sin(\alpha+\beta)$ $\cos(\alpha+\beta)$ 0	$ \cos \alpha / \cos \beta \\ \sin \alpha / \cos \beta \\ 1 $	$-\sin\alpha/\cos\beta$ $\cos\alpha/\cos\beta$ $-\mathrm{tg}\beta$

Tab. 3b: Coefficients in the couplings of neutral Higgs bosons to sfermion pairs.

$g_{1/2}^{LL}$	$g_{1/2}^{RR}$	$g_{1/2}^{LR}$	$g_{1/2}^{RL}$
$\frac{m_u^2/\tan\beta + m_d^2\tan\beta}{-\sin 2\beta}$	$m_u m_d (\operatorname{tg}\beta + 1/\operatorname{tg}\beta)$	$m_d(\mu + A_d \operatorname{tg}\beta)$	$m_u(\mu + A_u/\operatorname{tg}\beta)$

Tab. 3c: Coefficients in the couplings of charged Higgs bosons to sfermion pairs.

Mixing between sfermions occurs only in the third–generation sector. For the first two generations the decay pattern is rather simple. In the limit of massless fermions, the pseudoscalar Higgs boson does not decay into sfermions since by virtue of CP–invariance it couples only to pairs of left– and right–handed sfermions with the coupling proportional to m_f . In the asymptotic regime, where the masses $M_{H,H^{\pm}}$ are large, the decay widths of the heavy CP–even and charged [36] Higgs bosons into sfermions are proportional to

$$\Gamma(H, H^+ \to \tilde{f}\tilde{f}) \sim \frac{G_F M_W^4}{M_H} \sin^2 2\beta$$
 (4.30)

These decay modes can be significant only for low values $\operatorname{tg}\beta$ [which implies $\sin^2 2\beta \sim 1$]. However, in this regime the decay widths are inversely proportional to M_H , and thus cannot compete with the decay widths into charginos/neutralinos and ordinary fermions which increase with increasing Higgs mass. Therefore, the decays into first and second generations are unlikely to be important.

In the case of the third generation squarks, the Higgs decay widths can be larger by more than an order of magnitude. For instance the decay widths of the heavy neutral Higgs boson into top squarks of the same helicity is proportional to

$$\Gamma(H \to \tilde{t}\tilde{t}) \sim \frac{G_F m_t^4}{M_H \tan^2 \beta}$$
 (4.31)

in the asymptotic region, and it will be enhanced by large coefficients [for small $tg\beta$] compared to first/second generation squarks. Conversely, the decay widths into sbottom quarks can be very large for large $tg\beta$. Furthermore, the decays of heavy neutral CP–even and CP–odd Higgs bosons to top squarks of different helicities will be proportional in the asymptotic region [and for the CP–even, up to the suppression by mixing angle] to

$$\Gamma(H, A \to \tilde{t}\tilde{t}) \sim \frac{G_F m_t^2}{M_H} \left[\mu + A_t/\tan\beta\right]^2$$
 (4.32)

For μ and A_t values of the order of the Higgs boson masses, these decay widths will be competitive with the chargino/neutralino and standard fermion decays. Therefore, if kinematically allowed, these decay modes have to be taken into account.

4.4 Numerical results

The decay widths of the H,A and H^{\pm} Higgs bosons into the sum of charginos and neutralinos, squark or slepton final states, as well as the standard and the total decay widths are shown in Figs.6a, 7a and 8a as a function of $m_{1/2}$ for two values of the pseudoscalar Higgs boson mass $M_A=300$ and 600 GeV, and for positive and negative μ values; $\mathrm{tg}\beta$ is fixed to 1.75.

Fig.6a shows the various decay widths for the heavy CP-even Higgs boson. For $M_A = 300$ GeV, the $H \to t\bar{t}$ channel is still closed and the decay width into standard particles is rather small, being of $\mathcal{O}(250)$ MeV. In this case, the decays into the lightest stop squarks which are kinematically allowed for small values of $m_{1/2}$ will be by far the dominant decay channels. This occurs in most of the $m_{1/2}$ range if $\mu > 0$, but if $\mu < 0$ only for $m_{1/2} \lesssim 50$ GeV which is already ruled out by CDF and LEP1.5 data.

The decays into charginos and neutralinos, although one order of magnitude smaller than stop decays when allowed kinematically, are also very important. They exceed the standard decays in most of the $m_{1/2}$ range, except for large values of $m_{1/2}$ and $\mu < 0$ where no more phase space is available for the Higgs boson to decay into combinations of the heavy and light chargino/neutralino states. For small $m_{1/2}$ values, chargino and

neutralino decays can be larger than the standard decays by up to an order of magnitude.

As expected, the decay widths into sleptons are rather small and they never exceed the widths into standard particles, except for large values of $m_{1/2}$. Note that due to the isospin and charge assignments, the coupling of the H boson to sneutrinos is approximately a factor of two larger than the coupling to the charged sleptons. Since all the sleptons of the three generations are approximately mass degenerate [the mixing in the $\tilde{\tau}$ sector is very small for low values of $\operatorname{tg}\beta$], the small decay widths into sleptons are given by the approximate relation: $\Gamma(H \to \tilde{\nu}\tilde{\nu}) \simeq 4\Gamma(H \to \tilde{l}_L\tilde{l}_L) \simeq 4\Gamma(H \to \tilde{l}_R\tilde{l}_R)$.

For larger values of M_H , $M_H \gtrsim 350$ GeV, the decay widths into supersymmetric particles have practically the same size as discussed previously. However, since the $H \to t\bar{t}$ channel opens up, the decay width into standard model particles becomes rather large, $\mathcal{O}(10 \text{ GeV})$, and the supersymmetric decays are no longer dominant. For $M_H \simeq 600$ GeV, Fig.6a, only the $H \to \tilde{q}\tilde{q}$ decay width can be larger than the decay width to standard particles; this occurs in the lower range of the $m_{1/2}$ values. The chargino/neutralino decays have a branching ratio of $\sim 20\%$, while the branching ratios of the decays into sleptons are below the 1% level.

Fig.6b and 6c show the individual decay widths of the heavy H boson with a mass $M_H \simeq 600$ GeV into charginos, neutralinos, stop quarks and sleptons for the set of parameters introduced previously. For decays into squarks, only the channels $H \to \tilde{t}_1 \tilde{t}_1, \tilde{t}_1 \tilde{t}_2$, and in a very small range of $m_{1/2}$ values the channel $H \to \tilde{b}_1 \tilde{b}_1$, are allowed kinematically [see Fig.3c]. The decay into two different stop states is suppressed by the [small] mixing angle, and due to the larger phase space the decay $H \to \tilde{t}_1 \tilde{t}_1$ is always dominating.

For the decays into chargino and neutralinos, the dominant channels are decays into mixtures of light and heavy neutralinos and charginos, in particular $H \to \chi_1^+ \chi_2^-$ and $H \to \chi_1^0 \chi_3^0$ or $\chi_2^0 \chi_3^0$. This can be qualitatively explained, up to phase space suppression factors, by recalling the approximate values of the relative branching ratios in the large $|\mu|$ limit given in eqs.(4.18–20): $\Gamma(H \to \chi_1^\pm \chi_2^\mp) \sim 1$, while $\Gamma(H \to \chi_2^0 \chi_3^0) \sim 1$ and $\Gamma(H \to \chi_1^0 \chi_3^0) \sim \tan^2 \theta_W$ because $\sin 2\beta$ is close to one. The mixed decays involving χ_4^0 are suppressed since they are proportional to $(1 - \sin 2\beta)$, and all other decay channels are suppressed by powers of M_Z^2/μ^2 for large $|\mu|$ values.

The decay widths for the pseudoscalar Higgs boson are shown in Fig.7a. There are no decays into sleptons, since the only decay allowed by CP-invariance, $A \to \tilde{\tau}_1 \tilde{\tau}_2$, is strongly suppressed by the very small $\tilde{\tau}$ mixing angle. For $M_A = 300$ GeV, the decay into the two stop squark eigenstates, $A \to \tilde{t}_1 \tilde{t}_2$, is not allowed kinematically and the only possible supersymmetric decays are the decays into charginos and neutralinos. The sum of the decay widths into these states can be two orders of magnitude larger than the decay width into standard particles.

For values of M_A above the $t\bar{t}$ threshold, the decay width into charginos and neutralinos is still of the same order as for low M_A , but because of the opening of the $A \to t\bar{t}$ mode,

the total decay width increases dramatically and the chargino/neutralino decay branching ratio drops to the level of 20%. As in the case of the heavy CP–even Higgs boson H, the relative decay widths of the pseudoscalar boson into charginos and neutralinos, Fig.7b, are larger for the channels involving mixtures of light and heavy neutralinos or charginos; the dominant decay modes are, roughly, $A \to \chi_1^+ \chi_2^-$ and $A \to \chi_1^0 \chi_4^0$ or $\chi_2^0 \chi_4^0$. Again, this can be qualitatively explained, up to phase space suppression factors, by recalling the approximate formulae of eqs.(4.18–19), since the situation is the same as for H, with the two neutralino states χ_3^0 and χ_4^0 being interchanged.

For small values of the common gaugino mass, $m_{1/2} \lesssim 100$ GeV, the decay mode of the pseudoscalar Higgs boson into stop squarks, $A \to \tilde{t}_1 \bar{t}_2$, is phase space allowed. In this case, it is competitive with the top–antitop decay mode. As discussed previously, the $1/M_A^2$ suppression [and to a lesser extent the suppression due to the mixing angle] of the $A \to \tilde{t}_1 \bar{t}_2$ decay width compared to $\Gamma(A \to t\bar{t})$ will be compensated by the enhancement of the $A\tilde{t}_1\bar{t}_2$ coupling for large values of μ and A_t .

Fig.8a shows the decay widths for the charged Higgs boson. Since the dominant decay channel $H^+ \to t\bar{b}$ is already open for $M_{H^\pm} \simeq 300$ GeV [although still slightly suppressed by phase space], the charged Higgs decay width into standard particles is rather large and it increases only by a factor of ~ 4 when increasing the pseudoscalar mass to $M_A = 600$ GeV. The situation for the supersymmetric decays is quite similar for the two masses: the chargino/neutralinos decay modes have branching ratios of the order of a few ten percent, while the branching ratios for the decays into sleptons, when kinematically allowed, do not exceed the level of a few percent, as expected. Only the decay $H^+ \to \tilde{t}_1 \tilde{b}_1$, the only squark decay mode allowed by phase space [see Fig.3c] for relatively low values of $m_{1/2}$, is competitive with the $t\bar{b}$ decay mode.

The decay widths of the charged Higgs into the various combinations of charginos and neutralinos are shown in Fig.8b for $M_{H^{\pm}} \sim 600$ GeV. The dominant channels are again decays into mixtures of gauginos and higgsinos, since $|\mu|$ is large. The pattern follows approximately the rules of eq.(4.22), modulo phase suppression.

As discussed in section 2, since the chargino, neutralino and sfermion masses scale as M_A , the situation for even larger values of the pseudoscalar Higgs boson mass, $M_A \sim 1$ TeV, will be qualitatively similar to what has been discussed for $M_A \sim 600$ GeV. The only exception is that there will be slightly more phase space available for the supersymmetric decays to occur.

5. Final Decay Products of the Higgs Bosons

In this section, we will qualitatively describe the final decay products of the produced Higgs bosons. Assuming that M_A is large, $M_A \gtrsim 500$ GeV, the decays into standard particles [and more precisely, the $t\bar{t}$ for the neutral and the $t\bar{b}$ decays for the charged Higgs bosons] always have substantial branching ratios, even for the value $tg\beta = 1.75$ which will

be chosen for the discussion. Therefore, to investigate decays into SUSY particles in the main production processes, $e^+e^- \to HA$ and H^+H^- , one has to look for final states where one of the Higgs bosons decays into standard modes while the other Higgs boson decays into charginos, neutralinos or stop squarks. As discussed previously, the decays into the other squarks are disfavored by phase space, while the branching ratios into sleptons are always small and can be neglected.

Let us first discuss the case where one of the Higgs bosons decays into chargino and neutralino pairs,

$$e^+e^- \rightarrow H A \rightarrow [t\bar{t}][\chi^+\chi^-] \text{ and } [t\bar{t}][\chi^0\chi^0]$$

 $e^+e^- \rightarrow H^+H^- \rightarrow [tb][\chi^\pm\chi^0]$ (5.1)

The lightest chargino χ_1^+ and next-to-lightest neutralino χ_2^0 decay into [possibly virtual] W, Z and the lightest Higgs boson h, assuming that decays into sleptons and squarks are kinematically disfavored. In the limit of large $|\mu|$, the decay widths [in the decoupling limit] are proportional to [37]

$$\Gamma(\chi_1^+ \to \chi_1^0 W^+) \sim \sin^2 2\beta$$
 (5.2)

$$\Gamma(\chi_2^0 \to \chi_1^0 Z) \sim \cos^2 2\beta \left[(M_2 - M_1)/2\mu \right]^2$$

$$\Gamma(\chi_2^0 \to \chi_1^0 h) \sim \sin^2 2\beta$$
 (5.3)

In most of the parameter space, the W/Z/h are virtual [in addition to the three–body phase space factors, the decay widths are suppressed by powers of M_2M_Z/μ^2] except near the upper values of $m_{1/2}$. In the case of χ_2^0 , the channel $\chi_2^0 \to \chi_1^0 Z$ mode is always dominant although suppressed by additional powers of M_2^2/μ^2 compared to the $\chi_2^0 \to h \chi_1^0$ mode, since both h and Z are off–shell, and the Z boson width is much larger than the width of the h boson for small values of $\mathrm{tg}\beta$. The radiative decay $\chi_2^0 \to \chi_1^0 \gamma$ should play a marginal role except for very small values of $m_{1/2}$ where the difference between the χ_2^0 and Z boson masses becomes too large.

For large values of $m_{1/2}$, the sleptons become rather light compared to the gauginos and the decays of the light chargino and neutralino into leptons+sleptons are kinematically possible. In this case, these cascade decays become dominant since the partial widths for large $|\mu|$ are given by

$$\sum_{l} \Gamma(\chi_2^0 \to l\tilde{l}) = \sum_{l} 2\Gamma(\chi_1^{\pm} \to l\tilde{\nu}) = \frac{3G_F^2 M_W^2}{\sqrt{2}\pi} M_2$$
 (5.4)

and therefore not suppressed by powers of $M_Z M_2/\mu^2$, unlike the previous decay modes [we assume of course that there is no suppression by phase–space]. The sleptons will then decay into the LSP and massless leptons, leading to multi–lepton final states.

The heavier chargino, in the absence of squark and slepton decay modes, will decay preferentially into the lightest chargino and neutralinos plus gauge or light Higgs bosons.

The decay widths, in units of $G_F M_W^2 |\mu|/(8\sqrt{2}\pi)$ may be approximated in the decoupling limit by [37]

$$\chi_{2}^{+} \rightarrow \chi_{1}^{+}Z : \Gamma = 1$$

$$\rightarrow \chi_{1}^{+}h : \Gamma = 1$$

$$\rightarrow \chi_{1}^{0}W^{+} : \Gamma = \tan^{2}\theta_{W}$$

$$\rightarrow \chi_{2}^{0}W^{+} : \Gamma = 1$$
(5.5)

The branching ratios for the various final states are roughly equal. Since χ_2^+ is almost higgsino-like, the decay widths into sleptons and partners of the light quarks, when kinematically allowed, are extremely small since they are suppressed by powers of m_f^2/M_Z^2 . Because of the large m_t value, only the decays into stop squarks and bottom quarks will be very important. This decay is allowed in most of the parameter space for $M_A \gtrsim 600$ GeV and, up to suppression by mixing angles, it is enhanced by a power m_t^2 [37]

$$\frac{\Gamma(\chi_2^+ \to \tilde{t}b)}{\Gamma(\chi_2^+ \to W, Z, h)} \sim \frac{3m_t^2}{M_W^2} \frac{1}{\sin^2 \beta (3 + \tan^2 \theta_W)} \sim 4$$
 (5.6)

compared to the other decays. Therefore, when kinematically possible, this decay will be the dominant decay mode of the heavy charginos.

For the heavier neutralinos, $\chi_{3,4}^0$, the decay widths into W/Z/h bosons, again in units of $G_F M_W^2 |\mu|/(8\sqrt{2}\pi)$ may be be written in the decoupling limit as [37]

$$\chi_{3/4}^{0} \rightarrow \chi_{1}^{0}Z : \Gamma = \frac{1}{2} \tan^{2} \theta_{W} (1 \pm \sin 2\beta)$$

$$\rightarrow \chi_{1}^{0}h : \Gamma = \frac{1}{2} \tan^{2} \theta_{W} (1 \mp \sin 2\beta)$$

$$\rightarrow \chi_{2}^{0}Z : \Gamma = \frac{1}{2} (1 \pm \sin 2\beta)$$

$$\rightarrow \chi_{2}^{0}h : \Gamma = \frac{1}{2} (1 \mp \sin 2\beta)$$

$$\rightarrow \chi_{1}^{+}W^{-} : \Gamma = 2$$

$$(5.7)$$

The dominant mode is the charged decay, $\chi_{3,4}^0 \to \chi_1^+ W^-$, followed by the modes involving the h(Z) boson for $\chi_4^0(\chi_3^0)$. Because $\sin 2\beta \sim 1$, only one of the h or Z decay channels is important. Here again, because of the higgsino nature of the two heavy neutralinos, the decay widths into sleptons and the scalar partners of the light quarks are negligible; the only important decays are the stop decays, $\chi_{3,4}^0 \to t\tilde{t}_1$, when they are allowed kinematically [i.e. for not too large values of $m_{1/2}$]. The ratio between stop and W/Z/h decay widths, up to suppression by mixing angles, is also given by eq.(5.6), and the stop decays will therefore dominate.

We now turn to the case where one of the produced Higgs particles decays into stop squarks

$$e^+e^- \rightarrow HA \rightarrow [t\bar{t}][\tilde{t}_1\tilde{t}_1] \text{ and } [t\bar{t}][\tilde{t}_1\tilde{t}_2]$$

$$e^+e^- \rightarrow H^+H^- \rightarrow [tb][\tilde{t}_1\tilde{b}_1]$$
 (5.8)

From the squark mass plots, Fig. 3c, the only decay modes of the lightest stop squark allowed by phase space are

$$\tilde{t}_1 \to t \chi_1^0 \ , \ t \chi_2^0 \ , \ b \chi_1^+$$
 (5.9)

Only the last decay mode occurs for relatively small values of $m_{1/2}$, since $m_{\tilde{t}_1} < m_t + m_{\chi_{1,2}^0}$ in this case. For larger values of $m_{1/2}$, \tilde{t}_1 is heavy enough to decay into top quarks plus the lightest neutralinos. For these $m_{1/2}$ values, the three decay modes of eq.(5.9) will have approximately the same magnitude since the chargino and the neutralinos are gaugino–like and there is no enhancement due to the top mass for the $\tilde{t}_1 \to t\chi^0$ decays.

The heavier stop squark, in addition to the previous modes, has decay channels with \tilde{t}_1 and Z/h bosons in the final state

$$\tilde{t}_2 \to \tilde{t}_1 Z$$
 , $\tilde{t}_1 h$ (5.10)

These decays, in particular the decay into the lightest Higgs boson h, will be dominant in the large $|\mu|$ limit, since they will be enhanced by powers of μ^2 .

Appendix A: Chargino and Neutralino Masses and Couplings

In this Appendix we collect the analytical expressions of the chargino and neutralino masses and couplings, and we discuss the limit in which the Higgs-higgsino mass parameter $|\mu|$ is large.

The general chargino mass matrix [18],

$$\mathcal{M}_C = \begin{bmatrix} M_2 & \sqrt{2}M_W \sin \beta \\ \sqrt{2}M_W \cos \beta & \mu \end{bmatrix}$$
 (A1)

is diagonalized by two real matrices U and V,

$$U^* \mathcal{M}_C V^{-1} \rightarrow U = \mathcal{O}_- \text{ and } V = \begin{cases} \mathcal{O}_+ & \text{if } \det \mathcal{M}_C > 0\\ \sigma \mathcal{O}_+ & \text{if } \det \mathcal{M}_C < 0 \end{cases}$$
 (A2)

where σ is the matrix

$$\sigma = \begin{bmatrix} \pm 1 & 0 \\ 0 & \pm 1 \end{bmatrix} \tag{A3}$$

with the appropriate signs depending upon the values of M_2 , μ , and $\tan \beta$ in the chargino mass matrix. \mathcal{O}_{\pm} is given by:

$$\mathcal{O}_{\pm} = \begin{bmatrix} \cos \theta_{\pm} & \sin \theta_{\pm} \\ -\sin \theta_{\pm} & \cos \theta_{\pm} \end{bmatrix}$$
 (A4)

with

$$\tan 2\theta_{-} = \frac{2\sqrt{2}M_{W}(M_{2}\cos\beta + \mu\sin\beta)}{M_{2}^{2} - \mu^{2} - 2M_{W}^{2}\cos\beta}$$

$$\tan 2\theta_{+} = \frac{2\sqrt{2}M_{W}(M_{2}\sin\beta + \mu\cos\beta)}{M_{2}^{2} - \mu^{2} + 2M_{W}^{2}\cos\beta}$$
(A5)

This leads to the two chargino masses, the $\chi_{1,2}^+$ masses

$$m_{\chi_{1,2}^{+}} = \frac{1}{\sqrt{2}} \left[M_2^2 + \mu^2 + 2M_W^2 + \left[(M_2^2 - \mu^2)^2 + 4M_W^4 \cos^2 2\beta + 4M_W^2 (M_2^2 + \mu^2 + 2M_2\mu \sin 2\beta) \right]^{\frac{1}{2}} \right]^{\frac{1}{2}} (A6)$$

In the limit $|\mu| \gg M_2, M_Z$, the masses of the two charginos reduce to

$$m_{\chi_1^+} \simeq M_2 - \frac{M_W^2}{\mu^2} (M_2 + \mu \sin 2\beta)$$

 $m_{\chi_2^+} \simeq |\mu| + \frac{M_W^2}{\mu^2} \epsilon_\mu (M_2 \sin 2\beta + \mu)$ (A7)

where ϵ_{μ} is for the sign of μ . For $|\mu| \to \infty$, the lightest chargino corresponds to a pure wino state with mass $m_{\chi_1^+} \simeq M_2$, while the heavier chargino corresponds to a pure higgsino state with a mass $m_{\chi_1^+} = |\mu|$.

In the case of the neutralinos, the four-dimensional neutralino mass matrix depends on the same two mass parameters μ and M_2 , if the GUT relation $M_1 = \frac{5}{3} \tan^2 \theta_W M_2 \simeq \frac{1}{2} M_2$ [18] is used. In the $(-i\tilde{B}, -i\tilde{W}_3, \tilde{H}_1^0, \tilde{H}_2^0)$ basis, it has the form

$$\mathcal{M}_{N} = \begin{bmatrix} M_{1} & 0 & -M_{Z}s_{W}\cos\beta & M_{Z}s_{W}\sin\beta \\ 0 & M_{2} & M_{Z}c_{W}\cos\beta & -M_{Z}c_{W}\sin\beta \\ -M_{Z}s_{W}\cos\beta & M_{Z}c_{W}\cos\beta & 0 & -\mu \\ M_{Z}s_{W}\sin\beta & -M_{Z}c_{W}\sin\beta & -\mu & 0 \end{bmatrix}$$
(A8)

It can be diagonalized analytically [38] by a single real matrix Z; the [positive] masses of the neutralino states $m_{\chi_i^0}$ are given by

$$\epsilon_{1} m_{\chi_{1}^{0}} = C_{1} - \left(\frac{1}{2}a - \frac{1}{6}C_{2}\right)^{1/2} + \left[-\frac{1}{2}a - \frac{1}{3}C_{2} + \frac{C_{3}}{(8a - 8C_{2}/3)^{1/2}}\right]^{1/2}
\epsilon_{2} m_{\chi_{2}^{0}} = C_{1} + \left(\frac{1}{2}a - \frac{1}{6}C_{2}\right)^{1/2} - \left[-\frac{1}{2}a - \frac{1}{3}C_{2} - \frac{C_{3}}{(8a - 8C_{2}/3)^{1/2}}\right]^{1/2}
\epsilon_{3} m_{\chi_{3}^{0}} = C_{1} - \left(\frac{1}{2}a - \frac{1}{6}C_{2}\right)^{1/2} - \left[-\frac{1}{2}a - \frac{1}{3}C_{2} + \frac{C_{3}}{(8a - 8C_{2}/3)^{1/2}}\right]^{1/2}
\epsilon_{4} m_{\chi_{4}^{0}} = C_{1} + \left(\frac{1}{2}a - \frac{1}{6}C_{2}\right)^{1/2} + \left[-\frac{1}{2}a - \frac{1}{3}C_{2} - \frac{C_{3}}{(8a - 8C_{2}/3)^{1/2}}\right]^{1/2}$$
(A9)

where $\epsilon_i = \pm 1$; the coefficients C_i and a are given by

$$C_{1} = (M_{1} + M_{2})/4$$

$$C_{2} = M_{1}M_{2} - M_{Z}^{2} - \mu^{2} - 6C_{1}^{2}$$

$$C_{3} = 2C_{1} \left[C_{2} + 2C_{1}^{2} + 2\mu^{2} \right] + M_{Z}^{2} (M_{1}c_{W}^{2} + M_{2}s_{W}^{2}) - \mu M_{Z}^{2} \sin 2\beta$$

$$C_{4} = C_{1}C_{3} - C_{1}^{2}C_{2} - C_{1}^{4} - M_{1}M_{2}\mu^{2} + (M_{1}c_{W}^{2} + M_{2}s_{W}^{2})M_{Z}^{2}\mu \sin 2\beta$$
(A10)

and

$$a = \frac{1}{2^{1/3}} \text{Re} \left[S + i \left(\frac{D}{27} \right)^{1/2} \right]^{1/3}$$
 (A11)

with

$$S = C_3^2 + \frac{2}{27}C_2^3 - \frac{8}{3}C_2C_4$$

$$D = \frac{4}{27}(C_2^2 + 12C_4)^3 - 27S^2$$
(A12)

In the limit of large $|\mu|$ values, the masses of the neutralino states simplify to

$$m_{\chi_1^0} \simeq M_1 - \frac{M_Z^2}{\mu^2} (M_1 + \mu \sin 2\beta) s_W^2$$

$$m_{\chi_2^0} \simeq M_2 - \frac{M_Z^2}{\mu^2} (M_2 + \mu \sin 2\beta) c_W^2$$

$$m_{\chi_3^0} \simeq |\mu| + \frac{1}{2} \frac{M_Z^2}{\mu^2} \epsilon_\mu (1 - \sin 2\beta) \left(\mu + M_2 s_W^2 + M_1 c_W^2\right)$$

$$m_{\chi_4^0} \simeq |\mu| + \frac{1}{2} \frac{M_Z^2}{\mu^2} \epsilon_\mu (1 + \sin 2\beta) \left(\mu - M_2 s_W^2 - M_1 c_W^2\right)$$
(A13)

Again, for $|\mu| \to \infty$, two neutralinos are pure gaugino states with masses $m_{\chi_1^0} \simeq M_1$, $m_{\chi_2^0} = M_2$, while the two others are pure higgsino states, with masses $m_{\chi_3^0} \simeq m_{\chi_4^0} \simeq |\mu|$.

The matrix elements of the diagonalizing matrix, Z_{ij} with i, j = 1, ..4, are given by

$$Z_{i1} = \left[1 + \left(\frac{Z_{i2}}{Z_{i1}}\right)^{2} + \left(\frac{Z_{i3}}{Z_{i1}}\right)^{2} + \left(\frac{Z_{i4}}{Z_{i1}}\right)^{2}\right]^{-1/2}$$

$$\frac{Z_{i2}}{Z_{i1}} = -\frac{1}{\tan \theta_{W}} \frac{M_{1} - \epsilon_{i} m_{\chi_{i}^{0}}}{M_{2} - \epsilon_{i} m_{\chi_{i}^{0}}}$$

$$\frac{Z_{i3}}{Z_{i1}} = \frac{\mu(M_{1} - \epsilon_{i} m_{\chi_{i}^{0}})(M_{2} - \epsilon_{i} m_{\chi_{i}^{0}}) - M_{Z}^{2} \sin \beta \cos \beta [(M_{1} - M_{2})c_{W}^{2} + M_{2} - \epsilon_{i} m_{\chi_{i}^{0}}]}{M_{Z}(M_{2} - \epsilon_{i} m_{\chi_{i}^{0}})s_{W}[\mu \cos \beta + \epsilon_{i} m_{\chi_{i}^{0}} \sin \beta)}$$

$$\frac{Z_{i4}}{Z_{i1}} = \frac{-\epsilon_{i} m_{\chi_{i}^{0}}(M_{1} - \epsilon_{i} m_{\chi_{i}^{0}})(M_{2} - \epsilon_{i} m_{\chi_{i}^{0}}) - M_{Z}^{2} \cos^{2} \beta [(M_{1} - M_{2})c_{W}^{2} + M_{2} - \epsilon_{i} m_{\chi_{i}^{0}}]}{M_{Z}(M_{2} - \epsilon_{i} m_{\chi_{i}^{0}})s_{W}[\mu \cos \beta + \epsilon_{i} m_{\chi_{i}^{0}} \sin \beta)}$$

where ϵ_i is the sign of the *i*th eigenvalue of the neutralino mass matrix, which in the large $|\mu|$ limit are: $\epsilon_1 = \epsilon_2 = 1$ and $\epsilon_4 = -\epsilon_3 = \epsilon_{\mu}$.

Appendix B: Sfermion Masses and Mixing

We now present the explicit expressions of the squark and slepton masses. We will assume a universal scalar mass m_0 and gaugino mass $m_{1/2}$ at the GUT scale, and we will neglect the Yukawa couplings in the RGE's [see Appendix C]. For third generation squarks this is a poor approximation since these couplings can be large; these have been taken into account in the numerical analysis.

By performing the RGE evolution to the electroweak scale, one obtains for the left– and right–handed sfermion masses at one–loop order [we include the full two–loop evolution of the masses in the numerical analysis]

$$m_{\tilde{f}_{L,R}}^2 = m_0^2 + \sum_{i=1}^3 F_i(f) m_{1/2}^2 \pm (T_{3f} - e_f s_W^2) M_Z^2 \cos 2\beta$$
 (B1)

 T_{3f} and e_f are the weak isospin and the electric charge of the corresponding fermion f, and F_i are the RGE coefficients for the three gauge couplings at the scale $Q \sim M_Z$, given by

$$F_{i} = \frac{c_{i}(f)}{b_{i}} \left[1 - \left(1 - \frac{\alpha_{G}}{4\pi} b_{i} \log \frac{Q^{2}}{M_{G}^{2}} \right)^{-2} \right]$$
 (B2)

The coefficients b_i , assuming that all the MSSM particle spectrum contributes to the evolution from Q to the GUT scale M_G , are

$$b_1 = 33/5$$
 , $b_2 = 1$, $b_3 = -3$ (B3)

The coefficients $c(\tilde{f}) = (c_1, c_2, c_3)(\tilde{f})$ depend on the hypercharge and color of the sfermions $[F_L = L_L \text{ or } Q_L \text{ is the slepton or squark doublet}]$

$$c(\tilde{L}_L) = \begin{pmatrix} 3/10 \\ 3/2 \\ 0 \end{pmatrix} , c(\tilde{E}_R) = \begin{pmatrix} 6/5 \\ 0 \\ 0 \end{pmatrix}$$

$$c(\tilde{Q}_L) = \begin{pmatrix} 1/30 \\ 3/2 \\ 8/3 \end{pmatrix}, c(\tilde{U}_R) = \begin{pmatrix} 8/15 \\ 0 \\ 8/3 \end{pmatrix}, c(\tilde{D}_R) = \begin{pmatrix} 2/15 \\ 0 \\ 8/3 \end{pmatrix}$$
(B4)

With the input gauge coupling constants at the scale of the Z boson mass

$$\alpha_1(M_Z) \simeq 0.01 \ , \ \alpha_2(M_Z) \simeq 0.033 \ , \ \alpha_3(M_Z) \simeq 0.118$$
 (B5)

one obtains for the GUT scale M_G and for the coupling constant α_G

$$M_G \sim 1.9 \times 10^{16} \text{ GeV}$$
 and $\alpha_G = 0.041$ (B6)

Using these values, and including only gauge loops in the one–loop RGE's, one obtains for the left– and right–handed sfermion masses [39]

$$\begin{split} m_{\tilde{u}_L}^2 &= m_0^2 + 6.28 m_{1/2}^2 + 0.35 M_Z^2 \cos(2\beta) \\ m_{\tilde{d}_L}^2 &= m_0^2 + 6.28 m_{1/2}^2 - 0.42 M_Z^2 \cos(2\beta) \\ m_{\tilde{u}_R}^2 &= m_0^2 + 5.87 m_{1/2}^2 + 0.16 M_Z^2 \cos(2\beta) \\ m_{\tilde{d}_R}^2 &= m_0^2 + 5.82 m_{1/2}^2 - 0.08 M_Z^2 \cos(2\beta) \\ m_{\tilde{\nu}_L}^2 &= m_0^2 + 0.52 m_{1/2}^2 + 0.50 M_Z^2 \cos(2\beta) \\ m_{\tilde{e}_L}^2 &= m_0^2 + 0.52 m_{1/2}^2 - 0.27 M_Z^2 \cos(2\beta) \\ m_{\tilde{e}_R}^2 &= m_0^2 + 0.15 m_{1/2}^2 - 0.23 M_Z^2 \cos(2\beta) \end{split}$$
 (B7)

In the case of the third generation sparticles, left– and right–handed sfermions will mix; for a given sfermion $\tilde{f} = \tilde{t}, \tilde{b}$ and $\tilde{\tau}$, the mass matrices which determine the mixing are

$$\begin{bmatrix} m_{\tilde{f}_L}^2 + m_f^2 & m_f(A_f - \mu r_f) \\ m_f(A_f - \mu r_f) & m_{\tilde{f}_R}^2 + m_f^2 \end{bmatrix}$$
 (B8)

where the sfermion masses $m_{\tilde{f}_{L,R}}$ are given above, m_f are the masses of the partner fermions and $r_b = r_\tau = 1/r_t = \mathrm{tg}\beta$. These matrices are diagonalized by orthogonal matrices with mixing angles θ_f defined by

$$\sin 2\theta_f = \frac{2m_f(A_f - \mu r_f)}{m_{\tilde{f}_1}^2 - m_{\tilde{f}_2}^2} \quad , \quad \cos 2\theta_f = \frac{m_{\tilde{f}_L}^2 - m_{\tilde{f}_R}^2}{m_{\tilde{f}_1}^2 - m_{\tilde{f}_2}^2} \tag{B9}$$

and the masses of the squark eigenstates given by

$$m_{\tilde{f}_{1,2}}^2 = m_f^2 + \frac{1}{2} \left[m_{\tilde{f}_L}^2 + m_{\tilde{f}_R}^2 \mp \sqrt{(m_{\tilde{f}_L}^2 - m_{\tilde{f}_R}^2)^2 + 4m_f^2 (A_f - \mu r_f)^2} \right].$$
 (B10)

Appendix C: Renormalization Group Equations

Finally, we collect for completeness the renormalization group equations for the soft—SUSY breaking parameters [the trilinear couplings, scalar masses as well as for μ and B], including the dependence on A_t , A_b and A_τ . We restrict ourselves to the one–loop RGE's and we keep only the leading terms in the mass hierarchy in the MSSM with three fermion generations. The complete expressions for the RGE's can be found in Refs.[13,19].

For the trilinear couplings of the third generation sfermions, the RGE's are given by

$$\frac{dA_t}{dt} = \frac{2}{16\pi^2} \Big(\sum c_i g_i^2 M_i + 6\lambda_t^2 A_t + \lambda_b^2 A_b \Big)
\frac{dA_b}{dt} = \frac{2}{16\pi^2} \Big(\sum c_i' g_i^2 M_i + 6\lambda_b^2 A_b + \lambda_t^2 A_t + \lambda_\tau^2 A_\tau \Big)
\frac{dA_\tau}{dt} = \frac{2}{16\pi^2} \Big(\sum c_i'' g_i^2 M_i + 3\lambda_b^2 A_b + 4\lambda_\tau^2 A_\tau \Big)$$
(C1)

while for the scalar masses of the third generation sfermions, one has

$$\frac{dM_{Q_L}^2}{dt} = \frac{2}{16\pi^2} \left(-\frac{1}{15} g_1^2 M_1^2 - 3g_2^2 M_2^2 - \frac{16}{3} g_3^2 M_3^2 + \lambda_t^2 X_t + \lambda_b^2 X_b \right)
\frac{dM_{t_R}^2}{dt} = \frac{2}{16\pi^2} \left(-\frac{16}{15} g_1^2 M_1^2 - \frac{16}{3} g_3^2 M_3^2 + 2\lambda_t^2 X_t \right)
\frac{dM_{b_R}^2}{dt} = \frac{2}{16\pi^2} \left(-\frac{4}{15} g_1^2 M_1^2 - \frac{16}{3} g_3^2 M_3^2 + 2\lambda_b^2 X_b \right)
\frac{dM_{L_L}^2}{dt} = \frac{2}{16\pi^2} \left(-\frac{3}{5} g_1^2 M_1^2 - 3g_2^2 M_2^2 + \lambda_\tau^2 X_\tau \right)
\frac{dM_{\tau_R}^2}{dt} = \frac{2}{16\pi^2} \left(-\frac{12}{5} g_1^2 M_1^2 + 2\lambda_\tau^2 X_\tau \right) \tag{C2}$$

The evolution parameter is defined by $t = \log(Q/M_G)$,

$$b_{i} = (33/5, 1, -3)$$

$$c_{i} = (13/15, 3, 16/3)$$

$$c'_{i} = (7/15, 3, 16/3)$$

$$c''_{i} = (9/5, 3, 0)$$
(C3)

and

$$X_{t} = M_{Q_{L}}^{2} + M_{t_{R}}^{2} + M_{H_{2}}^{2} + A_{t}^{2}$$

$$X_{b} = M_{Q_{L}}^{2} + M_{b_{R}}^{2} + M_{H_{1}}^{2} + A_{b}^{2}$$

$$X_{\tau} = M_{L_{L}}^{2} + M_{\tau_{R}}^{2} + M_{H_{1}}^{2} + A_{\tau}^{2}$$
(C4)

For the first and second generation sfermions, these expressions reduce to

$$\frac{dA_u}{dt} = \frac{2}{16\pi^2} \Big(\sum c_i g_i^2 M_i + \lambda_t^2 A_t \Big)
\frac{dA_d}{dt} = \frac{2}{16\pi^2} \Big(\sum c_i' g_i^2 M_i + \lambda_b^2 A_b + \frac{1}{3} \lambda_\tau^2 A_\tau \Big)
\frac{dA_e}{dt} = \frac{2}{16\pi^2} \Big(\sum c_i'' g_i^2 M_i + \lambda_b^2 A_b + \frac{1}{3} \lambda_\tau^2 A_\tau \Big)$$
(C5)

and

$$\frac{dM_{q_L}^2}{dt} = \frac{2}{16\pi^2} \left(-\frac{1}{15} g_1^2 M_1^2 - 3g_2^2 M_2^2 - \frac{16}{3} g_3^2 M_3^2 \right)
\frac{dM_{u_R}^2}{dt} = \frac{2}{16\pi^2} \left(-\frac{16}{15} g_1^2 M_1^2 - \frac{16}{3} g_3^2 M_3^2 \right)
\frac{dM_{d_R}^2}{dt} = \frac{2}{16\pi^2} \left(-\frac{4}{15} g_1^2 M_1^2 - \frac{16}{3} g_3^2 M_3^2 \right)
\frac{dM_{l_L}^2}{dt} = \frac{2}{16\pi^2} \left(-\frac{3}{5} g_1^2 M_1^2 - 3g_2^2 M_2^2 \right)
\frac{dM_{e_R}^2}{dt} = \frac{2}{16\pi^2} \left(-\frac{12}{5} g_1^2 M_1^2 \right)$$
(C6)

For the gauge coupling constants and the other soft–SUSY breaking parameters, the RGE's are given by

$$\frac{dg_i}{dt} = \frac{1}{16\pi^2} b_i g_i^3 \tag{C7}$$

$$\frac{dM_i}{dt} = \frac{2}{16\pi^2} b_i g_i^2 M_i \tag{C8}$$

$$\frac{dB}{dt} = \frac{2}{16\pi^2} \left(\frac{3}{5} g_1^2 M_1 + 3g_2^2 M_2 + 3\lambda_b^2 A_b + 3\lambda_t^2 A_t + \lambda_\tau^2 A_\tau \right)$$
 (C9)

$$\frac{d\mu}{dt} = \frac{\mu}{16\pi^2} \left(-\frac{3}{5}g_1^2 - 3g_2^2 + 3\lambda_t^2 + 3\lambda_b^2 + \lambda_\tau^2 \right)$$
 (C10)

$$\frac{dm_{H_1}^2}{dt} = \frac{2}{16\pi^2} \left(-\frac{3}{5}g_1^2 M_1^2 - 3g_2^2 M_2^2 + 3\lambda_b^2 X_b + \lambda_\tau^2 X_\tau \right)$$
 (C11)

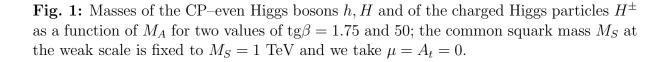
$$\frac{dm_{H_2}^2}{dt} = \frac{2}{16\pi^2} \left(-\frac{3}{5}g_1^2 M_1^2 - 3g_2^2 M_2^2 + 3\lambda_t^2 X_t \right) \tag{C12}$$

References

- [1] J. Wess and B. Zumino, Phys. Lett. B49 (1974) 52.
- [2] For reviews on supersymmetric theories, see P. Fayet and S. Ferarra, Phys. Rep. 32 (1977) 249; H. P. Nilles, Phys. Rep. 110 (1984) 1. R. Barbieri, Riv. Nuovo Cimento 11 (1988) 1; H. Haber and G. Kane, Phys. Rep. 117 (1985) 75.
- [3] P. W. Higgs, Phys. Rev. Lett. 12 (1964) 132 and Phys. Rev. 145 (1966) 1156; F. Englert and R. Brout, Phys. Rev. Lett. 13 (1964) 321; G. S. Guralnik, C. R. Hagen and T. W. Kibble, Phys. Rev. Lett. 13 (1964) 585.
- [4] For a review on the Higgs sector in the MSSM, see J.F. Gunion, H.E. Haber, G. Kane and S. Dawson, The Higgs Hunter's Guide, Addison-Wesley, Reading 1990.
- [5] H. Georgi, H. Quinn and S. Weinberg, Phys. Rev. Lett. 33 (1974) 451.
- [6] J. Ellis, S. Kelley and D. V. Nanopoulos, Phys. Lett. 260B (1991) 131; U. Amaldi, W. de Boer and H. Fürstenau, Phys. Lett. 260B (1991) 447; P. Langacker and M. Luo, Phys. Rev. D44 (1991) 817; G. G. Ross and R. G. Roberts, Nucl. Phys. B377 (1992) 571.
- [7] The LEP Electroweak Working Group, Report CERN-PPE/95-172.
- [8] K. Inoue, A. Kakuto, H. Komatsu and S. Takeshita, Prog. Theor. Phys. 68 (1982) 927; 71 (1984) 413; L. E. Ibañez and G. G. Ross, Phys. Lett. B110 (1982) 215; L. Alvarez-Gaumé, M. Claudson and M. B. Wise, Nucl. Phys. B207 (1982) 96; J. Ellis, D. V. Nanopoulos, and K. Tamvakis, Phys. Lett. B121 (1983) 123; M. Drees, Phys. Rev. D38 (1988) 718.

- [9] J. Ellis, L. Fogli and M. Lisi, Z. Phys. C69 (1996) 627; P. Chankowski and S. Pokorski, Phys. Lett. B356 (1995) 307.
- [10] M. Veltman, Nucl. Phys. **B123** (1977) 89.
- [11] M. Chanowitz, J. Ellis and M. Gaillard, Nucl. Phys. 128 (1977) 506.
- [12] B. Pendleton and G. G. Ross, Phys. Lett. 98B (1981) 291; C. T. Hill, Phys. Rev. D24 (1981) 691.
- [13] V. Barger, M.S. Berger, and P. Ohmann, Phys. Rev. **D47**, (1993) 1093.
- [14] V. Barger, M.S. Berger, P. Ohmann, and R.J.N. Phillips, Phys. Lett. B314 (1993)
 351; M. Carena, S. Pokorski, and C. E. M. Wagner, Nucl. Phys. B406 (1993) 59.
- [15] F. Abe et al., CDF Coll., Phys. Rev. Lett. 74 (1995) 2626; S. Abachi et al., DO Coll., Phys. Rev. Lett. 74 (1995) 2632; F. Abe et al., CDF Coll., FNAL-PUB-96/004.
- [16] H.E. Haber, Report CERN-TH/95-109, Proceedings Conference on Beyond the Standard Model IV, Lake Tahoe CA 1994; World Sci., J.F. Gunion et al., eds.
- [17] Y. Okada, M. Yamaguchi and T. Yanagida, Prog. Theor. Phys. 85 (1991) 1; H.E. Haber and R. Hempfling, Phys. Rev. Lett. 66 (1991) 1815; J. Ellis, G. Ridolfi and F. Zwirner, Phys. Lett. 257B (1991) 83; R. Barbieri, F. Caravaglios and M. Frigeni, Phys. Lett. 258B (1991) 167.
- [18] H.E. Haber and G. Kane in Ref.[2].
- [19] V. Barger, M. S. Berger, and P. Ohmann, Phys. Rev. **D49**, (1994) 4908.
- [20] W. de Boer et al., IEKP-KA/96-04, hep-ph/9603350.
- [21] F. M. Borzumati, M. Olechowski, and S. Pokorski, Phys. Lett. B349, 311 (1995);
 H. Murayama, M. Olechowski, and S. Pokorski, UCB-PTH-95/34, hep-ph/9510327.
- [22] M. Drees and M. Nojiri, Nucl. Phys. **B369** (1992) 54.
- $[23]\,$ S. Bethke, Proceedings of the QCD 1994, Montpellier 1994.
- [24] J.-F. Grivaz, Proc. Europhysics Conference on High Energy Physics, Brussels 1995; for the recent limits including LEP1.5 data, see: D. Buskulic et al., Aleph Collab. CERN-PPE-96-010; G. Alexander et al., OPAL Collab. CERN-PPE-019, 020; M. Acciarri et al., L3 Collab. CERN-PPE-96-029.
- [25] J. Ellis, G. Ridolfi, and F. Zwirner, Phys. Lett. **B262**, 477 (1991); A. Brignole,
 J. Ellis, G. Ridolfi, and F. Zwirner, Phys. Lett. **B271**, 123 (1991).

- [26] M. Drees, Phys. Lett. B181, (1986) 279; J. S. Hagelin and S. Kelley, Nucl. Phys. B342, (1990) 95.
- [27] A. Djouadi, G. Girardi, W. Hollik, F. Renard and C. Verzegnassi, Nucl. Phys. B349 (1991) 48; M. Boulware and D. Finnell, Phys. Rev. D44 (1991) 2054.
- [28] See for instance W. Hollik, Proc. Europhysics Conference on High Energy Physics, Brussels 1995; J. D. Wells, C. Kolda, and G. L. Kane Phys. Lett. B338 (1994) 219.
- [29] G. Kane, C. Kolda, L. Roszkowski, and J. D. Wells, Phys. Rev. **D49**, (1994) 6173.
- [30] A. J. Buras, M. Misiak, M. Münz, and S. Pokorski, Nucl. Phys. **B424**, (1994) 374.
- [31] V. Barger, M. S. Berger, P. Ohmann and R. J. N. Phillips, Phys. Rev. **D51**, (1995) 2438; B. de Carlos and J. A. Casas, Phys. Lett. **B349**, (1995) 300, erratum *ibid*. **351**, (1995) 604.
- [32] A. Djouadi, J. Kalinowski and P. M. Zerwas, Z. Phys. C57, (1993) 569.
- [33] A. Djouadi, J. Kalinowski and P. M. Zerwas, Z. Phys. C70 (1996) 435.
- [34] A. Djouadi, M. Spira and P. M. Zerwas, Z. Phys. C70 (1996) 427.
- [35] J.F. Gunion and H.E. Haber, Nucl. Phys. B272 (1986) 1; B278 (1986) 449; B307 (1988) 445; erratum hep-ph/9301201.
- [36] A. Bartl et al., Phys. Lett. **B373** (1996) 117.
- [37] J.F. Gunion and H.E. Haber, Phys. Rev. **D37** (1988) 2515.
- [38] M. El Kheishen, A. Shafik and A. Aboshousha, Phys. Rev. **D45** (1992) 4345.
- [39] L. E. Ibañez and and C. Lopez, Nucl. Phys. **B233** (1984) 511.



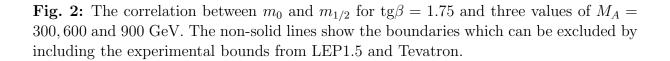


Fig. 3a: The masses of the Higgs bosons as a function of $m_{1/2}$ for $tg\beta=1.75$, for the two values $m_0=100$ and 500 GeV and both signs of μ .

Fig. 3b: The masses of the two charginos (dashed lines) and the four neutralinos (solid lines) as a function of $m_{1/2}$ for $\mathrm{tg}\beta=1.75,\,M_A=300$ and 600 GeV and for both signs of μ . The chargins/neutralinos are ordered with increasing masses. 66

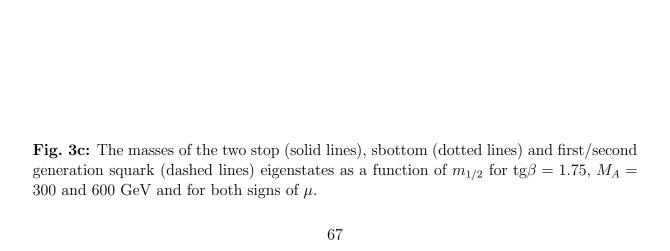


Fig. 3d: The masses of the charged sleptons (solid and dotted lines) and the sneutrino (dashed lines) of the three generations as a function of $m_{1/2}$ for $\mathrm{tg}\beta=1.75,\ M_A=300$ and 600 GeV and for both signs of μ .

Fig. 4: The correlation between m_0 and $m_{1/2}$ for $\mathrm{tg}\beta \simeq 50$, $\mu < 0$, and two values of $M_A = 300$ and 600 GeV. The boundary contours correspond to tachyonic solutions, $m_{\tilde{\tau}}^2 < 0$, $M_A^2 < 0$ and $M_h^2 < 0$ at the tree–level.

Fig. 5a: Cross sections for the pair production processes $e^+e^- \to HA$ and $e^+e^- \to H^+H^-$ as a function of \sqrt{s} for $\mathrm{tg}\beta=1.75$ (solid lines) and $\mathrm{tg}\beta=50$ (dashed lines) and three values of $M_A=300,600$ and 900 GeV.

Fig. 5b: Cross sections for the production processes $e^+e^- \to HZ$, $e^+e^- \to hA$ and $e^+e^- \to H\nu\bar{\nu}$ as a function of \sqrt{s} for $\mathrm{tg}\beta=1.75$ and the values $M_A=300$ and 600 GeV.

Fig. 6a: Decay widths (in GeV) of the heavy CP–even Higgs boson H into charginos and neutralinos (dotted lines), squarks (dashed lines), sleptons (dash–dotted lines), standard particles (dott–long–dashed lines) and the total decay widths (solid lines) as a function of $m_{1/2}$ for $\mathrm{tg}\beta=1.75,\ M_A=300$ and 600 GeV and for both signs of μ .

Fig. 6b: Partial decay widths (in GeV) of the heavy CP–even Higgs boson H into all combinations of chargino and neutralino pairs $[ij \equiv \chi_i \chi_j]$ as a function of $m_{1/2}$ for $tg\beta = 1.75$, $M_A = 600$ GeV and for both signs of μ .

Fig. 6c: Partial decay widths (in GeV) of the heavy CP–even Higgs boson H into stop and sbottom squarks and into slepton pairs as a function of $m_{1/2}$ for $\mathrm{tg}\beta=1.75,\,M_A=600$ GeV and for both signs of μ .

Fig. 7a: Decay widths (in GeV) of the pseudoscalar Higgs boson A into charginos and neutralinos (dotted lines), stop squarks (dashed lines), standard particles (dott-long-dashed lines) and the total decay widths (solid lines) as a function of $m_{1/2}$ for $\mathrm{tg}\beta=1.75$, $M_A=300$ and 600 GeV and for both signs of μ .

Fig. 7b: Partial decay widths (in GeV) of the pseudoscalar Higgs boson A into all combinations of chargino and neutralino pairs $[ij \equiv \chi_i \chi_j]$ as a function of $m_{1/2}$ for $tg\beta = 1.75$, $M_A = 600$ GeV and for both signs of μ .

Fig. 8a: Decay widths (in GeV) of the charged Higgs bosons into charginos and neutralinos (dotted lines), squarks (dashed lines), sleptons (dash–dotted lines), standard particles (dott–long–dashed lines) and the total decay widths (solid lines) as a function of $m_{1/2}$ for $tg\beta=1.75,\ M_A=300$ and 600 GeV and for both signs of μ .

Fig. 8b: Partial decay widths (in GeV) of the charged Higgs boson H^{\pm} into all combinations of charginos and neutralinos $[ij \equiv \chi_i^+ \chi_j^0]$ as a function of $m_{1/2}$ for $\mathrm{tg}\beta = 1.75$, $M_A = 600$ GeV and for both signs of μ .

Production of Heavy Neutral MSSM Higgs Bosons a complete 1-loop calculation.

V. Driesen, W. Hollik and J. Rosiek*

Institut für Theoretische Physik, Universität Karlsruhe, D-76128 Karlsruhe, Germany

Abstract

The complete 1-loop diagrammatic calculations of the cross sections for the neutral Higgs production processes $e^+e^- \to Z^0H^0(Z^0h^0)$ and $e^+e^- \to A^0H^0(A^0h^0)$ in the MSSM are presented and compared the with the corresponding results of the simpler and compact effective potential approximation.

1. Introduction

In order to experimentally detect possible signals of the neutral MSSM Higgs bosons, detailed studies for the decay and production processes of Higgs boson are required. As has been discovered several years ago [1-3], radiative corrections in the MSSM Higgs sector are large and have to be taken into account for phenomenological studies. Three main approaches have been developed to calculate the 1-loop radiative corrections to the MSSM Higgs boson masses, production and decay rates:

- a) The Effective Potential Approach (EPA) [2].
- b) The Renormalization Group approach (RGE) [3].
- c) The diagrammatic calculation in the on-shell renormalization scheme (Feynman Diagram Calculation, FDC) [4,5]: The masses are calculated from the pole positions of the Higgs propagators, and the cross sections are obtained from the full set of 1-loop diagrams contributing to the amplitudes, including [4]:
 - the most general form of the MSSM lagrangian with soft breaking terms,
 - the virtual contributions from all the particles of the MSSM spectrum,
 - all 2-, 3- and 4-point Green's functions for a given process with Higgs particles,
 - the momentum dependence of the Green's functions,
 - the leading reducible diagrams of higher orders corrections.

The experimental searches for Higgs bosons at LEP1 [6] and studies for the future searches at higher energies [7] conventionally make use of the most compact effective potential approximation. We present the complete 1-loop diagrammatic results for the cross sections for the neutral Higgs production processes $e^+e^- \to Z^0H^0(Z^0h^0)$ and $e^+e^- \to A^0H^0(A^0h^0)$, compare them with the corresponding ones of the simpler and compact EPA approximation and discuss the typical size of the differences.

^{*}Supported in part by the Alexander von Humboldt Stiftung and by the Polish Committee for Scientific Research.

2. Outline of the calculations

The tree level potential for the neutral MSSM Higgs bosons can be written as:

$$V^{(0)} = m_1^2 H_1^2 + m_2^2 H_2^2 + \epsilon_{ij} (m_{12}^2 H_1^i H_2^j + H.c.) + \frac{g^2 + g'^2}{8} (H_1^2 - H_2^2)^2 + \frac{g^2}{4} (H_1 H_2)^2$$
 (1)

Diagonalization of the mass matrices following from the potential (1) leads to three physical particles: two CP-even Higgs bosons H^0 , h^0 and one CP-odd Higgs boson A^0 , and defines their tree-level masses m_H , m_h and m_A , with $m_H > m_h$, and the mixing angles α , β . The way of calculating the radiative corrections in the EPA and FDC methods is briefly described as follows:

In the EPA, the tree level potential $V^{(0)}$ is improved by adding the 1-loop terms [2]:

$$V^{(1)}(Q^2) = V^{(0)}(Q^2) + \frac{1}{64\pi^2} \sum_{\substack{quarks \\ squarks}} \text{Str} \mathcal{M}^4 \left(\log \frac{\mathcal{M}^2}{Q^2} - \frac{3}{2} \right)$$
 (2)

Figure 1: Classes of diagrams contributing to the $e^+e^- \to Z^0h^0(H^0)$ process in the FDC approach.

where $V^{(0)}(Q^2)$ is the tree level potential evaluated with couplings renormalized at the scale Q^2 , and Str denotes the supertrace over the third generation of quark and squark fields contributing to the generalized mass matrix \mathcal{M}^2 . The 1-loop potential $V^{(1)}$ is rediagonalized yielding the 1-loop corrected physical masses M_H , M_h and the effective mixing angle α_{eff} (for explicit formulae see [2]).

In the FDC the 1-loop physical Higgs boson masses are obtained as the pole positions of the dressed scalar propagators. M_H^2 and M_h^2 are given by the solution of the equation (3). For the calculations of the cross sections we need the full set of 2-, 3- and 4-point functions. In Fig. 1 the diagrams contributing to the $e^+e^- \to Z^0h^0(H^0)$ process are collected. The diagrams contributing to the $e^+e^- \to A^0h^0(H^0)$ process can be obtained by changing Z^0 into A^0 on the external line and skipping the diagrams i), j).

$$\operatorname{Re}\left[\left(p^{2}-m_{h}^{2}-\Sigma_{hh}(p^{2})\right)\left(p^{2}-m_{H}^{2}-\Sigma_{HH}(p^{2})\right)-\Sigma_{hH}^{2}(p^{2})\right]=0$$
(3)

The formulae for the cross sections obtained in the FDC differ from the Born expressions, because not only the effective masses are corrected but also new form factors and momentum dependent effects are considered (see [4] for a detailed description).

3. Results on production cross sections

In this section we present the results for $Z^0H^0(Z^0h^0)$ and $A^0H^0(A^0h^0)$ production from the FDC and discuss the quality of simpler EPA approximation. In all figures we use as an example the set of parameters listed in Table 1. μ is the parameter describing the Higgs doublet mixing in the MSSM superpotential. M_2 denotes the SU(2) gaugino mass parameter. For the U(1) gaugino mass we use the value $M_1 = \frac{5}{3} \tan^2 \theta_W M_2$, suggested by GUT constraints. M_{sq} , M_{sl} , A_t and A_b are the parameters entering the sfermion mass matrices (for the detailed expressions see e.g. [8]). For simplicity we assume a common value M_{sq} for all generations of squarks, and a common M_{sl} for sleptons.

Parameter	m_t	M_A	M_{sq}	M_{sl}	M_2	μ	$A_t = A_b$
Value (GeV)	175	200	1000	300	1000	500	1000

Table 1: Parameters used for the numerical analysis.

From the theoretical point of view, the most convenient parameters for the Higgs sector are the mass M_A of the CP-odd Higgs boson and the ratio $\tan \beta = \frac{v_2}{v_1}$. From the experimental point of view it is more natural to use, depending on the process considered, the masses M_h or M_H of the CP-even Higgs instead of the formal quantity $\tan \beta$.

As a first step, we apply the conventional M_A , $\tan \beta$ parameterization. Figs. 2 and 3 show the production cross sections for the processes $\sigma(e^+e^- \to Z^0h^0, A^0h^0)$ and $\sigma(e^+e^- \to Z^0H^0, A^0H^0)$ for $\sqrt{s} = 500$ GeV. For the chosen set of parameters the numerical differences can reach 30% at $\sqrt{s} = 500$ GeV. They become more important with

Figure 2: Comparison of the cross sections $\sigma(e^+e^- \to Z^0h^0, A^0h^0)$ obtained in the EPA and FDC. Parameters as given in Table 1, $\sqrt{s} = 500$ GeV.

Figure 3: Comparison of the cross sections $\sigma(e^+e^- \to Z^0H^0, A^0H^0)$ obtained in the EPA and FDC. Parameters as given in Table 1, $\sqrt{s} = 500$ GeV.

increasing energies, exceeding 40% at 1 TeV. Note, however, that in the region of large cross sections the EPA accuracy is better (20% at 500 GeV). More detailed discussion of the lighter CP-even Higgs boson production can be found in ref. [9].

Fig. 4 shows the production cross sections for the processes $\sigma(e^+e^- \to Z^0H^0, A^0H^0)$ as a function of \sqrt{s} . The effect of the additional form factors included in the FDC grows when center-of-mass energy increases. For $\sqrt{s}=1.5$ TeV the differences between FDC and EPA can reach 50% for the $\sigma(e^+e^- \to Z^0H^0)$ production channel. In addition, the angular dependence of the cross section given by the FDC is modified in compare to the effective Born approximation.

We now turn to the more physical parameterization of the cross sections in terms of the two Higgs boson masses M_A and M_h or M_H . This parameterization is more clumsy in the calculations, but it has the advantage of physically well defined input quantities avoiding possible confusions from different renormalization schemes. Varying M_H (M_A and other input quantities fixed) we obtain $\tan \beta$ and σ_{ZH} , σ_{AH} as functions of M_H . For the parameter values given in Table 1, the differences between the $\tan \beta$ values obtained in the EPA and FDC can reach 10% (up to 20% for smaller $M_A \approx 100$ GeV). Also significant differences can occur for the cross sections, as displayed in Fig. 5 where the predictions of EPA and FDC for the σ_{ZH} and σ_{AH} are plotted as functions of M_H . The typical size of differences between the methods is 10-20% for $\sqrt{s} = 500$ GeV, but they may became as large as 60% in case of the process $\sigma(e^+e^- \to Z^0H^0)$. This particularly large deviation occurs for large M_H values, corresponding to small $\tan \beta \leq 1$ (compare Fig. 2).

We have analyzed also the dependence of the differences between the EPA and the FDC predictions on the SUSY parameters: sfermion and gaugino masses, μ parameter and sfermion mixing parameters. In most cases the variation of those parameters does not have a large effect on the size of the differences between the EPA and FDC (a more detailed discussion can be found in ref. [10]).

To give a more global impression of the typical size of the differences between the EPA and FDC results, we have chosen 1000 random points (for each \sqrt{s} value in Table 2) from

the hypercube in the MSSM parameters space with the following bounds:

$$\begin{array}{ll} 0.5 < \tan \beta < 50 & 50 \ {\rm GeV} < M_A < 250 \ {\rm GeV} \\ -500 \ {\rm GeV} < \mu < 500 \ {\rm GeV} & 200 \ {\rm GeV} < M_2 < 1000 \ {\rm GeV} \\ 200 \ {\rm GeV} < M_{sq} = 2M_{sl} < 1000 \ {\rm GeV} & -M_{sq} < A_t = A_b < M_{sq} \end{array}$$

We define the relative differences for the masses and cross sections as follows:

$$\delta X^{EPA} = \frac{X^{FDC} - X^{EPA}}{X^{FDC}}. (4)$$

where X can be chosen as M_h , M_H , σ_{ZH} , σ_{Zh} , σ_{AH} or σ_{Ah} . We calculated the quantities δM_h^{EPA} , δM_H^{EPA} , $\delta \sigma_{Zh}^{EPA}$, $\delta \sigma_{Ah}^{EPA}$, $\delta \sigma_{ZH}^{EPA}$ and $\delta \sigma_{AH}^{EPA}$ and averaged them (and also their absolute values) arithmetically over all generated points of the parameter space. The average mass differences are small and equal $|\delta M_h^{EPA}| = 2\%$ and $|\delta M_H^{EPA}| = 1\%$. The results for the cross sections are summarized in Table 2. It shows that the predictions of both methods deviate in particular for σ_{ZH} .

$\sqrt{s} \; (\text{GeV})$	$\delta\sigma_{Zh}^{EPA}$	$\delta\sigma_{Ah}^{EPA}$	$\delta\sigma_{ZH}^{EPA}$	$\delta\sigma_{AH}^{EPA}$	$ \delta\sigma_{Zh}^{EPA} $	$ \delta\sigma_{Ah}^{EPA} $	$ \delta\sigma_{ZH}^{EPA} $	$ \delta\sigma_{AH}^{EPA} $
500	16.4%	-2.4%	57%	4.4%	21%	31%	62%	14%
1000	10.3%	1.1%	56%	-3.0%	15%	31%	62%	14%
1500	4.2%	4.9%	53%	-9.0%	17%	32%	63%	18%

Table 2: Differences between the EPA and FDC predictions averaged over a random sample of parameters.

Summarizing, comparisons between the FDC predictions with the simpler EPA approximation have shown that at $\sqrt{s} = 500 \text{ GeV}$ the EPA has an accuracy of typically 10-20\% in the parameter regions where the cross sections are large. The differences become larger with increasing energy, where also modifications of the Born-like angular distributions are more visible. The use of the physical input variables M_A , M_h or M_A , M_H avoids ambiguities from the definition of tan β in higher order, but the observed differences remain of the same size. For a better accuracy, the full FDC would be required.

Recently some papers on the leading 2-loop corrections to the CP-even MSSM Higgs boson masses have been published [11]. The main conclusion is that 2-loop corrections are also significant and tend to compensate partially the effects of 1-loop corrections. The calculations are based on the EPA and RG methods. Since the main emphasis of this study is to figure out the difference between complete and approximate results in a given order, we have not implemented the 2-loop terms. They would improve the 1-loop FDC results in the same way as the approximations and thus do not influence the remaining differences which can only be obtained by an explicit diagrammatic calculation.

The library of FORTRAN codes for the calculation of the 1-loop radiative corrections in the on-shell renormalization scheme to the MSSM neutral Higgs production and decay rates [4] can be found at the URL address:

http://itpaxp1.physik.uni-karlsruhe.de/~rosiek/neutral_higgs.html

References

- S. P. Li, M. Sher, Phys. Lett. B140 (1984), 339; J. Gunion, A. Turski, Phys. Rev. D39 (1989) 2701; D40 (1989) 2325, 2333; M. Berger, Phys. Rev. D41 (1990) 225.
- J. Ellis, G. Ridolfi, F. Zwirner, *Phys. Lett.* **262B** (1991) 477; R. Barbieri, M. Frigeni, *Phys. Lett.* **258B** (1991) 395; A. Brignole, J. Ellis, G. Ridolfi, F. Zwirner *Phys. Lett.* **271B** (1991) 123.
- M. Carena, K. Sasaki, C.E.M. Wagner, Nucl. Phys. 381B (1992) 66; H.E. Haber,
 R. Hempfling, Phys. Rev. D48 (1993) 4280; P.H. Chankowski, S. Pokorski, J. Rosiek, Phys. Lett. 281B (1992) 100.
- P. Chankowski, S. Pokorski, J. Rosiek Nucl. Phys. B423 (1994) 437; B423 (1994) 497; V. Driesen, W. Hollik, Z. Phys. C68 (1995) 485.
- 5. A. Brignole, *Phys. Lett.* **281B** (1992) 284.
- ALEPH Collab., D. Buskulic et al., Phys. Lett. 313B (1993), 312; DELPHI Collab.,
 P. Abreu et al., Nucl. Phys. 373B (1992), 3; L3 Collab., O. Adriani et al., Z. Phys.
 57C (1993), 355; OPAL Collab., R. Akers et al., Preprint CERN, PPE/94-104 (1994); J. F. Grivaz, Proc. of the International Europhysics Conference on High Energies, Brussels, July 27 August 2, 1995; preprint LAL-95-83.
- 7. Higgs Physics, M. Carena, P. Zerwas et al., to appear in the Proceedings of LEP2 Workshop, CERN Yellow Report, eds. G. Altarelli et al.; Higgs Particles, in: e^+e^- Collisions at 500 GeV, DESY 92-123A,B,C, ed. P. Zerwas.
- 8. J. Rosiek, Phys. Rev. **D41** (1990) 3464; erratum hep-ph/9511250.
- 9. V. Driesen, W. Hollik, J. Rosiek, hep-ph/9512441, in print in Z. Phys. C.
- 10. J. Rosiek, A. Sopczak, Phys. Lett. **B341** (1994) 419.
- R. Hempfling, A. Hoang, *Phys. Lett.* B331 (1994) 99; M. Carena, J.R. Espinosa,
 M. Quiros, C.E.M. Wagner, *Phys. Lett.* B355 (1995) 209; M. Carena, M. Quiros,
 C.E.M. Wagner, preprint CERN-TH-95-157, hep-ph/9508343.

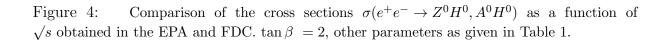


Figure 5: Comparison of the cross sections $\sigma(e^+e^- \to Z^0H^0, A^0H^0)$ as a function of M_H in the EPA and FDC. Parameters as given in Table 1, $\sqrt{s} = 500$ GeV.

Radiative corrections to $e^+e^- \rightarrow H^+H^-$

A. $Arhrib^{1,2}$ and G. $Moultaka^1$

¹ Physique Mathématique et Théorique, E.S.A. du CNRS Nº 5032, Université Montpellier II, F-34095 Montpellier France

² L.P.T.N., Faculté des Sciences Semlalia, B.P. S15, Marrakesh, Morocco

Abstract

We discuss the one-loop electroweak corrections to the pair production of charged Higgs bosons $e^+e^- \to H^+H^-$ in the Minimal Supersymmetric Standard Model.

In contrast to hadronic machines, a high energy e^+e^- collider in the TeV range will be a rather unique place to discover and study charged higgses in a clean environment. These would be produced either in pairs [1], our main concern here, or in associate (rare) production with W^{\pm} . It was first found in [2] that loop corrections from matter fermions and their susy partners (mainly the (t,b), (b,\tilde{t}) sector), are likely to change the tree-level result at $\sqrt{s} = 500$ GeV [1,3], by asmuch as 10% dip in the cross-section. The effect could even lie between -25% and 25% and perhaps grow out of perturbative control, though in a reasonable range of the model-parameters. Such a sensitivity to loop effects appears to be related to the fact that at tree-level the γ and Z mediated process is exclusively controlled by $U_B(1) \times U_{W_3}(1)$ gauge invariance and thus knows nothing about the non-standard extension whatsoever.

The aim of the present study is to improve on the previous one by including: **a)** the complete Higgs sector contributions (self-energies, vertices and boxes), **b)** the infrared part, including initial and final soft photon radiation as well as $\gamma\gamma$ and γZ boxes, **c)** The complete set of charginos/neutralinos/ $\tilde{e}/\tilde{\nu}$ box diagrams, and thus to identify the various origins of large effects, whether in the MSSM or in a type II two-Higgs-doublet model (THDM-II).

It turns out that besides the sensitivity to the heavy quark-squark sector there are, on one hand large effects from the soft photon radiation and on the other, possibly important effects in the purely Higgs sector. The latter case occurs when deviations from the tree-level supersymmetric $H^+H^- - H^0(h^0)$ couplings are allowed bringing in increasingly large effects for increasing values of $\tan \beta$ at a given \sqrt{s} . To quantify such effects we thus allow for a general deviation from the supersymmetric relations among the bare parameters of the Higgs potential as follows:

$$\lambda_{1} = \lambda_{2} + \delta_{12} \qquad , \qquad \lambda_{3} = \frac{1}{8}(g^{2} + g'^{2}) - \lambda_{1} + \delta_{31}$$

$$\lambda_{4} = 2\lambda_{1} - \frac{1}{2}g'^{2} + \delta_{41} \qquad , \qquad \lambda_{5} = -\frac{1}{2}(g^{2} + g'^{2}) + 2\lambda_{1} + \delta_{51}$$

$$\lambda_{6} = -\frac{1}{2}(g^{2} + g'^{2}) + 2\lambda_{1} + \delta_{61}$$

$$(1)$$

The $\lambda_i's$ are as defined in [4] and the (softly broken) susy case corresponds to $\delta_i = 0$. Eq.(1) translates in a definite way into deviations from the MSSM tree-level relations among the higgs masses, $\tan 2\alpha$ and $\tan \beta$, as well as the couplings of the higgs sector, leading to 6 free parameters. However, one can find conditions relating the $\delta's$ in such a way to preserve these relations even in a non-susy case. These conditions which we dub "quasisusy", are certainly not generic but constitute a good ground to test minimal deviations from the MSSM in a simple way, since one then has just one extra free parameter (ex. λ_3) besides $\tan \beta$ and $M_{H^{\pm}}$ in the higgs sector. In quasi-susy the only deviations from the MSSM tree-level triple Higgs couplings that contribute to one-loop order in our case are in $H^+ - H^- - (H^0, h^0)$. For large $\tan \beta$ these couplings behave as:

$$(H^+H^-(H^0, h^0))_{susy} - igM_W(cos(\beta - \alpha)\Delta_{(1,2)} + (1 \mp cos(2\alpha))cos(\alpha)\tan(\beta)\Delta_3$$
 (2)

the $\Delta's$ being functions of the $\delta's$ of eq.(1), and vanish in the MSSM.

Fig.1 illustrates how the Higgs sector contributions can counterbalance those of the heavy quarks found in [2] for large $\tan(\beta)$, but only near threshold. Far from threshold most of the effects become again negative, except for WW boxes. Furthermore the "neutral" model-independent contributions, including soft bremsstrahlung, obtained by adding one photon (or Z) line to the tree diagrams depend loosely on $M_{H^{\pm}}$ or \sqrt{s} and contribute at the level of -17% for $\Delta E_{\gamma} \sim 0.1 E_{beam}$. In Fig.2 we show (excluding those "neutral" contributions) the integrated cross-section for two values of $M_{H^{\pm}}$ and $\tan(\beta)$. In THDM-II the total loop effect increases (negatively) with increasing $\tan(\beta)$, the farther one goes from production threshold. In the MSSM ($\lambda_3 = \lambda_{3susy}$) the leading effects come exclusively from the heavy quark-squark sector and the conclusions of [2] remain unaltered in this case. [For instance the 150 boxes involving $\chi^{\pm}/\chi^0/\tilde{e}/\tilde{\nu}$ largely cancel among each other leading at most to 1-3% effect for a wide range of sparticle masses.]

- 1. S. Komamiya, Phys.Rev. D38 (1988) 2158.
- 2. A. Arhrib, M. Capdequi Peyranere, G. Moultaka Phys.Lett. B 341 (1995) 313;
- 3. A.Brignole et al., in Proceedings of the Workshop on e^+e^- Collisions at 500 GeV: The Physics Potential, ed. P.M.Zerwas, DESY 92-123, p.613; A.Djouadi, J.Kalinowski, P.M.Zerwas, *ibid.* p.83 and Z.Phys.C57 (1993) 569.
- 4. J.F.Gunion and H.E.Haber, Nucl. Phys. B272 (1986) 1.

Fig.1: Contributions in % to the integrated cross section in quasi-susy, $\lambda_3 = -0.61, M_{H^{\pm}} = 220$ i GeV; a) Higgs sector, $\tan \beta = 2$; b) Higgs sector, $\tan \beta = 30$; c) virtual Z, γ and soft bremsstrahlung; d) virtual W boxes; e) matter fermion sector, $m_{top} = 180 GeV$, $\tan \beta = 30$; f) same as e) but with $\tan \beta = 2$.

Fig.2: a) Tree-level, $M_{H^\pm}=220GeV$; b) quasi-susy, $\lambda_3=-0.61$ (MSSM value -0.71), $\tan\beta=30$; c) quasi-susy, $\lambda_3=-0.61$, $\tan\beta=2$; d) Tree-level, $M_{H^\pm}=430GeV$; e) quasi-susy, $\lambda_3=-2.6$ (MSSM value -2.84), $\tan\beta=30$; f) same as e) but with $\tan\beta=2$; $m_{top}=180GeV$.

Multiple Production of \mathcal{MSSM} Neutral Higgs Bosons at High–Energy e^+e^- Colliders

A. DJOUADI^{1,2*}, H.E. HABER³, AND P.M. ZERWAS²

 1 Institute für Theoretische Physik, Universität Karlsruhe, D–76128 Karlsruhe, FRG.

Abstract

The cross sections for the multiple production of the lightest neutral Higgs boson at high–energy e^+e^- colliders are presented in the framework of the Minimal Supersymmetric extension of the Standard Model (\mathcal{MSSM}). We consider production through Higgs–strahlung, associated production of the scalar and the pseudoscalar bosons, and the fusion mechanisms for which we use the effective longitudinal vector–boson approximation. These cross sections allow one to determine trilinear Higgs couplings λ_{Hhh} and λ_{hhh} , which are theoretically determined by the Higgs potential.

1. Introduction

The only unknown parameter in the Standard Model (\mathcal{SM}) is the quartic coupling of the Higgs field in the potential, which determines the value of the Higgs mass. If the Higgs mass is known, the potential is uniquely fixed. Since the form of the Higgs potential is crucial for the mechanism of spontaneous symmetry breaking, *i.e.* for the Higgs mechanism *per se*, it will be very important to measure the coefficients in the potential once Higgs particles have been discovered.

If the mass of the scalar particle is less than about 150 GeV, it very likely belongs to the quintet of Higgs bosons, h, H, A, H^{\pm} predicted in the two-doublet Higgs sector of supersymmetric theories [1] [h and H are the light and heavy CP-even Higgs bosons, A is the CP-odd (pseudoscalar) Higgs boson, and H^{\pm} is the charged Higgs pair]. The potential of the two doublet Higgs fields, even in the Minimal Supersymmetric Standard Model (\mathcal{MSSM}), is much more involved than in the Standard Model [2]. If CP is conserved by the potential, the most general two-doublet model contains three mass parameters and seven real self-couplings. In the \mathcal{MSSM} , the potential automatically

² Deutsches Elektronen-Synchrotron DESY, D-22603 Hamburg, FRG.

³ Santa Cruz Institute for Particle Physics, University of California, Santa Cruz, CA 95064, USA.

^{*}Supported by Deutsche Forschungsgemeinschaft DFG (Bonn).

conserves CP; in addition, supersymmetry fixes all the Higgs self-couplings in terms of gauge couplings. The remaining three free mass parameters can be traded in for the two vacuum expectation values (VEV's) of the neutral Higgs fields and one of the physical Higgs masses. The sum of the squares of the VEV's is fixed by the W mass, while the ratio of VEV's is a free parameter of the model called $\tan \beta$. It is theoretically convenient to choose the free parameters of the \mathcal{MSSM} Higgs sector to be $\tan \beta$ and M_A , the mass of the CP-odd Higgs boson A. The other Higgs masses and the mixing angle α of the CP-even neutral sector are then determined. Moreover, since all coefficients in the Higgs potential are also determined, the trilinear and quartic self-couplings of the physical Higgs particles can be predicted theoretically. By measuring these couplings, the Higgs mechanism as the basic mechanism for generating the masses of the fundamental particles.

The endeavor of measuring all Higgs self-couplings in the \mathcal{MSSM} is a daunting task. We will therefore discuss a first step by analyzing theoretically the production of two light Higgs particles of the \mathcal{MSSM} . These processes may be studied at the proton collider LHC [3] and at a high-energy e^+e^- linear collider. In this paper we will focus on the e^+e^- accelerators that are expected to operate in the first phase at an energy of 500 GeV with a luminosity of about $\mathcal{L} = 20 \text{ fb}^{-1}$, and in a second phase at an energy of about 1.5 TeV with a luminosity of order $\mathcal{L} = 200 \text{ fb}^{-1}$ per annum [4]. They will allow us to eventually study the couplings λ_{Hhh} and λ_{hhh} . The measurement of the coupling λ_{hAA} will be very difficult.

Multiple light Higgs bosons h can [in principle] be generated in the \mathcal{MSSM} by four mechanisms¹:

(i) Decay of the heavy CP-even neutral Higgs boson, produced either by H-strahlung and associated AH pair production, or in the WW fusion mechanisms, Fig. 1a,

$$\begin{cases}
e^+e^- \to ZH, AH \\
e^+e^- \to \nu_e\bar{\nu}_eH
\end{cases} \qquad H \to hh$$
(1)

Associated production $e^+e^- \to hA$ followed by $A \to hZ$ decays leads to hhZ background final states.

(ii) Double Higgs–strahlung in the continuum, with a final state Z boson, Fig. 1b,

$$e^+e^- \to Z^* \to hhZ \tag{2}$$

(iii) Associated production with the pseudoscalar A in the continuum, Fig. 1c,

$$e^+e^- \to Z^* \to hhA$$
 (3)

(iv) Non–resonant WW(ZZ) fusion in the continuum, Fig. 1d,

$$e^+e^- \to \bar{\nu}_e\nu_e W^*W^* \to \bar{\nu}_e\nu_e hh$$
 (4)

¹The production of two light Higgs bosons, $e^+e^- \to hh$, through loop diagrams does not involve any trilinear Higgs coupling; the production rates are rather small [5].

The cross sections for ZZ fusion in (1) and (4) are suppressed by an order of magnitude. The largest cross sections can be anticipated for the processes (1), where heavy on—shell H Higgs bosons decay into pairs of the light Higgs bosons. [Cross sections of similar size are expected for the backgrounds involving the pseudoscalar Higgs bosons.] We have derived the cross sections for the four processes analytically; the fusion process has been treated in the equivalent particle approximation for longitudinal vector bosons.

We will carry out the analysis in the \mathcal{MSSM} for the value $\tan \beta = 1.5$. [A summary will be given in the last section for all values of $\tan \beta$]. In the present exploratory study, squark mixing will be neglected, *i.e.* the supersymmetric Higgs mass parameter μ and the parameter A_t in the soft symmetry breaking interaction will be set to zero, and the radiative corrections will be included in the leading m_t^4 one–loop approximation parameterized by [6]

$$\epsilon = \frac{3G_F}{\sqrt{2}\pi^2 \sin^2 \beta} \log \left(1 + \frac{M_S^2}{m_t^2} \right) \tag{5}$$

with the common squark mass fixed to $M_S = 1$ TeV. In terms of $\tan \beta$ and M_A , the trilinear Higgs couplings relevant for our analysis are given in this approximation by

$$\lambda_{hhh} = 3\cos 2\alpha \sin(\beta + \alpha) + 3\frac{\epsilon}{M_Z^2} \frac{\cos^3 \alpha}{\sin \beta}$$

$$\lambda_{Hhh} = 2\sin 2\alpha \sin(\beta + \alpha) - \cos 2\alpha \cos(\beta + \alpha) + 3\frac{\epsilon}{M_Z^2} \frac{\sin \alpha}{\sin \beta} \cos^2 \alpha$$
(6)

In addition, the coupling

$$\lambda_{hAA} = \cos 2\beta \sin(\beta + \alpha) + \frac{\epsilon}{M_Z^2} \frac{\cos \alpha}{\sin \beta} \cos^2 \beta \tag{7}$$

will be needed even though it turned out – a posteriori – that it cannot be measured using the experimental methods discussed in this note². As usual, these couplings are defined in units of $(2\sqrt{2}G_F)^{1/2}M_Z^2$; the h, H, H^{\pm} masses and the mixing angle α can be expressed in terms of M_A and $\tan \beta$ [see e.g. Ref. [8] for a recent discussion].

In the decoupling limit [9] for large A, H and H^{\pm} masses, the lightest Higgs particle becomes \mathcal{SM} -like and the trilinear hhh coupling approaches the \mathcal{SM} value $\lambda_{hhh} \to M_h^2/M_Z^2$. In this limit, only the first three diagrams of Fig. 1b and 1d contribute and the cross-sections for the processes $e^+e^- \to hhZ$ and $WW \to hh$ approach the corresponding cross sections of the \mathcal{SM} [10,11].

2. H Production and hh Decays

If kinematically allowed, the most copious source of multiple h final states are cascade decays $H \to hh$, with H produced either by Higgs-strahlung or associated pair production

²For small masses the decay $h \to AA$ could have provided an experimental opportunity to measure this coupling. However, for tan $\beta > 1$, this area of the \mathcal{MSSM} parameter space is excluded by LEP [7].

$$\sigma(e^+e^- \to ZH) = \frac{G_F^2 M_Z^4}{96\pi s} (v_e^2 + a_e^2) \cos^2(\beta - \alpha) \frac{\lambda_Z^{1/2} [\lambda_Z + 12M_Z^2/s]}{(1 - M_Z^2/s)^2}$$
(8)

$$\sigma(e^+e^- \to AH) = \frac{G_F^2 M_Z^4}{96\pi s} (v_e^2 + a_e^2) \sin^2(\beta - \alpha) \frac{\lambda_A^{3/2}}{(1 - M_Z^2/s)^2}$$
(9)

The Z couplings to electrons are given by $a_e = -1$, $v_e = -1 + 4\sin^2\theta_W$ and λ_j is the usual two-body phase space function $\lambda_j = (1 - M_j^2/s - M_H^2/s)^2 - 4M_j^2M_H^2/s^2$. The cross sections (8) and (9) are shown in Fig. 2 for the total e^+e^- energies $\sqrt{s} = 500$ GeV and 1.5 TeV as a function of the Higgs mass M_H for a small value of $\tan\beta = 1.5$ where the H cascade decays are significant over a large mass range. As a consequence of the decoupling theorem, associated AH production is dominant for large Higgs masses.

The trilinear Hhh coupling can be measured in the decay process $H \to hh$

$$\Gamma(H \to hh) = \frac{G_F \lambda_{Hhh}^2}{16\sqrt{2}\pi} \frac{M_Z^4}{M_H} \left(1 - \frac{4M_h^2}{M_H^2}\right)^{1/2} \tag{10}$$

if the branching ratio is neither too small nor too close to unity. This is indeed the case, as shown in Fig. 3a, for H masses between 180 and 350 GeV and small to moderate $\tan \beta$ values. The other important decay modes are WW^*/ZZ^* decays. Since the H couplings to the gauge bosons can be measured through the production cross sections of the fusion and Higgs-strahlung processes, the branching ratio $BR(H \to hh)$ can be exploited to measure the coupling λ_{Hhh} .

The ZH final state gives rise to resonant two–Higgs [hh] final states. The AH final state typically yields three Higgs h[hh] final states since the channel $A \to hZ$ is the dominant decay mode in most of the mass range we consider. This is shown in Fig. 3b where the branching ratios of the pseudoscalar A are displayed for $\tan \beta = 1.5$.

Another type of two-Higgs hh final states is generated in the chain $e^+e^- \to Ah \to [Zh]h$, which does not involve any of the Higgs self-couplings. However, in this case, the two h bosons do not resonate while [Zh] does, so that the topology of these background events is very different from the signal events. The size of the $e^+e^- \to hA$ background cross section is shown in Fig. 2 together with the signal cross sections; for sufficiently large M_A , it becomes small, in line with the decoupling theorem [9].

A second large signal cross section is provided by the WW fusion mechanism. [Since the NC couplings are smaller compared to the CC couplings, the cross section for the ZZ fusion processes in (1) and (4) is $\sim 16\cos^4\theta_W$, i.e. one order of magnitude smaller than for WW fusion.] In the effective longitudinal W approximation [12] one obtains

$$\sigma(e^{+}e^{-} \to H\bar{\nu}_{e}\nu_{e}) = \frac{G_{F}^{3}M_{W}^{4}}{4\sqrt{2}\pi} \left[\left(1 + \frac{M_{H}^{2}}{s} \right) \log \frac{s}{M_{H}^{2}} - 2\left(1 - \frac{M_{H}^{2}}{s} \right) \right] \cos^{2}(\beta - \alpha) \tag{11}$$

The magnitude of the cross section³ $e^+e^- \to H\nu_e\bar{\nu}_e$ is also shown in Fig. 2 for the two energies $\sqrt{s} = 500$ GeV and 1.5 TeV as a function of the Higgs mass M_H and for $\tan\beta = 1.5$. The signals in $e^+e^- \to [hh] + \text{missing energy are very clear, competing only with } H$ -strahlung and subsequent neutrino decays of the Z boson. Since the lightest Higgs boson will decay mainly into $b\bar{b}$ pairs, the final states will predominantly include four and six b quarks.

At $\sqrt{s} = 500$ GeV, about 500 signal events are predicted in the mass range of $M_H \sim 200$ GeV for an integrated luminosity of $\int \mathcal{L} = 20$ fb⁻¹ per annum; and at $\sqrt{s} = 1.5$ TeV, about 8,000 to 1,000 signal events for the prospective integrated luminosity of $\int \mathcal{L} = 200$ fb⁻¹ per annum in the interesting mass range between 180 and 350 GeV. Note that for both energies, the Ah background cross section is significantly smaller.

3. Non-Resonant Double hh Production

The double Higgs-strahlung $e^+e^- \to Zhh$, the triple Higgs production process $e^+e^- \to Ahh$ and the WW fusion mechanism $e^+e^- \to \nu_e\bar{\nu}_e hh$ outside the resonant $H \to hh$ range are disfavored by an additional power of the electroweak coupling compared to the resonance processes. Nevertheless, these processes must be analyzed carefully in order to measure the value of the hhh coupling.

3.1
$$e^+e^- \to Zhh$$

The double differential cross section of the process $e^+e^- \to hhZ$, Fig. 1b, is given by

$$\frac{d\sigma(e^+e^- \to hhZ)}{dx_1 dx_2} = \frac{G_F^3 M_Z^6}{384\sqrt{2}\pi^3 s} \left(a_e^2 + v_e^2\right) \frac{\mathcal{A}}{(1 - \mu_Z)^2}$$
(12)

The couplings have been defined in the previous section. $x_{1,2} = 2E_{1,2}/\sqrt{s}$ are the scaled energies of the Higgs particles, $x_3 = 2 - x_1 - x_2$ is the scaled energy of the Z boson; $y_k = 1 - x_k$. The scaled masses squared are denoted by $\mu_i = M_i^2/s$. In terms of these variables, the coefficient \mathcal{A} in the cross section may be written as:

$$\mathcal{A} = \left\{ \frac{a^2}{2} f_0 + \frac{\sin^4(\beta - \alpha)}{4\mu_Z^2 (y_1 + \mu_h - \mu_Z)} \left[\frac{f_1}{y_1 + \mu_h - \mu_Z} + \frac{f_2}{y_2 + \mu_h - \mu_Z} \right] + \frac{\cos^4(\beta - \alpha)}{4\mu_Z^2 (y_1 + \mu_h - \mu_A)} \right] \times \left[\frac{f_3}{y_1 + \mu_h - \mu_A} + \frac{f_4}{y_2 + \mu_h - \mu_A} \right] + \frac{a}{\mu_Z} \left[\frac{\sin^2(\beta - \alpha) f_5}{y_1 + \mu_h - \mu_Z} + \frac{\cos^2(\beta - \alpha) f_6}{y_1 + \mu_h - \mu_A} \right] + \frac{\sin^2 2(\beta - \alpha)}{8\mu_Z^2 (y_1 + \mu_h - \mu_Z)} \left[\frac{f_7}{y_1 + \mu_h - \mu_Z} + \frac{f_8}{y_2 + \mu_h - \mu_Z} \right] \right\} + \left\{ y_1 \leftrightarrow y_2 \right\}$$
(13)

with

$$a = \frac{1}{2} \left[\frac{\sin(\beta - \alpha)\lambda_{hhh}}{y_3 + \mu_Z - \mu_h} + \frac{\cos(\beta - \alpha)\lambda_{Hhh}}{y_3 + \mu_Z - \mu_H} \right] + \frac{\sin^2(\beta - \alpha)}{y_1 + \mu_h - \mu_Z} + \frac{\sin^2(\beta - \alpha)}{y_2 + \mu_h - \mu_Z} + \frac{1}{2\mu_Z}$$
(14)

 $^{^{3}}$ In the effective W approximation, the cross section may be overestimated by as much as a factor of 2 for small masses and/or small c.m. energies. Therefore we display the exact cross sections [13] in Fig.2.

[omitting the small decay widths of the Higgs bosons]. Only the coefficient a includes the Higgs self-couplings λ_{Hhh} and λ_{hhh} . Introducing the notation $y_0 = (y_1 - y_2)/2$, the coefficients f_i which do not involve any Higgs couplings, are defined by

$$f_{0} = (y_{1} + y_{2})^{2} - 4\mu_{Z}(1 - 3\mu_{Z})$$

$$f_{1} = \left[(1 + y_{1})^{2} - 4\mu_{Z}(y_{1} + \mu_{h}) \right] \left[y_{1}^{2} + \mu_{Z}^{2} - 2\mu_{Z}(y_{1} + 2\mu_{h}) \right]$$

$$f_{2} = \left[2\mu_{Z}(\mu_{Z} - 2\mu_{h} + 1) - (1 + y_{1})(1 + y_{2}) \right] \left[\mu_{Z}(\mu_{Z} - y_{1} - y_{2} - 4\mu_{h} + 2) - y_{1}y_{2} \right]$$

$$f_{3} = \left[y_{0}^{2} + \mu_{Z}(1 - y_{1} - y_{2} + \mu_{Z} - 4\mu_{h}) \right] \left[1 + y_{1} + y_{2} + y_{0}^{2} + \mu_{Z}(\mu_{Z} - 4\mu_{h} - 2y_{1}) \right]$$

$$f_{4} = \left[y_{0}^{2} + \mu_{Z}(1 - y_{1} - y_{2} + \mu_{Z} - 4\mu_{h}) \right] \left[y_{0}^{2} - 1 + \mu_{Z}(\mu_{Z} - y_{1} - y_{2} - 4\mu_{h} + 2) \right]$$

$$f_{5} = 2\mu_{Z}^{3} - 4\mu_{Z}^{2}(y_{1} + 2\mu_{h}) + \mu_{Z} \left[(1 + y_{1})(3y_{1} - y_{2}) + 2 \right] - y_{1}^{2}(1 + y_{1} + y_{2}) - y_{1}y_{2}$$

$$f_{6} = 2\mu_{Z}^{3} - \mu_{Z}^{2}(y_{2} + 3y_{1} + 8\mu_{h} - 2) + 2\mu_{Z}y_{0}(1 + y_{1} + y_{0}) + 2y_{1}y_{0} - y_{0}^{2}(y_{1} + y_{2} - 2)$$

$$f_{7} = \left[\mu_{Z}(4\mu_{h} - \mu_{Z} - 1 + 2y_{1} - y_{0}) - y_{1}y_{0} \right] \left[\mu_{Z}(4\mu_{h} - \mu_{Z} - 1 + 3y_{1}) - (1 + y_{0})(1 + y_{1}) \right]$$

$$f_{8} = \left[\mu_{Z}(4\mu_{h} - \mu_{Z} - 1 + 2y_{1} - y_{0}) - y_{1}y_{0} \right] \left[\mu_{Z}(4\mu_{h} - \mu_{Z} - 2 + y_{1}) + (1 - y_{0})(1 + y_{1}) \right]$$

In the decoupling limit, the cross section is reduced to the \mathcal{SM} cross section for which

$$\mathcal{A} = \frac{a^2}{2} f_0 + \frac{1}{4\mu_Z^2 (y_1 + \mu_h - \mu_Z)} \left[\frac{f_1}{y_1 + \mu_h - \mu_Z} + \frac{f_2}{y_2 + \mu_h - \mu_Z} + 4a\mu_Z f_5 \right] + \{ y_1 \leftrightarrow y_2 \}$$

with the f_i 's as given above, and

$$a = \frac{1}{2} \frac{\lambda_{hhh}}{y_3 + \mu_Z - \mu_h} + \frac{1}{y_1 + \mu_h - \mu_Z} + \frac{1}{y_2 + \mu_h - \mu_Z} + \frac{1}{2\mu_Z}$$

The cross section $\sigma(e^+e^- \to hhZ)$ is shown for $\sqrt{s} = 500$ GeV at $\tan \beta = 1.5$ as a function of the Higgs mass M_h in Fig. 4a. For small masses, the cross section is built up almost exclusively by $H \to hh$ decays [dashed curve], except close to the point where the λ_{Hhh} coupling accidentally vanishes (cf. Ref.[8]) and for masses around ~ 90 GeV where additional contributions come from the decay $A \to hZ$ [this range of M_h corresponds to M_A values where BR($A \to hZ$) is large; c.f. Fig.3]. For intermediate masses, the resonance contribution is reduced and, in particular above 90 GeV where the decoupling limit is approached, the continuum hh production becomes dominant, falling finally down to the cross section for double Higgs production in the Standard Model [dashed line]. After subtracting the $H \to hh$ decays [which of course is very difficult], the continuum cross section is about 0.5 fb, and is of the same order as the \mathcal{SM} cross section at $\sqrt{s} = 500$ GeV. Very high luminosity is therefore needed to measure the trilinear hhh coupling. At higher energies, since the cross section for double Higgs-strahlung scales like 1/s, the rates are correspondingly smaller, c.f. Fig.4b.

Prospects are similar for large $\tan \beta$ values. The cascade decay $H \to hh$ is restricted to a small M_h range of less than 70 GeV, with a production cross section of ~ 20 fb at $\sqrt{s} = 500$ GeV and ~ 3 fb at 1.5 TeV. The continuum cross sections are of the order of 0.1 fb at both energies, so that very high luminosities will be needed to measure the

continuum cross sections in this case if the background problems can be mastered at all.

We have repeated the analysis for the continuum process $e^+e^- \to Ahh$ (cf. Fig.1c). However, it turned out that the cross section is built up almost exclusively by resonant $AH \to Ahh$ final states, with a very small continuum contribution, so that the measurement of the coupling λ_{hAA} is extremely difficult in this process.

3.2 $W_LW_L \rightarrow hh$

In the effective longitudinal W approximation⁴, the total cross section for the subprocess $W_LW_L \to hh$, Fig. 1d, is given by

$$\hat{\sigma}_{LL} = \frac{G_F^2 \hat{s}}{64\pi} \frac{\beta_h}{\beta_W} \left\{ (1 + \beta_W^2)^2 \left[\frac{\mu_Z \sin(\beta - \alpha)}{1 - \mu_h} \lambda_{hhh} + \frac{\mu_Z \cos(\beta - \alpha)}{1 - \mu_H} \lambda_{Hhh} + 1 \right]^2 + \frac{\beta_W^2}{\beta_W \beta_h} \left[\frac{\mu_Z \sin(\beta - \alpha)}{1 - \mu_h} \lambda_{hhh} + \frac{\mu_Z \cos(\beta - \alpha)}{1 - \mu_H} \lambda_{Hhh} + 1 \right] \left[\sin^2(\beta - \alpha) g_1 + \cos^2(\beta - \alpha) g_2 \right] + \frac{1}{\beta_W^2 \beta_h^2} \left[\sin^4(\beta - \alpha) g_3 + \cos^4(\beta - \alpha) g_4 + \sin^2 2(\beta - \alpha) g_5 \right] \right\}$$
(16)

with

$$g_{1} = 2[(\beta_{W} - x_{W}\beta_{h})^{2} + 1 - \beta_{W}^{4}]l_{W} - 4\beta_{h}(2\beta_{W} - x_{W}\beta_{h})$$

$$g_{2} = 2(x_{C}\beta_{h} - \beta_{W})^{2}l_{C} + 4\beta_{h}(x_{C}\beta_{h} - 2\beta_{W})$$

$$g_{3} = \beta_{h}[\beta_{h}x_{W}(3\beta_{h}^{2}x_{W}^{2} + 14\beta_{W}^{2} + 2 - 2\beta_{W}^{4}) - 4\beta_{W}(3\beta_{h}^{2}x_{W}^{2} + \beta_{W}^{2} + 1 - \beta_{W}^{4})][l_{W} + x_{W}y_{W}]$$

$$-[\beta_{W}^{4} + (1 - \beta_{W}^{4})(1 + 2\beta_{W}^{2} - \beta_{W}^{4})][l_{W}/x_{W} - y_{W}] - 2\beta_{h}^{2}y_{W}(2\beta_{W} - \beta_{h}x_{W})^{2}$$

$$g_{4} = \beta_{h}[\beta_{h}x_{C}(3\beta_{h}^{2}x_{C}^{2} + 14\beta_{W}^{2}) - 4\beta_{W}(3\beta_{h}^{2}x_{C}^{2} + \beta_{W}^{2})][l_{C} + x_{C}y_{C}]$$

$$-\beta_{W}^{4}[l_{C}/x_{C} - y_{C}] - 2y_{C}\beta_{h}^{2}(2\beta_{W} - \beta_{h}x_{C})^{2}$$

$$g_{5} = \frac{\beta_{h}\beta_{W}l_{W}}{x_{W}^{2} - x_{C}^{2}}[2x_{W}(2x_{W}^{2}\beta_{h}\beta_{W} - x_{C}x_{W}^{2}\beta_{h}^{2} - x_{C}\beta_{W}^{2}) - 2x_{W}^{2}(\beta_{h}^{2}x_{W}^{2} + \beta_{W}^{2} + 1 - \beta_{W}^{4})$$

$$+ \frac{x_{C}}{\beta_{W}\beta_{h}}((\beta_{h}^{2}x_{W}^{2} + \beta_{W}^{2})(1 - \beta_{W}^{4}) + (\beta_{h}^{2}x_{W}^{2} + \beta_{W}^{2})^{2})] - 4\beta_{h}^{3}\beta_{W}(x_{W} + x_{C})$$

$$+ \frac{\beta_{h}\beta_{W}l_{C}}{x_{C}^{2} - x_{W}^{2}}[4x_{C}^{3}\beta_{h}\beta_{W} - 2x_{C}x_{W}(\beta_{h}^{2}x_{C}^{2} + \beta_{W}^{2}) - 2x_{C}^{2}(\beta_{h}^{2}x_{C}^{2} + \beta_{W}^{2})$$

$$+ \frac{x_{W}}{\beta_{W}\beta_{h}}((\beta_{W}^{2} + \beta_{h}^{2}x_{C}^{2})(1 - \beta_{W}^{4}) + (\beta_{h}^{2}x_{C}^{2} + \beta_{W}^{2})^{2})] + 2\beta_{H}^{2}(x_{C}x_{W}\beta_{H}^{2} + 4\beta_{W}^{2})$$

$$+ \frac{x_{W}}{\beta_{W}\beta_{h}}((\beta_{W}^{2} + \beta_{h}^{2}x_{C}^{2})(1 - \beta_{W}^{4}) + (\beta_{h}^{2}x_{C}^{2} + \beta_{W}^{2})^{2})] + 2\beta_{H}^{2}(x_{C}x_{W}\beta_{H}^{2} + 4\beta_{W}^{2})$$

$$+ \frac{x_{W}}{\beta_{W}\beta_{h}}((\beta_{W}^{2} + \beta_{h}^{2}x_{C}^{2})(1 - \beta_{W}^{4}) + (\beta_{h}^{2}x_{C}^{2} + \beta_{W}^{2})^{2})] + 2\beta_{H}^{2}(x_{C}x_{W}\beta_{H}^{2} + 4\beta_{W}^{2})$$

$$+ (17)$$

The scaling variables are defined in the same way as before. $\hat{s}^{1/2}$ is the c.m. energy of the subprocess, $\beta_W = (1 - 4M_W^2/\hat{s})^{1/2}$ and $\beta_h = (1 - 4M_h^2/\hat{s})^{1/2}$ are the velocities of the W and h bosons, and

$$x_W = (1 - 2\mu_h)/(\beta_W \beta_h) , \quad x_C = (1 - 2\mu_h + 2\mu_{H^{\pm}} - 2\mu_W)/(\beta_W \beta_h)$$

$$l_i = \log(x_i - 1)/(x_i + 1) , \quad y_i = 2/(x_i^2 - 1)$$
(18)

⁴For qualifying comments see footnote 3.

The value of the charged Higgs boson mass $M_{H^{\pm}}$ in the H^{\pm} t-channel exchange diagram of Fig.1d is given by $M_{H^{\pm}}^2 = M_A^2 + M_W^2$.

In the decoupling limit, the cross section reduces again to the SM cross section which in terms of g_1 and g_2 , defined above, is given by:

$$\hat{\sigma}_{LL} = \frac{G_F^2 \hat{s}}{64\pi} \frac{\beta_h}{\beta_W} \left\{ (1 + \beta_W^2)^2 \left[\frac{\mu_Z \lambda_{hhh}}{1 - \mu_h} + 1 \right]^2 + \frac{1 + \beta_W^2}{\beta_W \beta_h} \left[\frac{\mu_Z \lambda_{hhh}}{1 - h_1} + 1 \right] g_1 + \frac{g_3}{\beta_W^2 \beta_h^2} \right\}$$
(19)

After folding $\hat{\sigma}_{LL}$ with the longitudinal W_LW_L luminosity [12], one obtains the total cross section $\sigma(e^+e^- \to \nu_e\bar{\nu}_e hh)$ shown in Fig. 4b as a function of the light Higgs mass M_h for $\tan\beta=1.5$ at $\sqrt{s}=1.5$ TeV. It is significantly larger than for double Higgs–strahlung in the continuum. Again, for very light Higgs masses, most of the events are $H\to hh$ decays [dashed line]. The continuum hh production is of the same size as pair production of \mathcal{SM} Higgs bosons [dotted line] which, as anticipated, is being approached near the upper limit of the h mass in the decoupling limit. The size of the continuum hh fusion cross section renders this channel more promising than double Higgs–strahlung for the measurement of the trilinear hhh coupling.

For large $\tan \beta$ values, strong destructive interference effects reduce the cross section in the continuum to very small values, of order 10^{-2} fb, before the \mathcal{SM} cross section is reached again in the decoupling limit. As before, the hh final state is almost exclusively built up by the resonance $H \to hh$ decays.

4. Summa

It is convenient to summarize our results by presenting Fig.5, which displays the areas of the $[M_A, \tan \beta]$ plane in which λ_{Hhh} [solid lines, 135° hatching] and λ_{hhh} [dashed lines, 45° hatching] could eventually be accessible by experiment. The size of these areas is based on purely theoretical cuts so that they are expected to shrink if background processes and detector effects are taken into account.

(i) In the case of $H \to hh$, we require a lower limit of the cross section $\sigma(H) \times \text{BR}(H \to hh) > 0.5$ fb and at the same time for the decay branching ratio $0.1 < \text{BR}(H \to hh) < 0.9$, as discussed earlier. Based on these definitions, λ_{Hhh} may become accessible in two disconnected regions denoted by I and II [1350 hatched] in Fig.5. For low $\tan \beta$, the left boundary of Region I is set by LEP1 data. The gap between Regions I and II is a result of the nearly vanishing λ_{Hhh} coupling in this strip. The right boundary of Region II is due to the overwhelming $t\bar{t}$ decay mode for heavy H masses, as well as due to the small H production cross section. For moderate values of $\tan \beta$, the left boundary of Region I is defined by $\text{BR}(H \to hh) > 0.9$. In the area between Regions I and II, H cannot decay into two h bosons, i.e. $M_H < 2M_h$. For large $\tan \beta \gtrsim 10$, $\text{BR}[H \to hh(AA)]$ is either too large or too small, except in a very small strip, $M_A \simeq 65$ GeV, towards the top of Region I. [Note that h and A are nearly mass-degenerate in this area.]

(ii) The dashed line in Fig.5 describes the left boundary of the area [45° hatched] in which λ_{hhh} may become accessible; it is defined by the requirement that the continuum $W_LW_L \to hh$ cross section, $\sigma_{\rm cont}$, is larger than 0.5 fb. Note that the resonant $H \to hh$ events in Region II must be subtracted in order to extract the λ_{hhh} coupling.

In conclusion, we have derived the cross sections for the double production of the lightest neutral Higgs boson in the \mathcal{MSSM} at e^+e^- colliders: in the Higgs-strahlung process $e^+e^- \to Zhh$, [in the triple Higgs production process $e^+e^- \to Ahh$], and in the WW fusion mechanism. These cross sections are large for resonant $H \to hh$ decays so that the measurement of the triple Higgs coupling λ_{Hhh} is expected to be fairly easy for $H \to hh$ decays in the M_H mass range between 150 and 350 GeV for small $\tan \beta$ values. The continuum processes must be exploited to measure the triple Higgs coupling λ_{hhh} . These continuum cross sections, which are of the same size as in the \mathcal{SM} , are rather small so that high luminosities are needed for the measurement of the triple Higgs coupling λ_{hhh} .

Acknowledgements:

Discussions with G. Moultaka and technical help by T. Plehn are gratefully acknowledged. A.D. thanks the Theory Group for the warm hospitality extended to him at DESY, and H.E.H. acknowledges the partial support of the U.S. Department of Energy.

- For reviews on the Higgs sector in the SM and MSSM, see J.F. Gunion, H.E. Haber, G. Kane and S. Dawson, The Higgs Hunter's Guide, Addison-Wesley 1990;
 A. Djouadi, Int. J. Mod. Phys A10 (1995) 1.
- 2. J.F. Gunion and H.E. Haber, Nucl. Phys. B272 (1986) 1; B278 (1986) 449.
- 3. T. Plehn, M. Spira and P. M. Zerwas, DESY 95–215 and Z. Phys. C (in press).
- 4. See e.g. P.M. Zerwas, Proceedings, Les Rencontres de Physique de la Vallée d'Aoste, La Thuile 1994 and DESY 94–001.
- 5. K. Gaemers and F. Hoogeveen, Z. Phys. C26 (1984) 249; A. Djouadi, V. Driesen and C. Jünger, Report KA–TP–02–96.
- H.E. Haber and R. Hempfling, Phys. Rev. Lett. 66 (1991) 1815; Y. Okada, M. Yamaguchi and T. Yanagida, Prog. Theor. Phys. 85 (1991) 1; J. Ellis, G. Ridolfi and F. Zwirner, Phys. Lett. 257B (1991) 83.
- 7. J.-F. Grivaz, Proceedings, Int. Conference on High-Energy Physics, Brussels 1995.
- 8. A. Djouadi, J. Kalinowski and P. M. Zerwas, DESY 95–211 (hep-ph 9511342) and Z. Phys. C (in press).
- 9. H.E. Haber, CERN-TH/95-109 and SCIPP-95/15, Proceedings, Conference on Physics Beyond the Standard Model IV, Lake Tahoe CA 1994; and Perspectives for Electroweak Interactions in e⁺e⁻ Collisions, Ringberg Castle, Tegernsee 1995.
- 10. G. Gounaris, D. Schildknecht and F. Renard, Phys. Lett. B83 (1979) 191 and (E) 89B (1980) 437.

- V. Barger and T. Han, Mod. Phys. Lett. A5 (1990) 667; V. Barger, T. Han and R.J. Phillips, Phys. Rev. D38 (1988) 2766; J. F. Gunion et al., Phys. Rev. D38 (1988) 3444; D. Dicus, K. Kallianpur and S. Willenbrock, Phys. Lett. B200 (1988) 187; K. Kallianpur, Phys. Lett. B215 (1988) 392; A. Abbasabadi, W. Repko, D. Dicus and R. Vega, Phys. Rev. D38 (1988) 2770; V. Ilyin, A. Pukhov, Y. Kurihara, Y. Shimitzu and T. Kaneko, KEK CP-030; F. Boudjema and E. Chopin, ENSLAPP-A534/95.
- 12. R.N. Cahn and S. Dawson, Phys. Lett. B136 (1984) 196; S. Dawson, Nucl. Phys. B249 (1984) 42; S. Chanowitz and M.K. Gaillard, Phys. Lett. B142 (1984) 85; I. Kuss and H. Spiesberger, Report BI-TP-95/25.
- 13. A. Djouadi, D. Haidt, B. Kniehl, B. Mele and P.M. Zerwas, Proceedings, e^+e^- collisions at 500 GeV: The Physics Potential, Munich—Annecy—Hamburg, DESY 92–123A.

Fig.1: Main mechanisms for the double production of the light MSSM Higgs boson in e^+e^- collisions: a) $e^+e^- \to ZH$, $e^+e^- \to AH$ and $WW \to H$ followed by $H \to hh$; (b) $e^+e^- \to hhZ$, (c) $e^+e^- \to hhA$ and (d) $WW \to hh$.

Fig. 2: Cross sections for the production of the heavy CP–even Higgs boson H in e^+e^- collisions, $e^+e^- \to ZH/AH$ and $e^+e^- \to H\nu_e\bar{\nu}_e$, and for the background process $e^+e^- \to Ah$ [the dashed curve shows $\frac{1}{2} \times \sigma(Ah)$ for clarity of the figures]. The c.m. energies are chosen $\sqrt{s}=500$ GeV in (a), and 1.5 TeV in (b).



Fig. 4: The cross sections for hh production in the continuum for $\tan\beta=1.5$: $e^+e^-\to hhZ$ at a c.m. energy of $\sqrt{s}=500$ GeV (a) and $W_LW_L\to hh$ at $\sqrt{s}=1.5$ TeV (b).

Fig. 5: The areas of the $[M_A, \tan\beta]$ plane in which the Higgs self–couplings λ_{Hhh} and λ_{hhh} could eventually be accessible by experiment at $\sqrt{s}=1.5$ TeV [see text for further discussions].

Loop Induced Higgs Boson Pair Production

A. DJOUADI, V. DRIESEN AND C. JÜNGER Institut für Theoretische Physik, Universität Karlsruhe, D-76128 Karlsruhe, Germany.

Abstract

We discuss the loop induced production of Higgs boson pairs at high–energy e^+e^- colliders, both in the Standard Model and in its minimal supersymmetric extension. The cross sections are rather small, but these processes could be visible with high-enough luminosities and if longitudinal polarization is available.

1. Introduction

If the genuine supersymmetric particles were too heavy to be kinematically accessible in collider experiments, the only way to distinguish between the Standard Model (SM) and the lightest Higgs boson of its minimal extension (MSSM) in the decoupling limit [where all the other MSSM Higgs bosons are heavy, and the lightest Higgs boson h has exactly the same properties [1] as the SM Higgs boson except that its mass is restricted to be smaller than $M_h \lesssim 140 \text{ GeV}$], is to search for loop induced contributions of the supersymmetric particles, which could give rise to sizeable deviations from the predictions of the SM. Well known examples of this loop induced processes are the $\gamma\gamma$ widths of the Higgs particles [2] or the process $e^+e^- \to Z$ +Higgs which in the MSSM receive extra contributions from supersymmetric gaugino and sfermion loops [3].

Another type of such discriminating processes is the pair production of Higgs bosons which will be analyzed here. In the SM, where it has been first discussed in Ref.[4], the process $e^+e^- \to H^0H^0$ is mediated only by W and Z boson loops, Fig.1a, while in the Minimal Supersymmetric extension, additional contributions to the corresponding process $e^+e^- \to hh$ will originate from chargino, neutralino, selectron and sneutrino loops, as well as loops built up by the associated A and H^\pm bosons; Fig.1b. The cross sections for these two processes [as well as for the production of the heavy MSSM Higgs bosons, $e^+e^- \to HH$, AA and hH] have been derived in [5] and here we will summarize the results.

2. SM Higgs Pair Production

In the SM, non–zero contributions to the process $e^+e^- \to H^0H^0$ can only come from one–loop diagrams, in the limit of vanishing electron mass. Among these, the diagrams involving the one–loop He^+e^- vertex [because $m_e \simeq 0$] and those with γ and Z boson s–channel exchanges [because of CP invariance] give zero–contribution; additional contributions from vertex diagrams involving the quartic WWH^0H^0/ZZH^0H^0 couplings are proportional m_e and also negligible. The only contribution to Higgs pair production in the SM will therefore come from W and Z box diagrams, Fig.1a. The expressions of the cross sections, allowing for longitudinal polarization of the initial beams are given in [5].

Fig. 1: Feynman diagrams contributing to the Higgs boson pair production process in e^+e^- collisions in the SM (a) and in the MSSM (b).

The cross sections are shown in Fig.2 as a function of the Higgs boson mass for two center-of-mass energies, $\sqrt{s} = 500$ GeV and 1.5 TeV. Except when approaching the $2M_H$ threshold [and the small dip near the WW threshold], the cross sections are practically constant for a given value of the c.m. energy, and amount to $\sigma \sim 0.2$ fb at $\sqrt{s} = 500$ GeV in the unpolarized case. The decrease of the cross sections with increasing center-of-mass energy is very mild: at $\sqrt{s} = 1.5$ TeV, the cross section is still at the level of $\sigma \sim 0.15$ fb for Higgs boson masses less than $M_H \lesssim 350$ GeV.

With left-handed polarized electrons, the cross section $e_L^-e^+ \to H^0H^0$ is larger by a factor of two, while for left-handed electrons and right-handed positrons, the cross section $e_L^-e_R^+ \to H^0H^0$ is larger by a factor of four, compared to the unpolarized case. Therefore, the availability of longitudinal polarization of the initial beams is very important. With integrated luminosities of the order of $\int \mathcal{L} \sim 100 \text{ fb}^{-1}$ which are expected to be available for future high-energy linear colliders, one could expect a few hundred events in the course of a few years, if both initial beams can be longitudinally polarized.

For $M_H \lesssim 140$ GeV, the signal will mainly consist of four b quarks in the final state, $e^+e^- \to H^0H^0 \to b\bar{b}b\bar{b}$, since the dominant decay mode of the Higgs boson in this mass range is $H^0 \to b\bar{b}$. This calls for very efficient μ -vertex detectors to tag the b jets. Since these rare events will be searched for only after the discovery of the Higgs boson in the main production processes [5], M_H will be precisely known and the two mass constraints $m(b\bar{b}) = M_H$, together with the large number of final b quarks, give a reasonable hope to experimentally isolate the signals despite of the low rates. For $M_H \gtrsim 140$ GeV, since $H^0 \to W^+W^-$ and $H^0 \to ZZ$ will be the dominant decay modes of the Higgs boson, the signals will consist of four gauge bosons in the final state, $e^+e^- \to H^0H^0 \to VVVV$, leading to eight final fermions. These rather spectacular events should also help to experimentally isolate the signal.

3. MSSM Higgs Pair Production

For the pair production of the light CP-even Higgs boson of the MSSM, $e^+e^- \to hh$,

Fig. 2: The cross sections for, $e^+e^- \to H^0H^0$, as a function of M_H for $\sqrt{s} = 500$ GeV [dashed lines] and $\sqrt{s} = 1.5$ TeV [solid lines]. The lower, middle and upper curves correspond to the cross sections with unpolarized, e_L^- and $e_R^+e_L^-$ beams respectively.

several additional diagrams will contribute to the process; Fig.1b. Besides the W and Z boson box diagrams, one has the box diagrams with the exchange of the pseudoscalar and the charged Higgs bosons, A and H^{\pm} and the box diagrams built up by chargino/sneutrino and neutralino/selectron loops. The analytical expressions of the cross sections, allowing for longitudinal polarization of the initial beams are also given in [5].

In Fig.3, we show the cross section for the process $e^+e^- \to hh$ as a function of M_h for two c.m. energies $\sqrt{s} = 500$ GeV and 1.5 TeV and two values of $\tan \beta = 1.5$ and 50. The solid lines are for the full cross sections, while the dashed lines are for the cross sections without the SUSY contributions. To include the latter we have chosen the parameters $M_2 = -\mu = 150$ GeV, while the common slepton and squark masses are taken to be $M_L = 300$ GeV and $M_S = 500$ GeV; the parameter A_t and A_b are set to zero. Only the unpolarized cross sections are discussed: as mentioned previously, they are simply increased by a factor of 2(4) when the initial beam(s) are longitudinally polarized.

Let us first discuss the case where the supersymmetric contributions are not included, for small $\tan \beta$ the cross section is of the same order as the SM cross section and does not strongly depend on M_h especially at very high–energies. Although the WWh/Zhh couplings are suppressed by $\sin(\beta - \alpha)$ factors, the suppression is not very strong and the W/Z box contributions are not much smaller than in the SM; the diagrams where A/H^{\pm} are exchanged will give compensating contributions since the $hAZ/hH^{\pm}W$ couplings are proportional to the complementary factor $\cos(\beta - \alpha)$. As in the SM case, the cross sections slightly decrease with increasing energy. For large $\tan \beta$ values, the factors $\sin/\cos(\beta - \alpha)$ vary widely when M_h is varied. For small M_h , the factor $\sin(\beta - \alpha) \to 0$, and the contribution of the diagrams with A/H^{\pm} exchange dominates. The latter contribution decreases with increasing M_h [i.e. with decreasing $\cos(\beta - \alpha)$], until the decoupling limit

Fig. 3: The cross sections for $e^+e^- \to hh$ in the MSSM, as a function of M_h for $\sqrt{s}=500$ GeV and $\sqrt{s}=1.5$ TeV and for $\tan\beta=1.5$ and 50. The solid curves correspond to the full cross sections, while the dashed curves correspond to the cross sections without the SUSY contributions.

is reached for $M_h \simeq 110$ GeV. In this case, the factor $\sin(\beta - \alpha) \to 1$ and the W/Z boson loops are not suppressed anymore; one then obtains the SM cross section.

The contributions of the chargino/selectron and neutralino/sneutrino loops lead to a destructive interference. At high–energies, the supersymmetric boxes practically do not contribute; but at low energies, and especially below the decoupling limit, the SUSY contributions can be of the order of $\sim 10\%$. We have scanned the SUSY parameter space, and the maximum contribution of the SUSY loops that we have found was about $\sim -15\%$. In the decoupling limit, the SUSY contributions are, at most, of the order of a few percent. Because of the rather low production rates, it will therefore be difficult to experimentally see this effect.

4. Summary

We have discussed the one-loop induced production of Higgs boson pairs at future high-energy e^+e^- colliders in the SM and the MSSM. In the SM, the unpolarized cross section is rather small, of the order 0.1–0.2 fb. The longitudinal polarization of both the e^- and e^+ beams will increase the cross section by a factor of 4. With integrated luminosities $\int \mathcal{L} \gtrsim 100 \text{ fb}^{-1}$ as expected to be the case for future high-energy linear colliders, one could expect a few hundred events in the course of a few years if longitudinal polarization is available. The final states are rather clean, giving a reasonable hope to isolate the signals experimentally. In the MSSM, additional contributions to the processes $e^+e^- \to hh$ come from chargino/ neutralino and slepton loops. For hh production, the contributions of the supersymmetric loops are in general rather small, being of the order of a few percent; the cross sections are therefore of the same order as in the SM. For the processes involving heavy Higgs bosons, the cross sections are even smaller than for $e^+e^- \to hh$, and the signals will be hard to be detected experimentally.

References

- [1] For reviews see, J. Gunion, H. Haber, G. Kane and S. Dawson, *The Higgs Hunter's Guide*, Addison–Wesley, Reading 1990; D. Haidt, P. Zerwas et al., Proceedings of the workshop e^+e^- collisions at 500 GeV: The Physics Potential, Munich–Annecy–Hamburg, DESY 92–123A+C, P.M. Zerwas (ed.); A. Djouadi, Int. J. Mod. Phys. A10 (1995)1.
- [2] J. Ellis, M.K. Gaillard and D.V. Nanopoulos, Nucl. Phys. B106 (1976) 292; for recent discussions of the Higgs- $\gamma\gamma$ coupling in the MSSM see: G.L. Kane, G.D. Kribs, S.P. Martin and J.D. Wells, Phys. Rev. D53 (1996) 213; B. Kileng, P. Osland and P.N. Pandita, NORDITA-95-48-P (1995).
- [3] For a discussion of the radiative corrections to the process $e^+e^- \to hZ$, see V. Driesen, W. Hollik and J. Rosiek, Report KA-TP-16-1995, hep-ph/9512441.
- [4] K. Gaemers and F. Hoogeveen, Z. Phys. C26 (1984) 249.
- [5] A. Djouadi, V. Driesen and C. Jünger, hep-ph/9602341, Phys. Rev. D (in press).

Search for the Higgs Bosons of the NMSSM at Linear Colliders

B. R. Kim¹, G. Kreyerhoff¹ and S. K. Oh²

 $^{\rm 1}$ III. Physikalisches Institut A, RWTH Aachen, D-52056 Aachen, Germany

² Department of Physics, Kon-Kuk University, Seoul, Korea.

Abstract

We show that at least one of the Higgs bosons of the Next to Minimal Supersymmetric Standard Model can be detected at future Linear Colliders of 500, 1000 and 2000 GeV c.m. energies.

1. Introduction

The Next to Minimal Supersymmetric Standard Model (NMSSM) [1–3] is a minimal extension to the Minimal Supersymmetric Standard Model [4]. The NMSSM provides the most economic solution of the so called μ -problem of the MSSM by introducing an additional Higgs singlet superfield $\mathcal{N} = (N, \psi_N, F_N)$ with a Higgs singlet N, a higgsino singlet V and an auxiliary field V. Together with the two Higgs doublets superfields $\mathcal{H}_{1,2} = (H_{1,2}, \psi_{1,2}, F_{1,2})$ the superpotential of the NMSSM is given by

$$W = \lambda \mathcal{H}_1^T \epsilon \mathcal{H}_2 \mathcal{N} - \frac{1}{3} k \mathcal{N}^3 \tag{1}$$

The soft breaking part of the Higgs sector is given by

$$V_{soft} = -\lambda A_{\lambda} H_1^T \epsilon H_2 N - \frac{1}{3} k A_k N^3 + h.c.$$
 (2)

where A_{λ} and A_k are soft breaking mass parameters.

 H_1, H_2 and N develop vacuum expectation values v_1, v_2 and x respectively. The NMSSM contains three scalar Higgs bosons S_1, S_2 and S_3 with masses $m_{S_1} \leq m_{S_2} \leq m_{S_3}$, two pseudoscalar Higgs bosons P_1 and P_2 with masses $m_{P_1} \leq m_{P_2}$ and a charged one H^+ with mass m_C .

The Higgs sector has 6 free parameters $\lambda, k, \tan \beta = v_1/v_2, x, A_{\lambda}$ and A_k .

2. Constraints on parameters

A remarkable result of the MSSM is the tree level bound of $m_{S_1} \leq m_Z \cos 2\beta$. This is due to the fact that all quartic terms have gauge coupling constants. In case of the NMSSM there is a quartic term with the coupling constant λ . It turns out that the upper bound of λ may be relevant for m_{S_1} . An effective way of determining this bound is RG-analysis [1–8].

The one loop RG-equation of λ is coupled with that of k and h_t , the Yukawa coupling constant of the top quark (neglecting other quarks) and is given by

$$\frac{d\lambda}{dt} = \frac{1}{8\pi^2} \left(k^2 + 2\lambda^2 + \frac{3}{2}h_t^2 + \frac{3}{2}g_2^2 - \frac{1}{2}g_1^2 \right) \lambda \tag{3}$$

$$\frac{dk}{dt} = \frac{3}{8\pi^2} \left(k^2 + \lambda^2\right) k \tag{4}$$

$$\frac{dh_t}{dt} = \frac{1}{8\pi^2} \left(\frac{1}{2}\lambda^2 + 3h_t^2 - \frac{8}{3}g_3^2 - \frac{3}{2}g_2^2 - \frac{13}{18}g_1^2 \right) h_t \tag{5}$$

where $t = \ln \mu$ and μ being the renormalization scale. By demanding no Landau pole up to the GUT scale one can determine from eq. (5) the upper bound of λ and k and the lower bound of $\tan \beta$ at the electroweak scale. We plot our results in Fig. 1 (Fig. 2) for $m_t = 175 \text{ GeV}$ (190 GeV). They show that λ_{max} decreases with increasing k^* . The lower bound of $\tan \beta$ is about 1.24 for $m_t = 175 \text{GeV}$ and 2.6 for $m_t = 190 \text{GeV}$. For $\tan \beta \gtrsim 3$ λ_{max} is almost independent on $\tan \beta$. The upper bound of k is about 0.7.

3. Mass upper bounds

The tree level bound of m_{S_1} is given by [3]

$$m_{S_1}^2 \le m_Z^2 \left(\cos^2 2\beta + \frac{2\lambda^2}{g_1^2 + g_2^2} \sin^2 2\beta\right) = m_{S_1^{max}}^2$$
 (6)

The upper bound of m_{S_2} and m_{S_3} can be expressed in terms of $m_{S_1^{max}}$ and m_{S_1}

$$m_{S_2}^2 \le m_{S_2^{max}}^2 = \frac{m_{S_1^{max}}^2 - R_1^2 m_{S_1}^2}{1 - R_1^2}$$
 (7)

$$m_{S_3}^2 \le m_{S_3^{max}}^2 = \frac{m_{S_1^{max}}^2 - (R_1^2 + R_2^2) m_{S_1}^2}{1 - (R_1^2 + R_2^2)}$$
 (8)

where $R_i = U_{i1} \cos \beta + U_{i2} \sin \beta$ and U_{ij} is the 3×3 orthogonal matrix which diagonalizes the scalar mass matrix.

 R_1 and R_2 satisfy the unitarity condition $0 \le R_1^2 + r_2^2 \le 1$. The tree level upper bound (6) yields $m_{S_1} \le m_Z$ for $\lambda^2 \le (g_1^2 + g_2^2)/2 = (0.52)^2$ and $m_{S_1} \le \sqrt{2/(g_1^2 + g_2^2)}\lambda m_Z = 1.92\lambda m_Z$ for $\lambda^2 > (0.52)^2$. Using $\lambda_{max} = 0.64 - 0.74$ from section 2 the tree level relation yields $m_{S_1} \le 113 \text{GeV} - 131 \text{GeV}$.

As in the case of the MSSM the contributions of radiative corrections may change this result considerably. Several groups calculated higher order contributions to the mass matrices using the one loop effective potential and determined the corrected upper bound [8,9,10,11].

^{*}We obtain $\lambda_{max} = 0.64 - 0.74$ for $m_t = 175 - 190$ GeV.

The result in our notation [8] is given by

$$m_{S_1}^2 \le m_Z^2 \left(\cos^2 2\beta + \frac{2\lambda^2}{g_1^2 + g_2^2} \sin^2 2\beta\right) + \alpha \cos^2 \beta + \beta \sin 2\beta + \gamma \sin^2 \beta$$
 (9)

with $(A_T = -A_t + \lambda x \cot \beta)$

$$\alpha = -\frac{1}{16\pi^2} \left(\frac{\lambda x A_T}{v_1}\right)^2 \left(\frac{m_t}{m_{\tilde{t}}}\right)^4 \tag{10}$$

$$\beta = \frac{3}{8\pi} \lambda x A_T \left(\frac{m_t^2}{m_{\tilde{t}} v_1}\right)^2 \left(1 + \frac{A_t A_T}{6m_{\tilde{t}}^2}\right) \tag{11}$$

$$\gamma = \frac{3}{8\pi} \left(\frac{m_t^2}{v_1^2}\right)^2 \left[2 \ln \frac{m_{\tilde{t}}^2}{m_t^2} - \frac{2A_t A_T}{m_{\tilde{t}}^2} - \frac{A_t^2 A_T^2}{6m_{\tilde{t}}^4} \right]$$
(12)

In this result only top and stop contributions were taken into account. We numerical calculated $m_{S_1^{max}}$ in the region 175GeV $\leq m_t \leq$ 190GeV, 250GeV $\leq x, A_{\lambda}, A_t, m_{\tilde{t}} \leq$ 1000GeV and $2 \leq \tan \beta \leq 20$ and obtained [8]

$$120 \le m_{S_1^{max}} \le 156 \text{GeV}$$
 (13)

4. Production of scalar Higgs bosons at e^+e^- Colliders

The upper bound $m_{S_1} \leq 120 - 156 \text{GeV}$ suggests that the accessible area of the parameter space at LEP1 with $\sqrt{s} = m_Z$ might be very small. Actually we showed that the existing LEP1 data do not exclude the existence of S_1 with $m_{S_1} = 0 \text{GeV}$ [12].

For colliders with $\sqrt{s} = 500,1000$ or 2000GeV the situation is different. In this case the production cross section of one S_i via the Higgsstrahlung $e^+e^- \to ZS_i$ with real Z and S_i is always possible as the collider energy is larger than $E_T = 212 - 248$ GeV. E_T is a kind of threshold energy and is an important quantity of a model.

In this case it is possible to derive a lower bound for the production cross section σ_i of S_i as a function of the collision energy only. This lower bound would give information about how far the model could be tested.

In order to derive the lower bound of σ_i we consider the production cross sections of S_1, S_2, S_3 via the Higgsstrahlungs process, denoted by $\sigma_1, \sigma_2, \sigma_3$, which can be expressed in terms of the standard model Higgs production cross section σ_{SM} and R_1 and R_2 defined in section 2:

$$\sigma_1(m_{S_1}) = R_1^2 \sigma_{SM}(m_{S_1}) \tag{14}$$

$$\sigma_2(m_{S_2}) = R_2^2 \sigma_{SM}(m_{S_2}) \tag{15}$$

$$\sigma_3(m_{S_3}) = (1 - R_1^2 - R_2^2)\sigma_{SM}(m_{S_3}) \tag{16}$$

A useful observation is that $\sigma_i(m_{S_i}^{max}) \leq \sigma_i(m_{S_i})$ which allows one to derive parameter independent lower limits on σ_i as we will see in the following.

First we determine at a fixed set of m_{S_1} , R_1 , R_2 the cross sections $\sigma_1(R_1, R_2, m_{S_1})$, $\sigma_2(R_1, R_2, m_{S_2^{max}})$ and $\sigma_3(R_1, R_2, m_{S_3^{max}})$. Then we keep R_1 and R_2 fixed, but vary m_{S_1} from its minimum to its maximum value and determine the quantity $\sigma(R_1, R_2)$ defined by

$$\sigma(R_1, R_2) = \min_{0 \le m_{S_1} \le m_{S_1^{max}}} \left[\max(\sigma_1, \sigma_2, \sigma_3) \right]$$
 (17)

where $\sigma_1 = \sigma_1(R_1, R_2, m_{S_1})$, $\sigma_2 = \sigma_2(R_1, R_2, m_{S_2^{max}})$ and $\sigma_3 = \sigma_3(R_1, R_2, m_{S_3^{max}})$. As a last step we vary R_1^2 and R_2^2 from 0 to 1 with $R_1^2 + R_2^2 \le 1$ and plot $\sigma(R_1, R_2)$ in the R_1 - R_2 -plane. It is plausible that $\sigma(R_1, R_2) = 0$ for $\sqrt{s} < E_T = m_z + m_{S_1^{max}} = 212 - 248 \text{GeV}$ in the entire R_1 - R_2 -plane. This is the case for LEP2 with $\sqrt{s} \le 205 \text{ GeV}$. Therefore this method does not give any results for LEP2. For $\sqrt{s} > E_T \sigma(R_1, R_2)$ never vanishes and the minimum of $\sigma(R_1, R_2)$ is a parameter independent lower limit of one of the σ_i . This minimum is thus a characteristic quantity of the model.

In Fig. 3 we plotted $\sigma(R_1, R_2)$ for $\sqrt{s} = 500\,$ GeV and $m_{S_1^{max}} = 145\,$ GeV. The minimum is about 16 fb. When the discovery limit is about 30 events, one would need a luminosity of about 25 fb, which is a realistic one. Fig. 4 (Fig. 5) shows $\sigma(R_1, R_2)$ for $\sqrt{s} = 1000(2000)\,$ GeV with minimum cross section of 4 fb (1 fb). Fig. 6 shows the minimum of $\sigma(R_1, R_2)$ as a function of \sqrt{s} and $m_{S_1^{max}}$ as a parameter. We see that the effect of $m_{S_1^{max}}$ on σ_{min} is very big around $\sqrt{s} = 300\,$ GeV, but rather small for $\sqrt{s} \geq 500\,$ GeV.

Fig. 7 shows the tree level cross sections σ_1 , σ_2 and σ_3 for an exemplary set of parameters with the contributions from (i) the Higgsstrahlungsprocess $e^+e^- \to ZS_i \to b\bar{b}S_i$, (ii) the process where S_i is radiated off from b or \bar{b} and (iii) $e^+e^- \to Z \to P_jS_i \to b\bar{b}S_i$, where $P_i(j=1,2)$ is a pseudoscalar Higgs boson.

Fig. 8 shows the same as Fig. 7, but with one loop contributions via the effective potential. The higher order contribution is rather important for the energy region around 150 GeV and decreases with \sqrt{s} . In this parameter region the dominant production is that of S_2 at $\sqrt{s} = 500$ GeV and is about 13 fb.

We conclude that the Higgs sector of the NMSSM can most probably be tested conclusively at the future linear e^+e^- -colliders with 500, 1000 or 2000 GeV c.m. energies.

- 1. J. P. Deredinger and C. A. Sarvoy, Nucl. Phys. **B237** (1984) 307
- 2. J. Ellis, J. E. Ellis, J. E. Gunion, H. E. Haber, L. Roszkowski and F. Zwirner, Phys. Rev. **D39** (1989) 844
- 3. M. Drees, Int. J. Mod. Phys. **A4** (1989) 3635
- 4. H. P. Nilles, Phys. Rep. 110 (1984)H. E. Haber and G. L. Kane, Phys. Rep. 117 (1985) 75
- 5. J. R. Espinosa and M. Quiros, Phys. Lett. **B279** (1992) 92
- 6. P. Binetury and C. A. Savoy, Phys. Lett. **B277** (1992) 453
- 7. U. Ellwanger and M. Lindner, Phys. Lett. **B301** (1993) 365

- 8. B. R. Kim and S. K. Oh, PITHA 94/46, 1994
- 9. P. N. Pandita, Z. Phys. C59 (1993) 575
- 10. U. Ellwanger, Phys. Lett. **B303** (1993) 271
- 11. T. Elliot, S. F. King and P. L. White, Phys. Rev. **D49** (1994) 2435
- 12. B. R. Kim, S. K. Oh and A. Stephan, in *Proceedings of the Workshop on Physics and Experiments with Linear* e^+e^- -Colliders, eds. F. A. Harris et. al., World Scientific (Singapure 1993) p. 860

Figure 1: Upper bound for λ as a funtion of $\tan \beta$ for $m_{top} = 175$ GeV.

Figure 2: Upper bound for λ as a funtion of $\tan \beta$ for $m_{top} = 190$ GeV.

Figure 3: $\sigma(R_1, R_2)$ as definded in the text for $\sqrt{s} = 500$ GeV.

Figure 4: $\sigma(R_1, R_2)$ for $\sqrt{s} = 1000$ GeV.

Figure 5: $\sigma(R_1, R_2)$ for $\sqrt{s} = 2000$ GeV.

Figure 6: Minimal value of $\sigma(R_1, R_2)$ as a function of \sqrt{s} for various values of $m_{S_1^{max}}$

Figure 7: Cross section for $e^+e^- \to Zb\overline{b}$ for $A_{\lambda}=220$ GeV, $A_k=160$ GeV, x=1000 GeV, $\tan\beta=2, k=0.04, \lambda=0.12$. Masses and mixing angles have calculated from the tree level protential.

Figure 8: The same as above, but with masses and mixing angles obtained from the one loop effective potential. The top mass is 175 GeV, $m_{\tilde{t}_l} = m_{\tilde{t}_R} = 1$ TeV and $A_t = 0$ GeV.